NAVAL POSTGRADUATE SCHOOL
Monterey, California

THESIS

DESIGN AND ANALYSIS OF DISCRETE LATERAL AUTOPILOTS FOR COORDINATED BANK-TO-TURN MISSILES

by

Christos I. Karadimas

December 1985

Thesis Advisor: Daniel J. Collins

Approved for public release; distribution unlimited.

Unclassified

RITY CLASSIFICATION OF THIS PAGE

REPORT DOCUMENTATION PAGE

EPORT SECURITY CLASSIFICATION	1b. RESTRICTIVE MARKINGS
ECURITY CLASSIFICATION AUTHORITY	3. DISTRIBUTION / AVAILABILITY OF REPORT Approved for public release; distribution unlimited.
ECLASSIFICATION / DOWNGRADING SCHEDULE	
RFORMING ORGANIZATION REPORT NUMBER(S)	5. MONITORING ORGANIZATION REPORT NUMBER(S)
AME OF PERFORMING ORGANIZATION: aval Postgraduate School 6b. OFFICE SYMBOL (If applicable): Code 67	7a. NAME OF MONITORING ORGANIZATION Naval Postgraduate School
DDRESS (City, State, and ZIP Code) onterey, California 93943-5100	7b. ADDRESS (City, State, and ZIP Code) Monterey, California 93943-5100
AME OF FUNDING / SPONSORING RGANIZATION 8b. OFFICE SYMBOL (If applicable)	9. PROCUREMENT INSTRUMENT IDENTIFICATION NUMBER
DDRESS (City, State, and ZIP Code)	10. SOURCE OF FUNDING NUMBERS PROGRAM ELEMENT NO. / PROJECT NO. / TASK NO. / WORK UNIT ACCESSION NO.

TLE (Include Security Classification)
SIGN AND ANALYSIS OF DISCRETE LATERAL AUTOPILOTS FOR
ORDINATED BANK-TO-TURN MISSILES

ERSONAL AUTHOR(S)
RADIMAS, Christos I.

TYPE OF REPORT	13b. TIME COVERED	14. DATE OF REPORT (Year, Month, Day)	15 PAGE COUNT
ster's Thesis	FROM _____ TO _____	1985 December	165

UPPLEMENTARY NOTATION

COSATI CODES			18. SUBJECT TERMS (Continue on reverse if necessary and identify by block number)
IELD	GROUP	SUB-GROUP	Bank-to-turn, autopilot, yaw, roll, pitch, classical, modern, state-feedback, estimator, robustness.

BSTRACT (Continue on reverse if necessary and identify by block number)

This thesis addresses the design and analysis of discrete lateral utopilots for application to BTT missiles.

The first part reviewed the classical design and analysis of the ntinuous uncoupled yaw and roll channels as developed in [Ref. 6]. en, applying analog-to-digital conversion, the corresponding discrete utopilots were designed and analyzed in terms of their transient sponses.

The second part utilized modern control design techniques for the ngle-input discrete lateral autopilots. At first, assuming avail- ility of all states for feedback purposes, a discrete state-feedback utopilot was obtained. Next, since the state vector is not always

ISTRIBUTION / AVAILABILITY OF ABSTRACT UNCLASSIFIED/UNLIMITED ☐ SAME AS RPT. ☐ DTIC USERS	21. ABSTRACT SECURITY CLASSIFICATION Unclassified
NAME OF RESPONSIBLE INDIVIDUAL J. Collins	22b. TELEPHONE (Include Area Code): (408) 646-2826 22c. OFFICE SYMBOL: 67 Co

ORM 1473, 84 MAR 83 APR edition may be used until exhausted
All other editions are obsolete.

SECURITY CLASSIFICATION OF THIS PAGE

Unclassified

available to direct measurement, an estimator was introduced to implement control. The state-feedback and estimator designs were analyzed for both lateral channels and found to have satisfactory time responses.

Finally, coupling the discrete pitch and roll channel autopilots, a state-feedback and estimator were designed and found to be robust.

Approved for public release; distribution unlimited.

Design and Analysis of Discrete Lateral Autopilots for Coordinated Bank-to-Turn Missiles

by

Christos I. Karadimas
Lieutenant, Hellenic Navy
B.S., Hellenic Naval Academy, 1976

Submitted in partial fulfillment of the
requirements for the degree of

MASTER OF SCIENCE IN ENGINEERING SCIENCE

from the

NAVAL POSTGRADUATE SCHOOL
December 1985

ABSTRACT

This thesis addresses the design and analysis of discrete lateral autopilots for application to BTT missiles.

The first part reviewed the classical design and analysis of the continuous uncoupled yaw and roll channels as developed in [Ref. 6]. Then, applying analog-to-digital conversion, the corresponding discrete autopilots were designed and analyzed in terms of their transient responses.

The second part utilized modern control design techniques for the single-input discrete lateral autopilots. At first, assuming availability of all states for feedback purposes, a discrete state-feedback autopilot was obtained. Next, since the state vector is not always available to direct measurement, as estimator was introduced to implement control. The state-feedback and estimator designs were analyzed for both lateral channels and found to have satisfactory time responses.

Finally, coupling the discrete pitch and roll channel autopilots, a state-feedback and estimator were designed and found to be robust.

TABLE OF CONTENTS

LIST OF TABLES

LIST OF FIGURES

TABLE OF SYMBOLS AND ABBREVIATIONS

BTT	Bank-to-Turn
CBTT	Coordinated Bank-to-Turn (minimum sideslip, positive $\alpha, \phi_e \leq 180^o$)
C_ℓ	rolling moment coefficient
$C_{\ell_{\delta_R}}$	change in rolling moment coefficient (C_ℓ) per degree roll control incidence (δ_R)
C_m	pitching moment coefficient
C_{m_α}	slope of curve of pitching moment coefficient (C_m) vs angle-of-attack
C_N	normal force coefficient
C_n	yawing moment coefficient
C_{n_β}	slope of curve of yawing moment coefficient (C_n) vs angle-of-sideslip (β)
$C_{n_{\delta_Y}}$	change in yawing moment coefficient (C_n) per degree yaw control incidence (δ_Y)
C_Y	side force coefficient
C_{Y_β}	slope of curve of side force coefficient (C_Y) vs angle-of-sideslip (β)
$C_{Y_{\delta_Y}}$	change in side force coefficient (C_Y) per degree yaw control incidence (δ_Y)
d	reference length for coefficients
I_{zz}	moment of inertia about $\bar{z}_B$ axis
I_{xx}	moment of inertia about $\bar{x}_B$ axis
OPTSYS	Optimal System Control Fortran Program
ORACLS	Optimum Regulator Analysis and Control of Linear Systems
p	roll rate about $\bar{x}_B$

$\dot{p}$	roll acceleration about $\bar{x}_B$
POC	Preferred Orientation Control
POPLAR	Pole Placement and Robustness Design Program
$\bar{q}$	dynamic pressure
q	pitch rate about $\bar{y}_B$
r	yaw angular rate about $\bar{z}_B$
r_c	yaw angular rate command (coordinated command)
$\dot{r}$	yaw angular acceleration about $\bar{z}_B$
S	reference are for coefficients
STT	Skid-to-Turn (roll attitude stabilized)
u	velocity component in $\bar{x}_B$ direction
v	velocity component in $\bar{y}_B$ direction (assumed constant)
V	constant missile flight path velocity
$\bar{V}$	missile velocity vector
w	velocity component in $\bar{z}_B$ direction
W	missile weight
x	body-fixed roll axis (along axis of symmetry, positive forward)
y	body-fixed pitch axis (positive forward)
z	body-fixed yaw axis (forms right-handed orthogonal system with $\bar{x}_B$ and $\bar{y}_B$)
η_z	achieved normal acceleration in $\bar{z}_B$ direction
η_y	achieved normal acceleration in $\bar{y}_B$ direction
η_z	achieved normal acceleration in $\bar{z}_v$ direction
η_y	achieved normal acceleration in $\bar{y}_v$ direction
n_c	normal acceleration command from guidance computer in $\bar{z}_v$ direction plus anti-gravity bias command

η_{Y_c}	normal acceleration guidance command in $\bar{Y}_V$ direction
Φ_c	roll attitude command from guidance computer (zero degrees in $-\bar{Z}_V$ direction and 90 degrees in $\bar{Y}_V$ direction)
Φ	roll attitude (zero degrees in $-\bar{Z}_V$ direction and 90 degrees in $\bar{Y}_V$ direction)
Θ	elevation Euler Angle (second rotation)
Ψ	azimuth Euler angle (first rotation about $\bar{Y}_V$)
δ_P	pitch control incidence (positive tail incidence produces negative pitching moment)
δ_{P_c}	commanded pitch control incidence
δ_Y	yaw control incidence (positive tail incidence produces negative yawing moment)
δ_{Y_c}	commanded yaw control incidence
δ_R	roll control incidence (positive tail incidence produces positive rolling moment)
δ_{R_c}	commanded roll control incidence
α_e	constant or equilibrium angle-of-attack
α	angle-of-attack
β	angle-of-sideslip

ACKNOWLEDGEMENT

The author wishes to express his sincere appreciation to Professor Daniel J. Collins whose guidance, assistance and encouragement contributed immeasurably to this research.

The author would also like to dedicate this thesis to his wife Irini and his son Ioannis for their constant support, patience and understanding.

I. INTRODUCTION

Modern tactical missiles require increased stand-off ranges and need to meet threats from highly maneuverable air targets. The high maneuverability of air targets has directed the use of defence missiles capable to develop higher lift accelerations and more complex control laws. In order to accomplish the requirement of large stand-off ranges, propulsion systems using air-breathing engines have been studied and developed in recent years. The advent of air-breathing engines has naturally led to the consideration of BTT missiles in order to minimize the inlet angle-of-attack.

The necessity of more complex control laws has introduced the application of modern control and estimation theory, since more complicated information of the missiles states are needed. BTT controlled missiles are generally characterized by increased maneuverability and considerable drag reduction over conventional cruciform, roll stabilized STT controlled missiles. Certain limitations in technology [Ref. 1] have delayed the development of BTT control systems, and consequently any progress in the area of BTT autopilots.

Major technological improvements during the last decade, as the availability of advanced digital computers, reopened the issue and made BTT control feasible in spite the added complexity of control laws for the autopilots. In addition, certain types

of ramjet engines [Ref. 2], which are candidate propulsion systems for modern tactical mission requirements of range and high altitude [Ref.3], have presented a need for a missile control technique to maintain effective inlet flow. This was the main reason for given further impetus to the investigation and development of BTT control.

Despite the fact that BTT steering may provide improved performance for a missile system, there are still unanswered questions concerning stability during homing phase, guidance performance, autopilot guidance logic and subsystem requirements. All these questions have to be investigated and properly answered in order for BTT steering to be considered as a viable control method for high performance missiles.

During the past decade many missile programs [Ref. 3] were initiated to improve the capability of steering tactical missile via BTT control with results that have greatly advanced the understanding of the various missile subsystems. In the autopilot area many different types have been designed and developed. All of them force the missile to roll or bank, so that the steering maneuver occurs with the missile axis oriented in a specific or preferred direction with respect to the incoming airstream. This class of autopilots is usually known as POC autopilots.

The main criterion for the selection of a particular type of autopilot is based upon the guidance, airframe and propulsion system requirements. Generally, missiles with either one or two

planes of symmetry use a POC autopilot which forces the missile to bank in order to turn as an aircraft. If this motion is coordinated, then the autopilot is referred to as a CBTT autopilot.

In the guidance area, radome aberation effects for frequency guidance are of major concern [Ref. 3] and are being investigated in great extent. Also, the interaction between BTT control, antenna stabilization and sensor orientation are some of the additional concerns that have to be properly addressed. However, simplified studies [Ref. 4], which neglect radome effects and assume that the missile motion is entirely coordinated, have proven that BTT control can provide acceptable performance with roll rates that are not excessive for autopilot design. These studies were made for a medium range area and long suppression mission, and considered both high lift (i.e., planar) and moderate lift (i.e., cruciform) airframe configurations.

In order to take full advantage of CBTT control, planar airframes have been designed to increase the lifting capability in one direction without the weight and drag penalty associated with orthogonal lifting surfaces [Ref. 5]. These airframes have aerodynamic properties characterized by increased potential to enhance CBTT control.

The present thesis addresses the design and analysis of discrete lateral autopilots for application to CBTT missiles.

The first part reviewed the design procedure of the two individual lateral channels as developed by Arrow [Ref. 6]. The

design was performed using classical techniques and involved the uncoupled yaw and roll channels for the elliptical and circular airframes respectively. The resulted continuous open loop designs were analyzed in terms of their transient and frequency responses and found to be in accordance with the desired requirements specified in [Ref. 6]. Then, applying analog-to-digital conversion, the corresponding discrete lateral autopilots were obtained and analyzed.

The second part utilized modern control design methods to the already discussed discrete single-input lateral autopilots. This allowed comparison with the preceding classical design, and more importantly established a technique to extend some of the results to the more general multivariable case. At first, assuming availability of all states for feedback purposes, application of the Ackermann formula led to a discrete state-feedback designed autopilot. Next, since the state vector of the state-feedback model is not usually accessible to direct measurement, an estimator was introduced as an additional dynamic design in order to implement control to the original system. The state-feedback and estimator designed autopilots were analyzed for both lateral channels and found to have satisfactory responses.

Finally, coupling the discrete pitch and roll channel autopilots, the state-feedback and estimator designs were obtained and proved to be robust.

The analysis in all the above cases was performed using the existed at Naval Postgraduate School OPTSYS and ORACLS Fortran

program for the continuous and discrete systems respectively. Additionally, the last part that dealt with the coupled pitch and roll channel autopilot utilized the POPLAR design program developed by Gordon [Ref. 7].

II. CLASSICAL DESIGN AND ANALYSIS OF LINEAR UNCOUPLED LATERAL AUTOPILOTS

A. GENERAL

The initial phase in the design of lateral CBTT autopilots involved the design and analysis of the individual uncoupled lateral channels (i.e., yaw and roll) with prescribed relationships between speeds-of-response. These relationships when coupled with the corresponding ones of the longitudinal uncoupled channel (i.e., pitch) would meet the requirements of the overall CBTT autopilot.

The uncoupled autopilot design method was classical and used a combination of frequency response and root locus techniques. Utilization of this particular design method led to the achievement of practical bandwidths (i.e., sufficient high frequency attenuation), and in turn provided the range of required missile body angular rates and control motions. In addition, the resulting design minimized the influence of aerodynamic variations on desired responses. The application of the uncoupled channels to the whole CBTT autopilot was accomplished by an appropriate choice of the relative time constants of the individual channels. In order to achieve the desired maneuver plane acceleration the roll channel was designed to have a time constant of 0.5 seconds. The yaw uncoupled channel, which follows the roll motion to produce the required coordination (i.e., minimization of sideslip angle), is designed to have a

more rapid response with a time constant of 0.39 seconds for the circular airframe. The detailed requirements for the classical design of the uncoupled yaw and roll channel autopilots are presented in Appendix A.

A fixed flight condition (i.e., constant Mach number and altitude) was selected for this preliminary performance study. Fixed flight conditions are typically used in autopilot designs to identify and cure critical areas of concern. When autopilot requirements are satisfied at fixed flight conditions, then areas of concern caused by varying them are addressed. The selected flight condition of 60000 feet altitude and Mach number 3.95 provided sufficient dynamic pressure, so that the missile maneuvers resulted in large enough angles-of-attack to exercise sideslip control. Aerodynamic data for this particular flight condition are provided in Appendix A.

The aerodynamic models developed for stability studies in the frequency domain were linearized about a trim angle-of-attack for both lateral channels. The following three assumptions were made:

1. The plane $\bar{x}_B$ - $\bar{z}_B$ of Figure 2.1 was the maneuver plane.
2. The missile was trimmed in pitch (i.e., $M_Y = 0$, at fixed values of α , q, and $\bar{c}_p$.

Rather than use the assumption that the missile roll rate is approximately zero as it is normally done for the roll stabilized STT control, the following assumption was made for BTT:

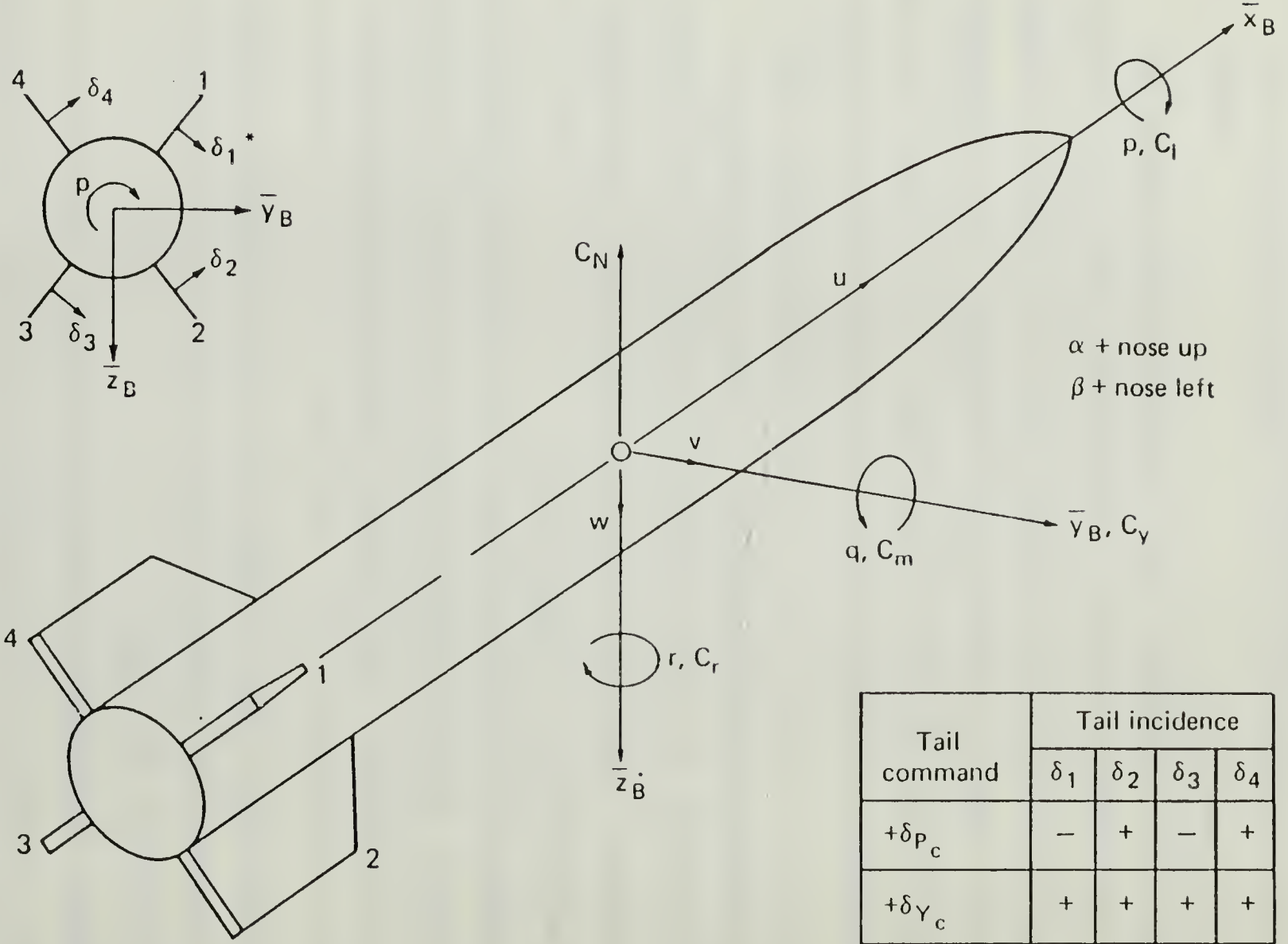

*Arrow indicates direction of positive leading edge deflection

Tail command	Tail incidence			
	δ_1	δ_2	δ_3	δ_4
$+\delta_{P_c}$	−	+	−	+
$+\delta_{Y_c}$	+	+	+	+
$+\delta_{R_c}$	+	−	−	+

Figure 2.1 Aerodynamic Sign Convention and Axis

3. The missile roll rate was constant.

Linearized aerodynamic derivatives are given in Appendix C.

In this chapter the analysis of both continuous and discrete uncoupled lateral channels of a BTT autopilot was based on the transient and frequency responses of maneuver plane accelerations, body angular rates and tail incidence angles. A general block diagram of a BTT autopilot with all its channels is shown in Figure 2.2. Inertial acceleration command were applied in polar coordinates (i.e., magnitude of the command n_c applied to pitch and the direction Φ_c to roll autopilot). The yaw autopilot was slaved to the roll autopilot in order to minimize the yaw and roll motions. Achieved maneuver plane accelerations in rectangular coordinates (i.e., n_z and n_y) were determined by resolving achieved body-fixed accelerations (i.e., n_z and n_y) through missile roll rate (i.e., Euler angles θ and ψ were assumed to be sufficiently small).

B. AIRFRAME CONFIGURATIONS

The two airframe configurations studied in this work were taken from [Ref. 6] and are shown in Figure 2.3 and Figure 2.4. Although the configuration in Figure 2.3 reveals a body of circular cross section and that of Figure 2.4 an elliptical one, both airframes have the same cross sectional area distribution. In specific, the circular cross sectional body has a closure ratio Abase/Amax of 0.69 with Amax occurring at 68% missile body, whereas the elliptical airframe has a 3:1 cross section.

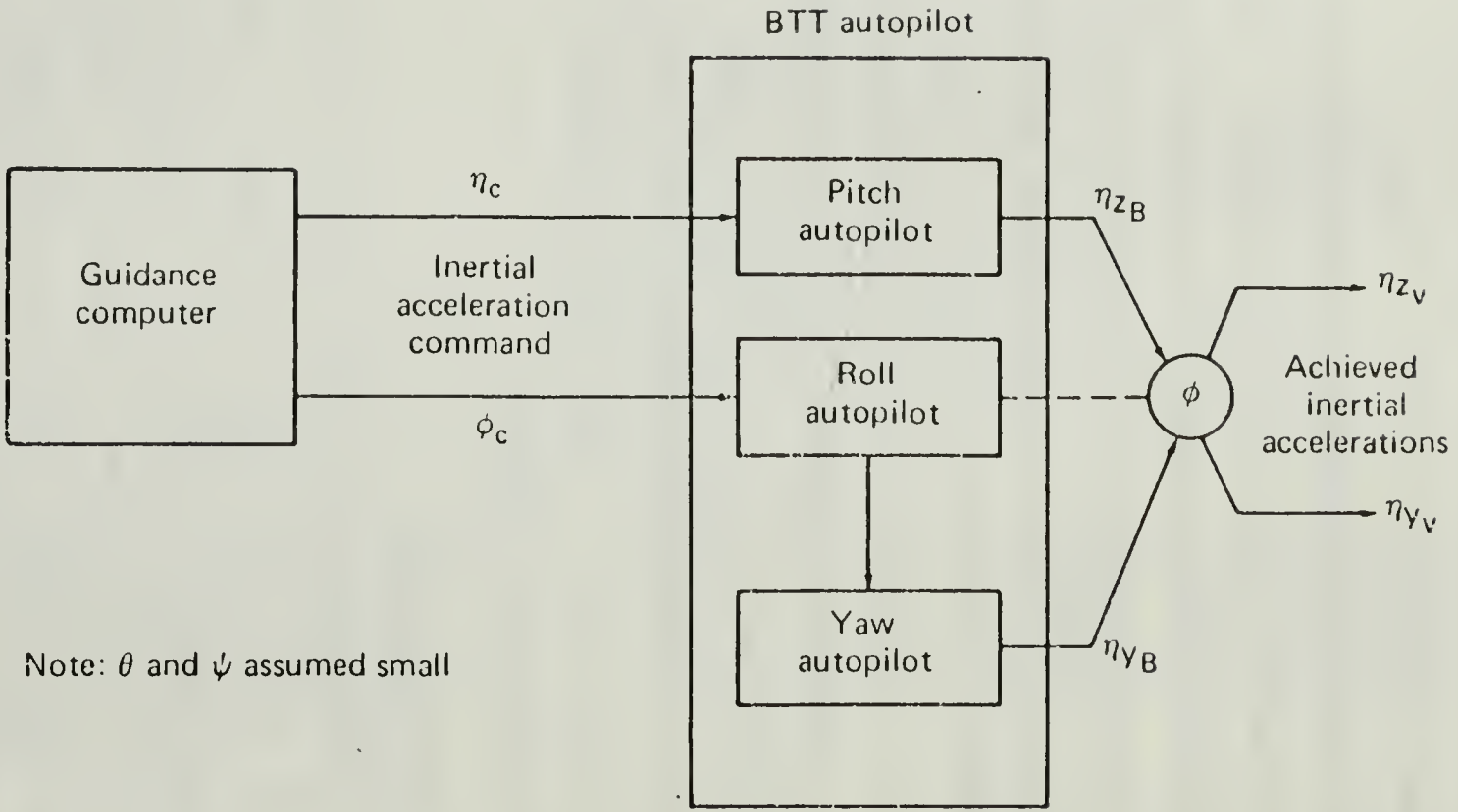

Figure 2.2 Bank-to-Turn Autopilot

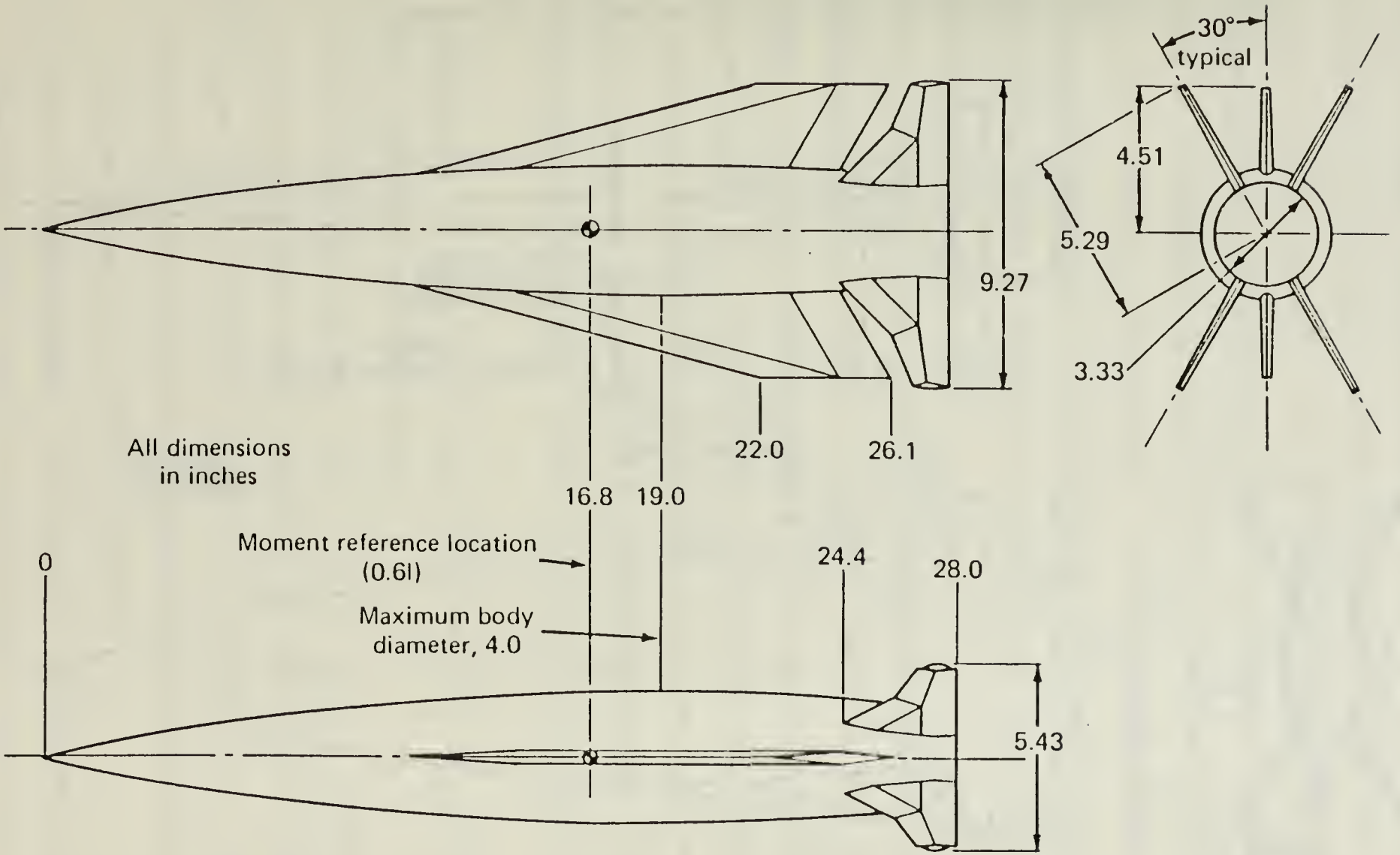

Figure 2.3 Model of Circular Airframe Configuration 1/6-scale

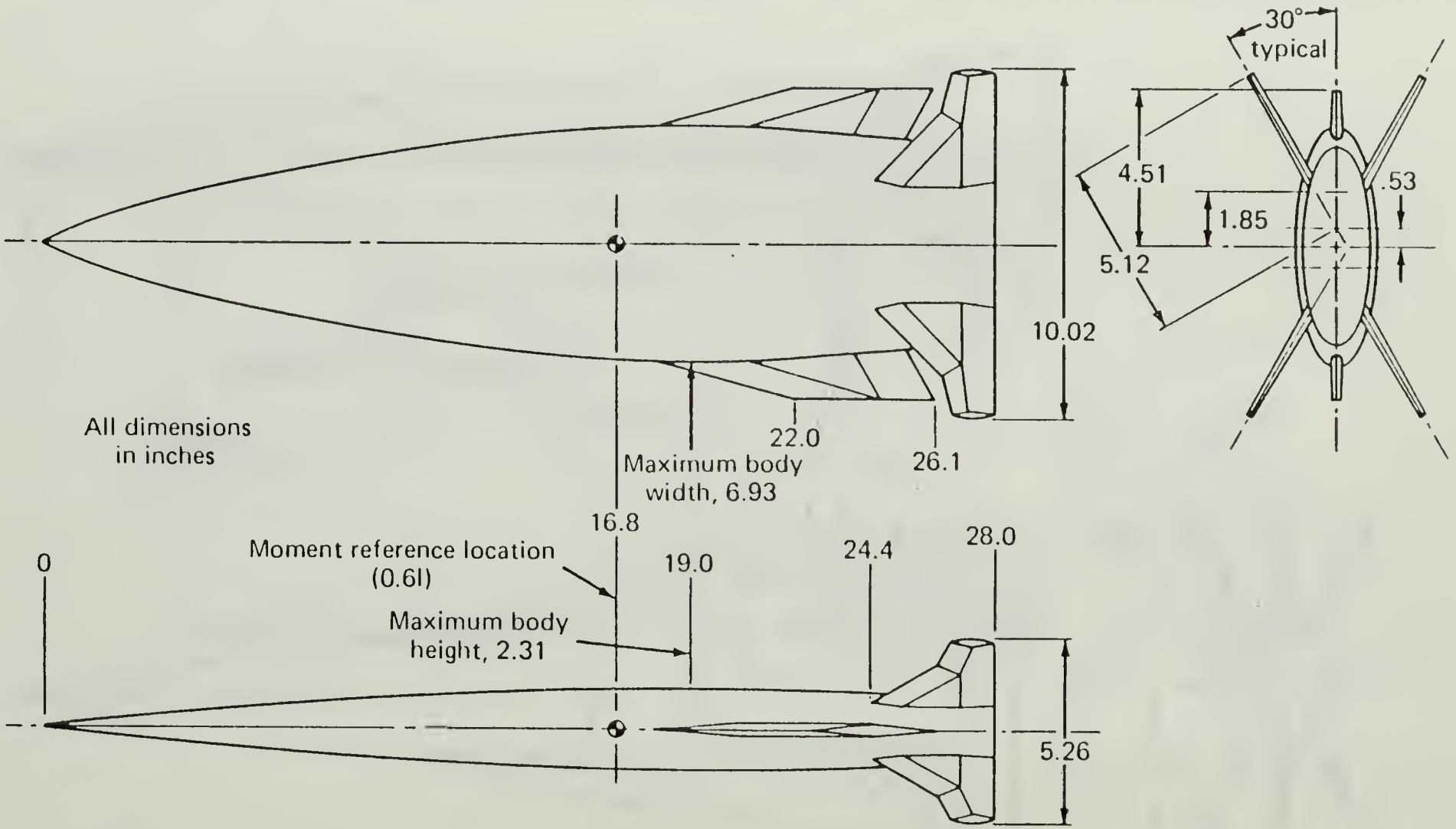

Figure 2.4 Model of Elliptical Airframe Configuration 1/6-scale

Both airframe configurations are tail-controlled using four identical control surfaces which are located flush with the body base with a $\pm 30^{\circ}$ dihedral. In the case of the elliptical body, the hinge line was skewed such that a 10° control deflection measured at the body-tail juncture had a resultant 7.04° surface deflection. Thus, the aerodynamic control effectiveness in terms of deflection measured at the body-tail is lower for the elliptical airframe although it is nearly the same in terms of resultant surface deflection.

The total span of the mono-wings is the same for each configuration, which results in larger wing area for the circular airframe. The wing area and span for the circular airframe were chosen as typical of current maneuvering missiles. The wing for the elliptical concept was determined by projecting the elliptical body on the circular body-wing planform. The resultant when exposed wing planform became the wing for the elliptical body.

Comparison of the elliptical airframe with the corresponding circular indicates the following:

1. About 30% more normal force that is nearly independent of angle-of-attack can be achieved at supersonic speeds.
2. Values of longitudinal stability parameter $C_{m_{\alpha}}$ are more positive, and with more pronounced nonlinearities in pitching moment at subsonic speeds.
3. Levels of directional stability are increased and more compatible with levels of longitudinal stability.

4. More yaw control is available although suitable locations for tails on the body are more limited because of the geometry of the elliptical airframe.

The two airframe configurations were sized to provide realistic geometric and mass properties. The details are presented in Appendix D.

C. UNCOUPLED YAW CHANNEL AUTOPILOT FOR ELLIPTICAL AIRFRAME

The purpose of the uncoupled yaw channel autopilot of a CBTT missile is to minimize the sideslip angle (β), or provide coordinate motion between the yaw and roll channels. The easiest way to accomplish this is by designing the uncoupled yaw channel (i.e., roll and pitch dynamic effects neglected) as a regulator (i.e., no guidance command and with rate and acceleration feedback) to help minimize the sideslip angle.

A block diagram of the uncoupled yaw channel is shown in Figure 2.5. In this diagram both the aerodynamic model and yaw control law are involved. The normal acceleration (n_{Y_c}) is not used to command the CBTT autopilot. Instead, it is used for the design and analysis of the uncoupled channel. The command used by the coupled system is shown in dashed lines and is a yaw angular rate command (r_c). The yaw control law shown in Figure 2.6 [Ref. 6] is governed by missile body angular rate (r) and yaw normal acceleration (n_Y). At the flight condition of interest (i.e., 60 kft altitude and Mach number 3.95) the yaw control law determines the required command ($\bar{\delta}_{Y_c}$) to an actuator which is

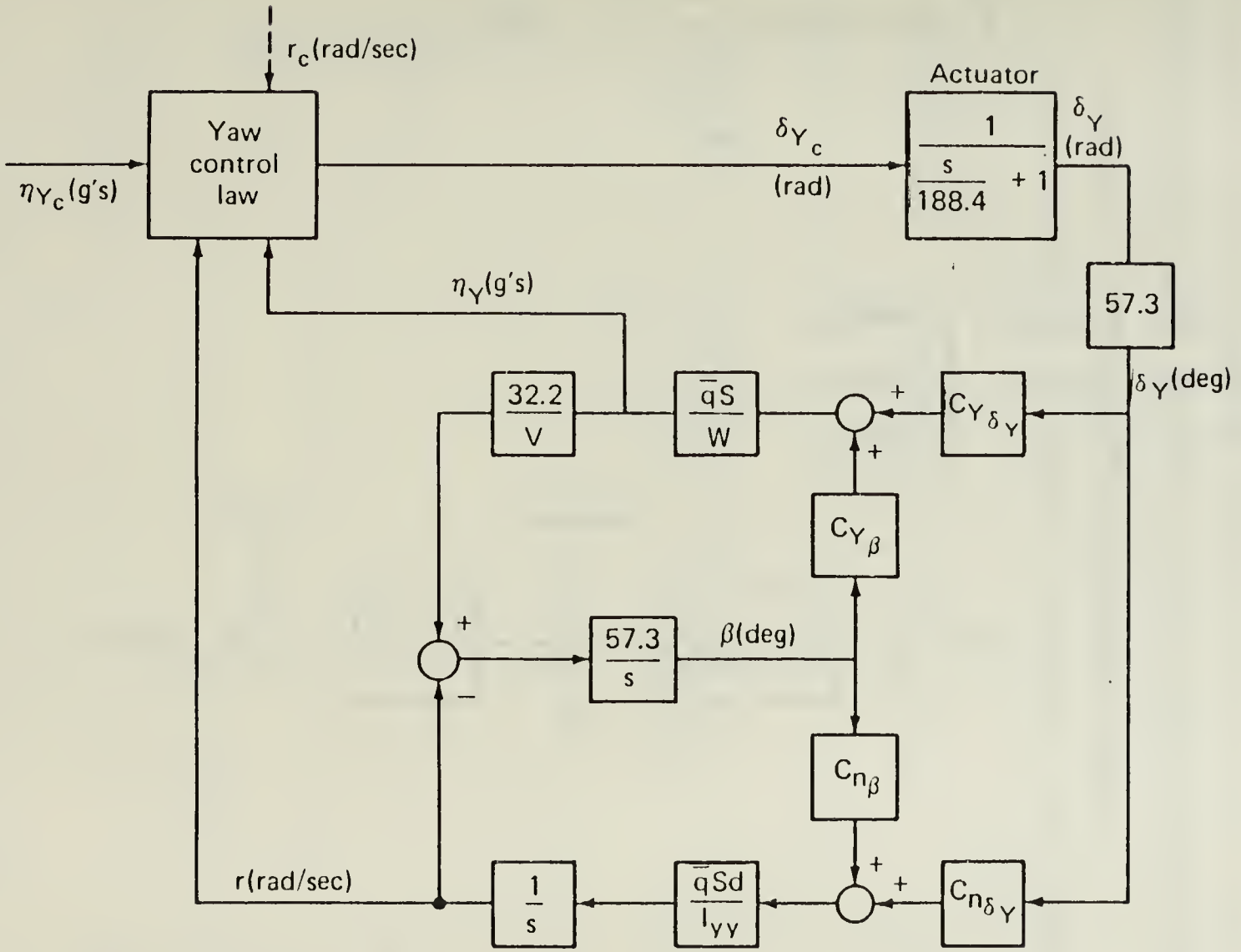

Figure 2.5 Uncoupled Yaw Channel

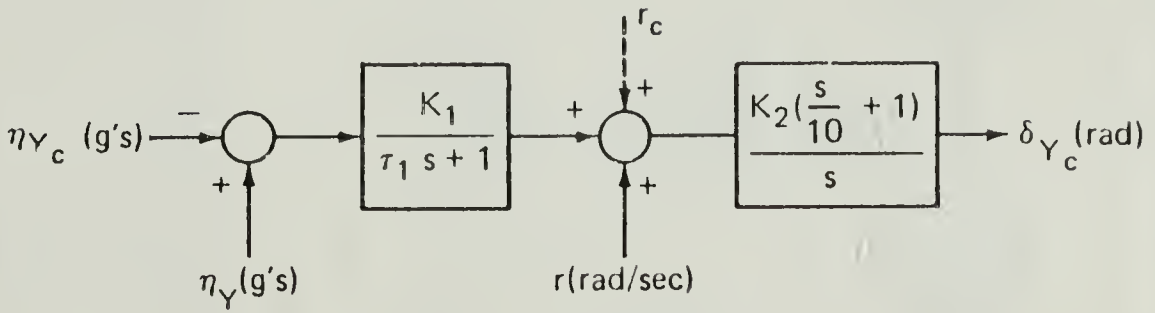

Airframe	K_1	τ_1	K_2
Circular	0.31946	0.2	4.85
Elliptical	0.33935	0.25	6.08

Figure 2.6 Yaw Control Law

approximated as a first-order lag at 30 Hz. The rate compensator computes the high frequency attenuation and is used to minimize aerodynamic variations on the quality of the regulator. On the other hand, the acceleration compensator measures the acceleration bandwidth via the time constant of the acceleration response of n_{Y_c}.

1. Transfer Functions of Aerodynamic Model

The aerodynamic transfer functions of the uncoupled yaw channel autopilot are:

$$\frac{z}{\delta_Y} = \frac{K(-\bar{A}\bar{E}+\bar{B}\bar{C})}{\bar{C}} \quad \frac{\frac{\bar{E}}{K(-\bar{A}\bar{E}+\bar{B}\bar{C})}s+1}{\frac{1}{\bar{C}}s^2-\frac{\bar{A}K}{\bar{C}}s+1} \text{ (deg/sec/deg)} \qquad \text{(II.C.1-1)}$$

$$\frac{n_Y}{\delta_Y} = \frac{-\bar{A}\bar{E}+\bar{B}\bar{C}}{\bar{C}} \quad \frac{\frac{\bar{B}}{-\bar{A}\bar{E}+\bar{B}\bar{C}}s^2+1}{\frac{1}{\bar{C}}s^2-\frac{\bar{A}K}{\bar{C}}s+1} \text{ (g's/deg)} \qquad \text{(II.C.1-2)}$$

where:

$$\bar{A} = \frac{\bar{q}S}{W} C_{Y_\beta} \qquad \text{(II.C.1-3)}$$

$$\bar{B} = \frac{\bar{q}S}{W} C_{Y_{\delta_Y}} \qquad \text{(II.C.1-4)}$$

$$\bar{C} = \frac{(57.3)\bar{q}Sd}{I_{ZZ}} C_{n_\beta} \qquad \text{(II.C.1-5)}$$

$$\bar{C} = \frac{(57.3)\,\bar{q}\,S\,d}{I_{zz}} \qquad \text{(II.C.1-6)}$$

$$K = \frac{1854}{V} \qquad \text{(II.C.1-7)}$$

Substituting the values of aerodynamic data (Table VII), linearized aerodynamic derivatives (Table VIII), and geometric and mass properties (Table IX), equations (II.C.1-3) through (II.C.1-7) become:

$$\bar{A} = -0.1351 \qquad \text{(II.C.1-8)}$$

$$\bar{B} = 0.0436 \qquad \text{(II.C.1-9)}$$

$$\bar{C} = -17.2748 \qquad \text{(II.C.1-10)}$$

$$\bar{E} = 34.5495 \qquad \text{(II.C.1-11)}$$

$$K = 0.4823 \qquad \text{(II.C.1-12)}$$

Introducing the above equations (II.C.1-8) through (II.C.1-12) to (II.C.1-1) and (II.C.1-2), the aerodynamic transfer functions of the uncoupled yaw channel for the circular airframe and zero angle-of-attack can be obtained.

a. Transfer Function of Yaw Angular Rate:

$$\frac{r}{\bar{\delta}_Y} = \frac{0.15\left(\frac{1}{0.0748}s+1\right)}{\left(\frac{1}{4.5}s+1\right)\left(\frac{1}{-4.25}s+1\right)} \qquad \text{(II.C.1-13)}$$

b. Transfer Function of Yaw Normal Acceleration:

$$\frac{n_Y}{\bar{\delta}_Y} = \frac{17.76\left(\frac{1}{11.48}s+1\right)\left(\frac{1}{-11.48}s+1\right)}{\left(\frac{1}{4.5}s+1\right)\left(\frac{1}{-4.25}s+1\right)} \qquad \text{(II.C.1-14)}$$

Rearranging the above transfer functions in terms of the variable pairs $(r, \bar{\delta}_Y)$ and $(n_Y, \bar{\delta}_Y)$ respectively, they become:

$$z s^2 + 0.0494 z s - 18.2815 z = -36.66 \delta_Y s - 2.7422 \delta_Y \quad \text{(II.C.1-15)}$$

$$\eta_Y s^2 + 0.0494 \eta_Y s - 18.2815 \eta_Y = 2.4625 \delta_Y s^2 - 0.0018 \delta_Y s - 324.6801 \delta_Y \quad \text{(II.C.1-16)}$$

Applying inverse Laplace transformation, the following set of linear differential equations can be obtained:

$$\ddot{z} + 0.0494 \dot{z} - 18.2815 z = -36.66 \dot{\delta}_Y - 2.7422 \delta_Y \quad \text{(II.C.1-17)}$$

$$\ddot{\eta}_Y + 0.0494 \dot{\eta}_Y - 18.2815 \eta_Y = 2.4625 \ddot{\delta}_Y - 0.0018 \dot{\delta}_Y - 324.6801 \delta_Y \quad \text{(II.C.1-18)}$$

Both equations (II.C.1-17) and (II.C.1-18) form a second-order system of linear differential equations in which the forcing function involves derivative terms. Using rules of state-space representation [Ref. 8] the following equations are obtained:

$$\dot{X}_1 = X_2 - 36.66 \delta_Y \quad \text{(II.C.1-19)}$$

$$\dot{X}_2 = 18.2815 X_1 - 0.0494 X_2 - 0.9312 \bar{\epsilon}_Y \quad \text{(II.C.1-20)}$$

$$\dot{Z}_1 = Z_2 - 0.1234 \bar{\epsilon}_Y \quad \text{(II.C.1-21)}$$

$$\dot{Z}_2 = 18.2815 Z_1 - 0.0494 Z_2 - 280.6555 \epsilon_Y \quad \text{(II.C.1-22)}$$

$$z = X_1 \quad \text{(II.C.1-23)}$$

$$\dot{z} = X_2 - 36.66 \bar{\delta}_Y \quad \text{(II.C.1-24)}$$

$$\dot{\eta}_Y = Z_1 + 2.4625 \eta_Y \quad \text{(II.C.1-25)}$$

2. Equations of Yaw Control Law and Actuator

a. Acceleration Compensator Equation

The acceleration compensator equation obtained from Figure 2.6 is:

$$Y = \frac{0.31946}{0.2s+1}(\eta_Y - \eta_{Y_c}) \qquad \text{(II.C.2-1)}$$

Rearranging and applying inverse Laplace transformation, (II.C.2-1) turns into the following linear differential equation:

$$\dot{y} = -5y + 1.5973\eta_Y - 1.5973\eta_{Y_c} \qquad \text{(II.C.2-2)}$$

Substituting equation (II.C.1-25) into (II.C.2-2), the last becomes:

$$\dot{y} = 1.5973z_1 - 5y + 3.9334\bar{\sigma}_Y - 1.5973\eta_{Y_c} \qquad \text{(II.C.2-3)}$$

b. Rate Compensator Equation

The rate compensator equation also obtained from Figure 2.6 is:

$$\bar{\sigma}_{Y_c} = \frac{4.85\left(\frac{1}{10}s+1\right)}{.5}(y+z) \qquad \text{(II.C.2-4)}$$

Rearranging and applying inverse Laplace transformation to (II.C.2-5), it turns into:

$$\dot{\bar{\sigma}}_{Y_c} = 0.485\dot{y} + 0.485\dot{z} + 4.85y + 4.85z \qquad \text{(II.C.2-5)}$$

Substituting equations (II.C.1-23), (II.C.1-24) and (II.C.2-3) into the above, it becomes:

$$\dot{\bar{\sigma}}_{Y_c} = 4.85x_1 + 0.485x_2 + 0.7747z_1 + 2.425y - 15.8124\bar{\sigma}_Y - 0.7747\eta_{Y_c} \qquad \text{(II.C.2-6)}$$

c. Actuator Equation

The actuator equation obtained from Figure 2.5 is:

$$\bar{\delta}_Y = \frac{1}{\frac{1}{188.4}s+1}\,\bar{\delta}_{Y_c} \qquad \text{(II.C.2-7)}$$

Rearranging and applying inverse Laplace transformation, the last equation turns into:

$$\dot{\bar{\delta}}_Y = 188.4\,\bar{\delta}_{Y_c} - 188.4\,\bar{\delta}_Y \qquad \text{(II.C.2-8)}$$

3. Design Approach and Analysis of Continuous System

Utilizing state-space representation, the equations (II.C.1-19) through (II.C.1-22), (II.C.2-2) (II.C.2-6) and (II.C.2-8) can be modeled in a seventh-order system of the form $\underline{\dot{x}}=\underline{F}\underline{x}+\underline{G}\underline{u}$. The continuous plant system and input matrixes $\underline{F}$ and $\underline{G}$ are shown in Table I, and the state vector is:

$$\begin{bmatrix} X_1 \\ X_2 \\ Z_1 \\ Z_2 \\ Y \\ \bar{\delta}_{Y_c} \\ \bar{\delta}_Y \end{bmatrix} \qquad \text{(II.C.3-1)}$$

where the state variables are:

x_1, x_2: yaw angular rates

z_1, z_2: yaw normal accelerations

y : output of acceleration compensator

$\bar{\delta}_{Y_c}$: input command in the actuator

$\bar{\delta}_Y$: yaw tail incidence

TABLE I

PLANT SYSTEM AND INPUT MATRICES; UNCOUPLED YAW CHANNEL AUTOPILOT; CLASSICAL DESIGN; CONTINUOUS OPEN LOOP SYSTEM; ELLIPTICAL AIRFRAME

F MATRIX 7 ROWS 7 COLUMNS

0.0000000E+00	1.0000000E+00	0.0000000E+00	0.0000000E+00	0.0000000E+00	0.0000000E+00	-2.9232100E+01
-1.6722400E+01	-4.3400000E-02	0.0000000E+00	0.0000000E+00	0.0000000E+00	0.0000000E+00	2.5870000E-01
0.0000000E+00	0.0000000E+00	0.0000000E+00	1.0000000E+00	0.0000000E+00	0.0000000E+00	-8.0100000E-02
0.0000000E+00	0.0000000E+00	-1.6722400E+01	-4.3500000E-02	0.0000000E+00	0.0000000E+00	-1.5077240E+02
0.0000000E+00	0.0000000E+00	3.3574000E+00	0.0000000E+00	-4.0000000E+00	0.0000000E+00	6.4341000E+00
6.0800000E+00	6.0800000E-01	2.0413000E+00	0.0000000E+00	3.5480000E+00	0.0000000E+00	-1.3861200E+01
0.0000000E+00	0.0000000E+00	0.0000000E+00	0.0000000E+00	0.0000000E+00	1.8640000E+02	-1.8840000E+02

G MATRIX 7 ROWS 1 COLUMNS

0.0000000E+00
0.0000000E+00
0.0000000E+00
0.0000000E+00
-3.3574000E+00
-2.0413000E+00
0.0000000E+00

Executing the OPTSYS program, using an input step function which represents "1 gee command" at zero trim angle-of-attack, the pole-zero and time and frequency response plots are obtained.

The pole-zero plot of Figure 2.7 indicates that the continuous open loop system is stable, since the s-plane poles are:

$s_1 = -174.376$ (II.C.3-2)

$s_2 = -6.1042 + j\,10.6396$ (II.C.3-3)

$s_3 = -6.1042 - j\,10.6396$ (II.C.3-4)

$s_4 = -0.0217475 + j\,4.08919$ (II.C.3-5)

$s_5 = -0.0217475 - j\,4.08919$ (II.C.3-6)

$s_6 = -2.9296 + j\,2.99929$ (II.C.3-7)

$s_7 = -2.9296 - j\,2.99929$ (II.C.3-8)

The time response plots of the yaw normal acceleration, angular rate and tail incidence are shown in Figures 2.8 through 2.10. In particular the yaw normal acceleration time response plot has a 0.39 seconds time constant, 7% overshoot and a steady-state error of 0.018. These results are in accordance with the requirements referred in Appendix A, that is a time constant of 0.4 seconds, overshoot less than 10% and steady-state error not necessarily equal to zero. All the above three time response plots are identical with those presented in [Ref. 6].

Figures 2.11 through 2.16 show the frequency response plots of the yaw normal acceleration, angular rate and tail

incidence, from which the phase crossover frequencies and gain margins of Table II can be obtained. The positive gain and phase margins of the open loop system ensure the relative stability of the closed loop (controlled) system.

4. Design Approach and Analysis of Discrete System

Utilizing analog-to-digital conversion by the aid of ORACLS program and for a sample period of 0.0125 seconds, a seventh-order discrete system of the form $\underline{x}(k+1)=\underline{A}\underline{x}(k)+\underline{B}\underline{u}(k)$ is obtained. The discrete pant system and input matrices $\underline{A}$ and $\underline{B}$ are shown in Table III.

The pole-zero plot of Figure 2.17 indicates that the discrete open loop system is also stable, since the z-plane poles are:

$$z_1 = 0.113076 \qquad \text{(II.C.4-1)}$$

$$z_2 = 0.918354 + j0.122862 \qquad \text{(II.C.4-2)}$$

$$z_3 = 0.918354 - j0.122862 \qquad \text{(II.C.4-3)}$$

$$z_4 = 0.998422 + j0.0510788 \qquad \text{(II.C.4-4)}$$

$$z_5 = 0.998422 - j0.0510788 \qquad \text{(II.C.4-5)}$$

$$z_6 = 0.963365 + j0.0361346 \qquad \text{(II.C.4-6)}$$

$$z_7 = 0.963365 - j0.0361346 \qquad \text{(II.C.4-7)}$$

The time response plots of the yaw normal acceleration, angular rate and tail incidence for the discrete uncoupled yaw channel are presented in Figures 2.18 through 2.20. A close observation of these plots indicates that they are identical with those of the continuous classical system found in the previous section.

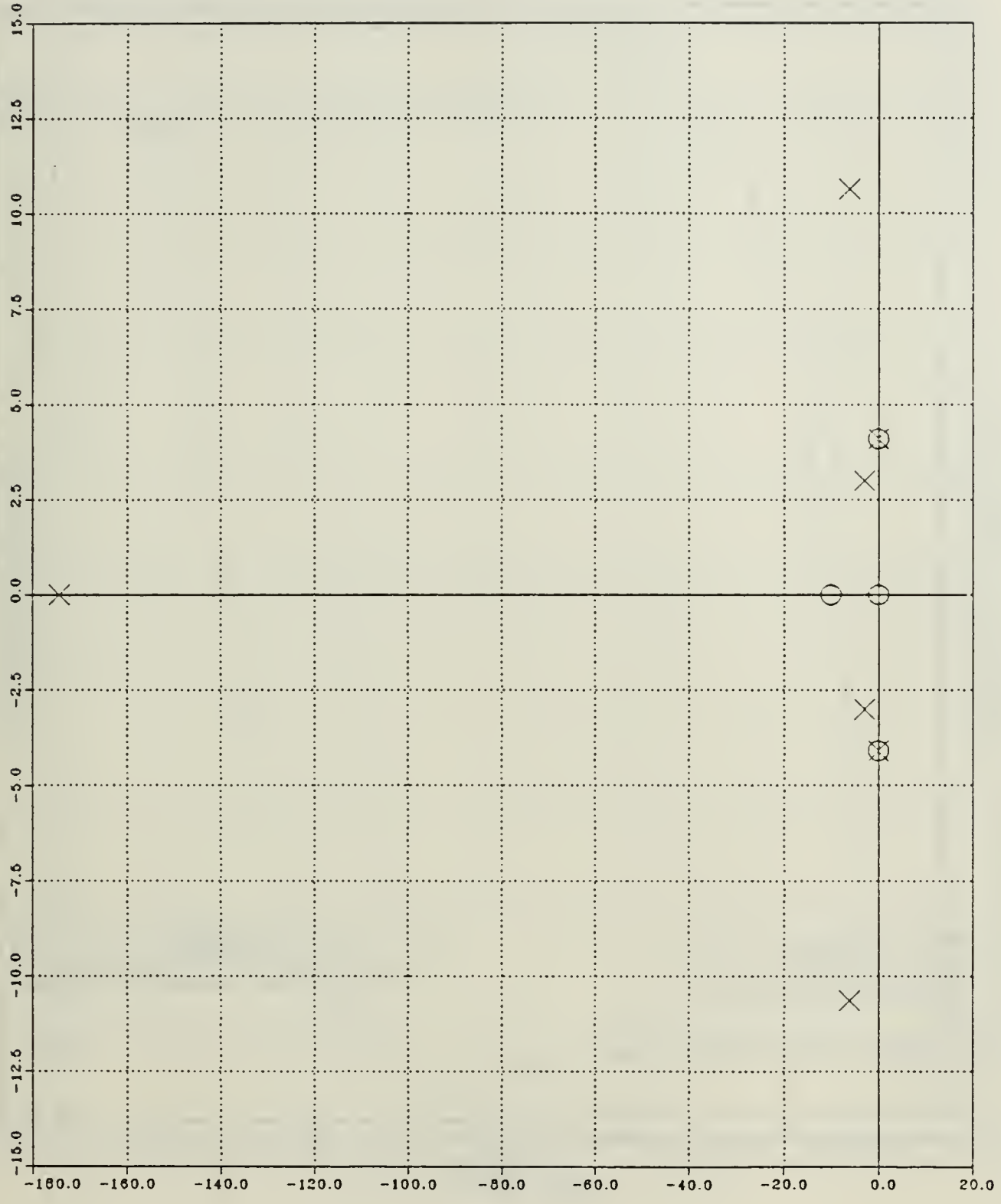

Figure 2.7 Pole-Zero Plot; Uncoupled Yaw Channel Autopilot; Classical Design Continuous Open Loop System; Elliptical Airframe

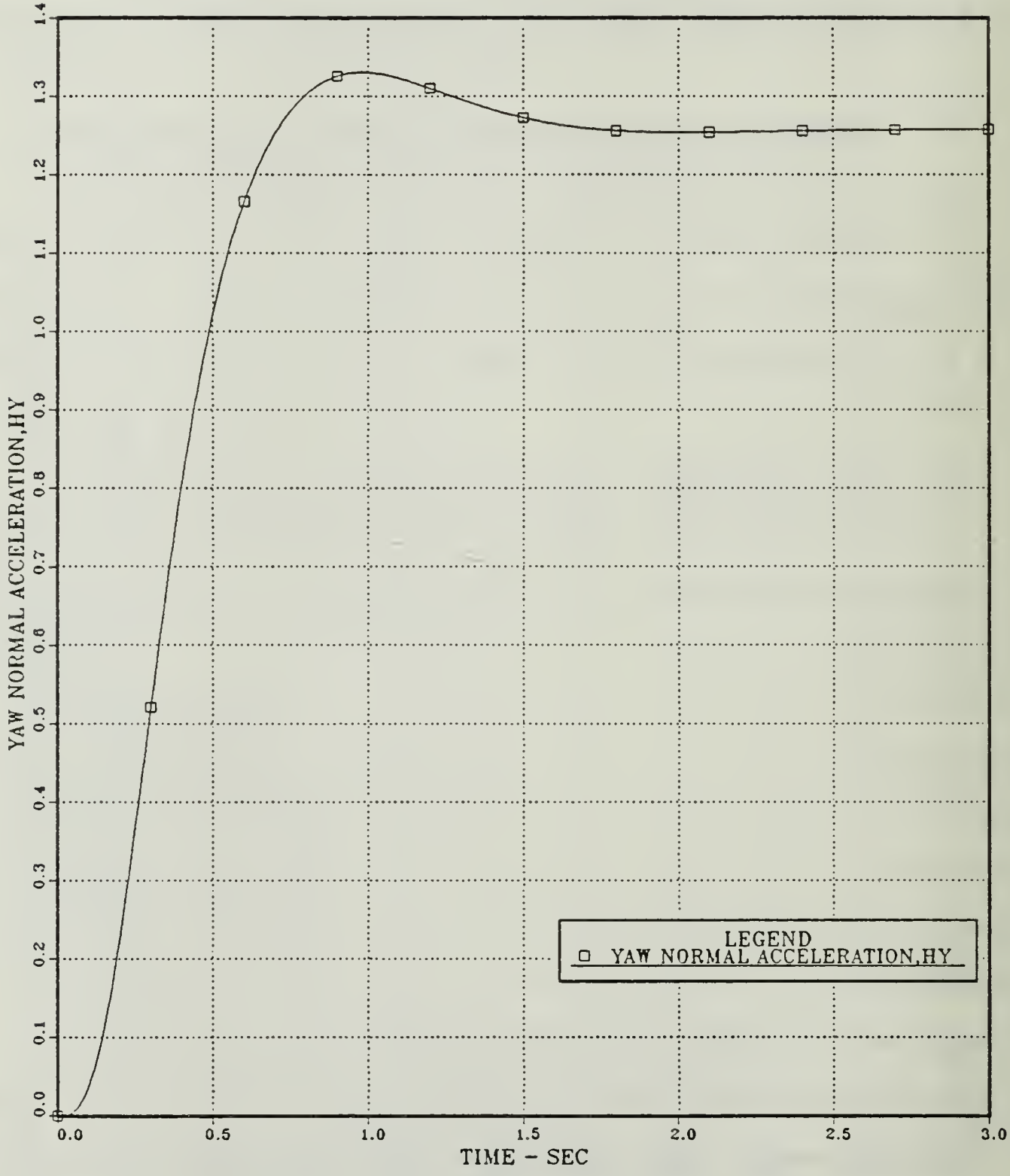

Figure 2.8 Yaw Normal Acceleration vs Time; Uncoupled Yaw Channel Autopilot; Classical Design; Continuous Open Loop System; Elliptical Airframe

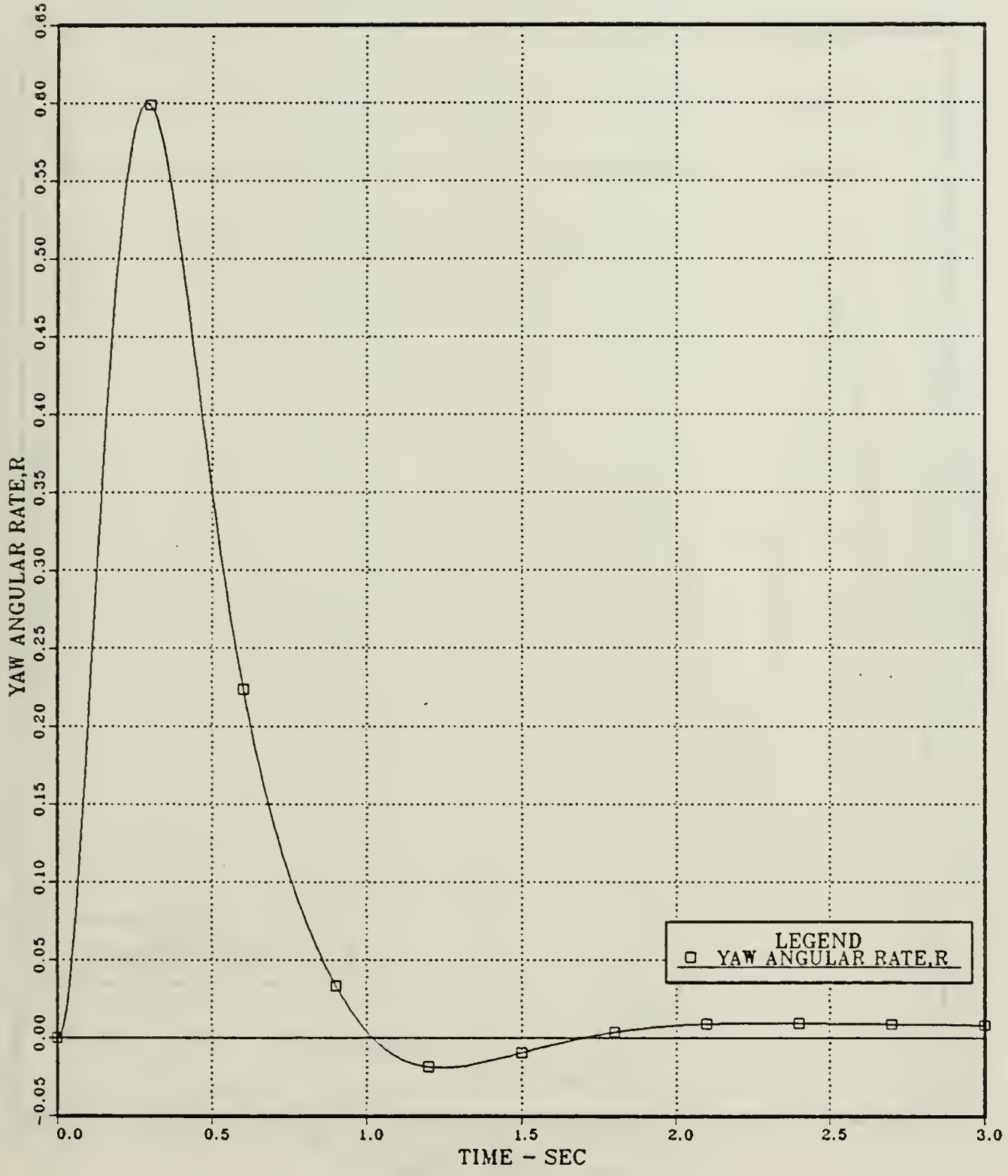

Figure 2.9 Yaw Angular Rate vs Time; Uncoupled Yaw Channel Autopilot; Classical Design; Continuous Open Loop System; Elliptical Airframe

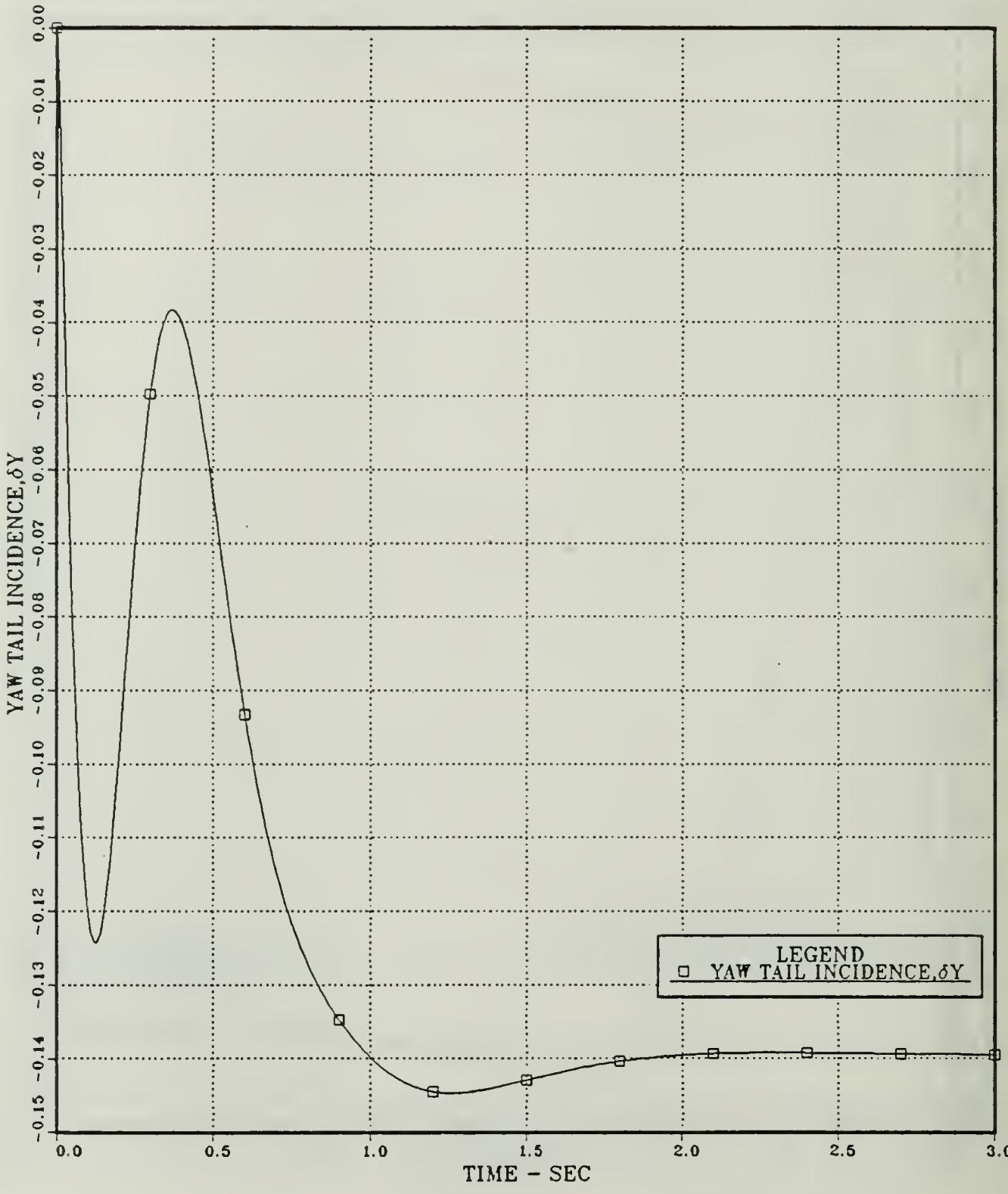

Figure 2.10 Yaw Tail Incidence vs Time; Uncoupled Yaw Channel Autopilot; Classical Design; Continuous Open Loop System; Elliptical Airframe

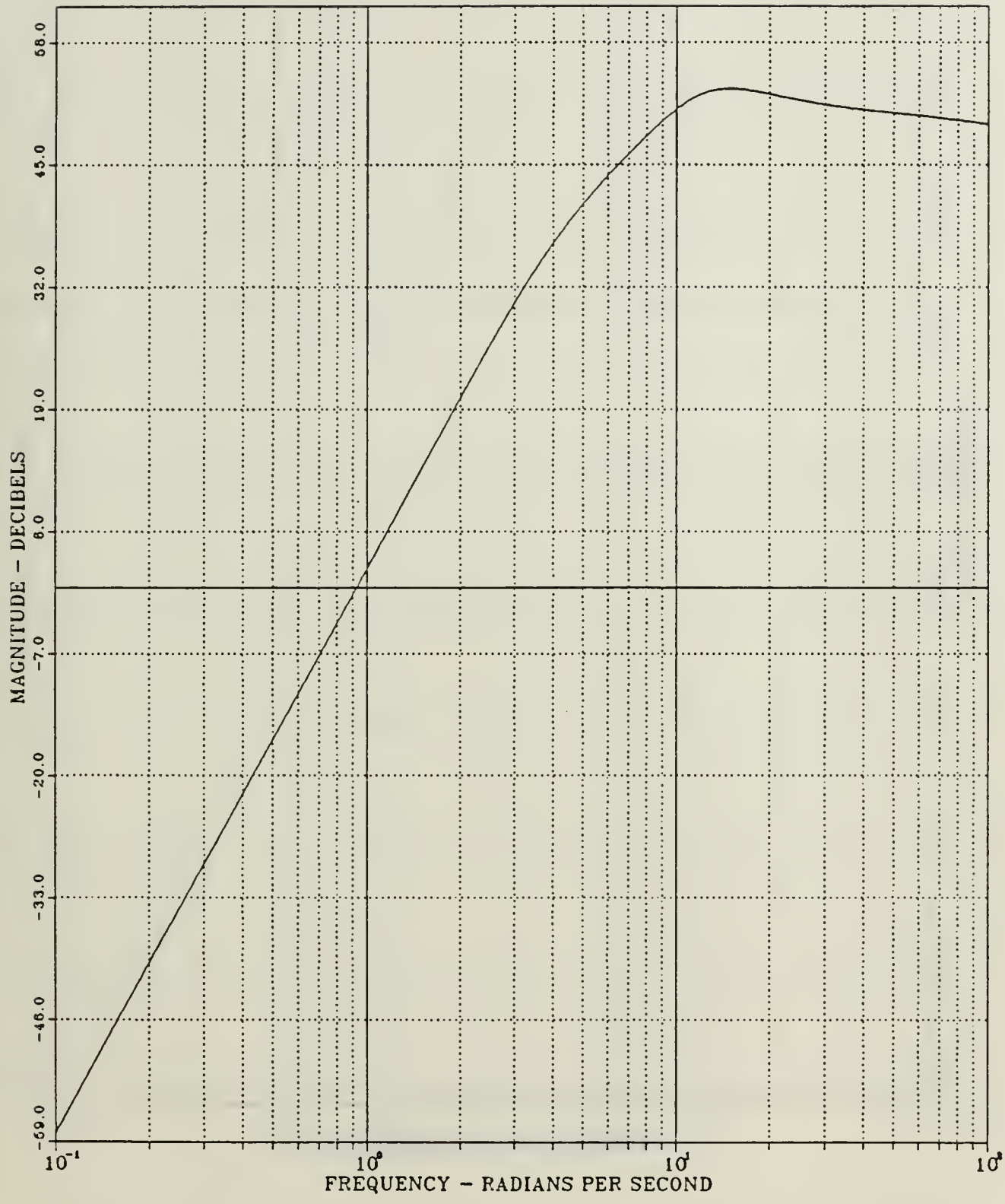

Figure 2.11 Yaw Normal Acceleration-Gain vs Frequency; Uncoupled Yaw Channel Autopilot; Classical Design; Continuous Open Loop System; Elliptical Airframe

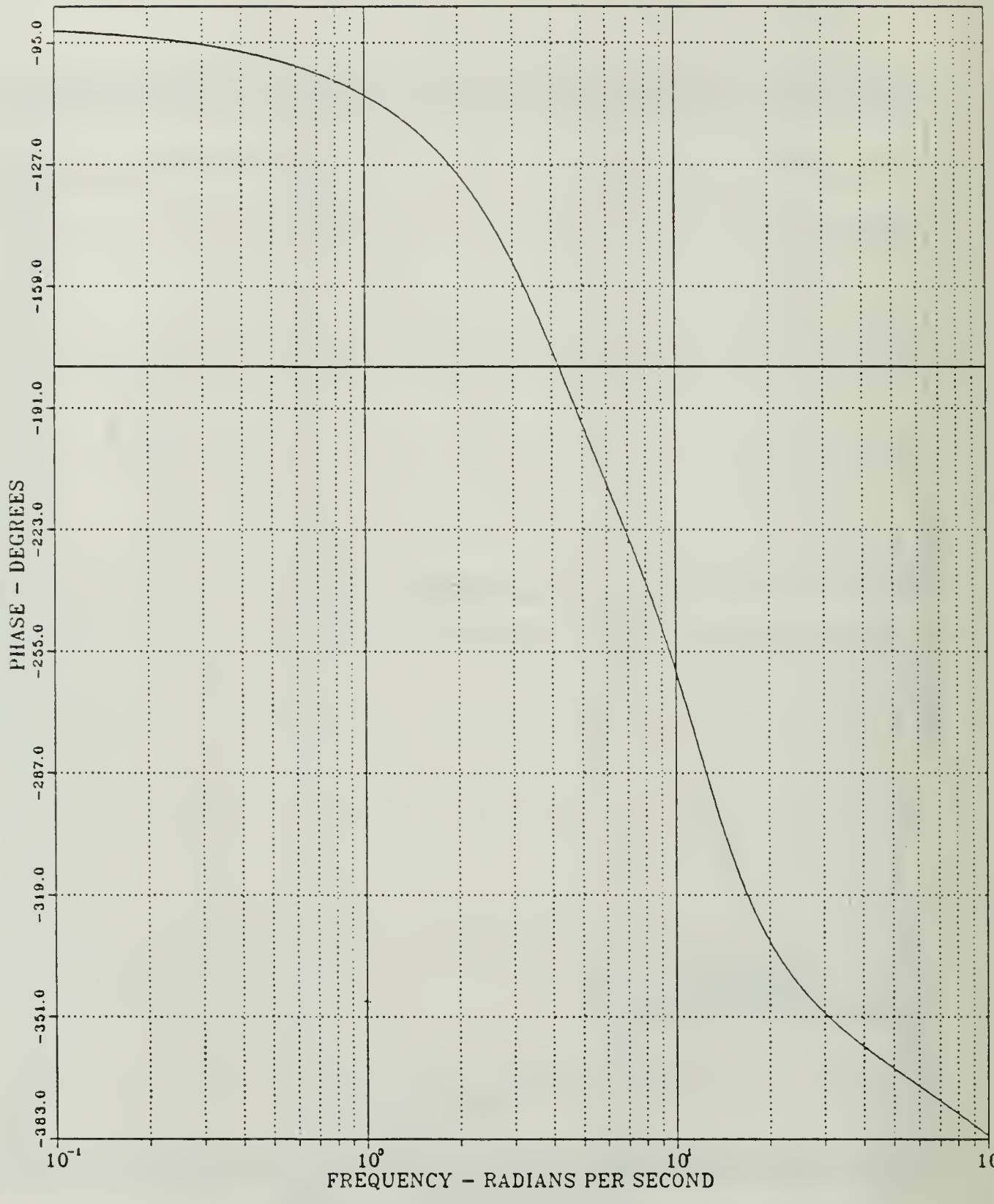

Figure 2.12 Yaw Normal Acceleration-Phase vs Frequency; Uncoupled Yaw Channel Autopilot; Classical Design; Continuous Open Loop System; Elliptical Airframe

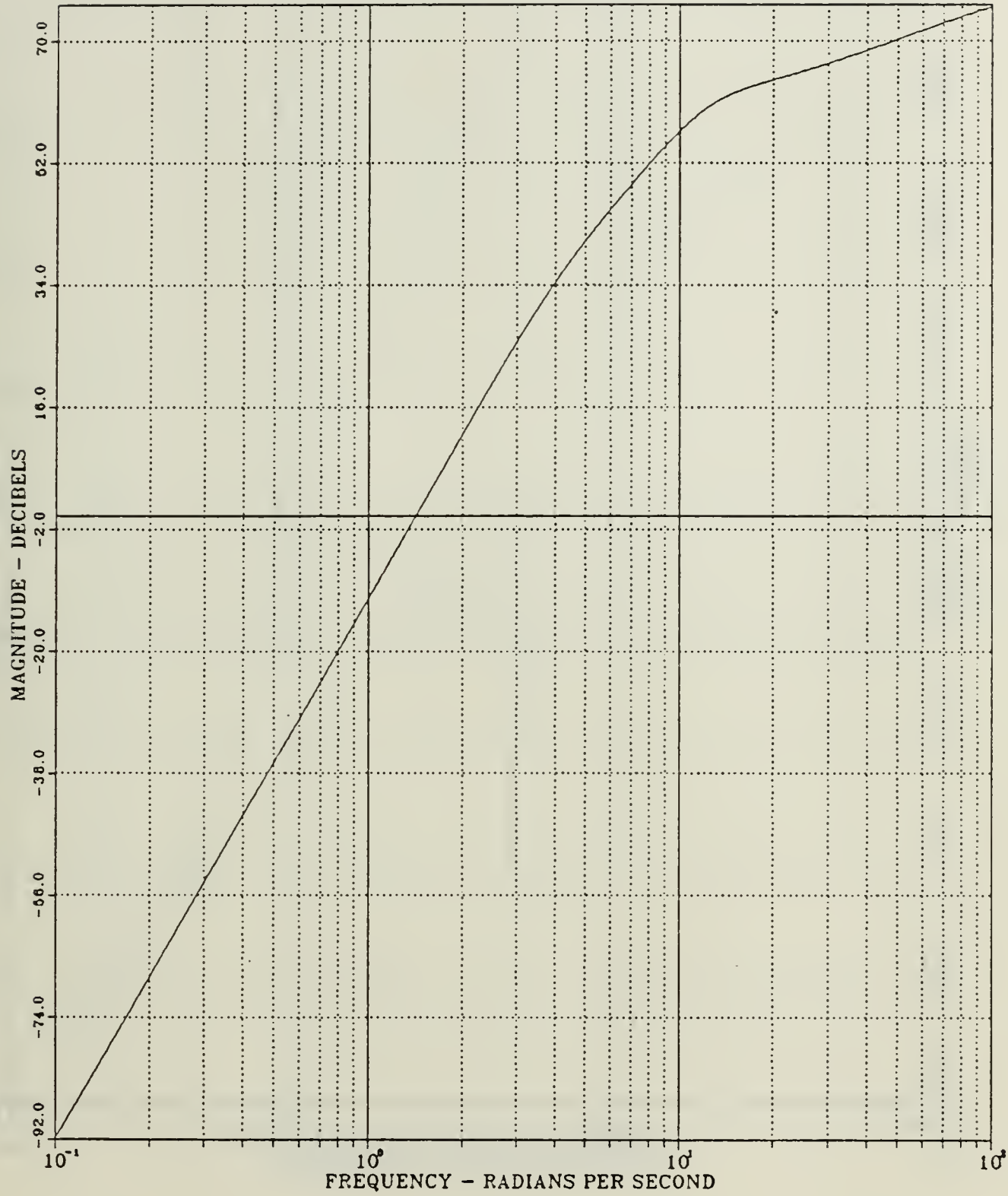

Figure 2.13 Yaw Angular Rate-Gain vs Frequency; Uncoupled Yaw Channel Autopilot; Classical Design; Continuous Open Loop System; Elliptical Airframe

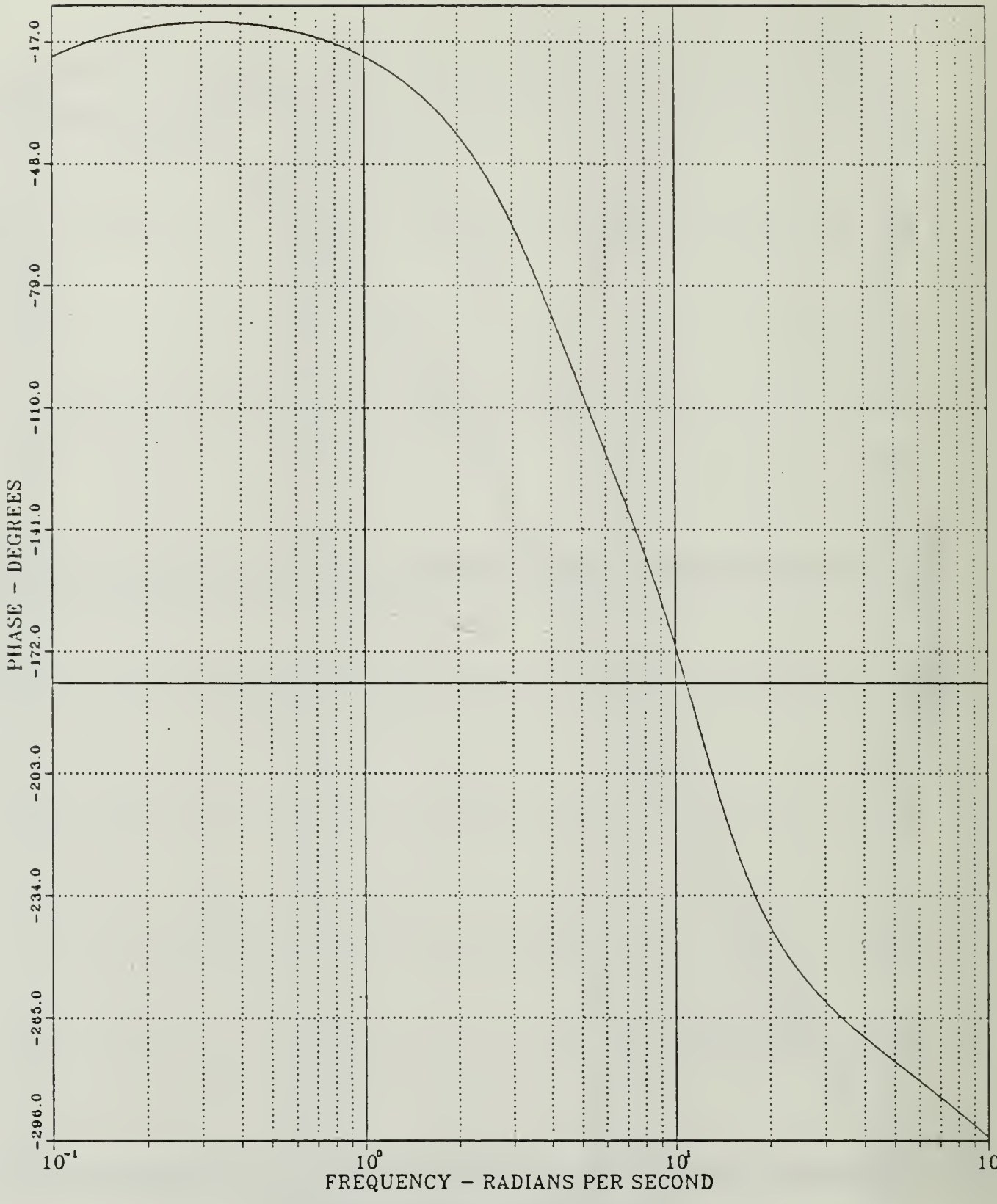

Figure 2.14 Yaw Angular Rate-Phase vs Frequency; Uncoupled Yaw Channel Autopilot; Classical Design; Continuous Open Loop System; Elliptical Airframe

Figure 2.15 Yaw Tail Incidence-Gain vs Frequency; Uncoupled Yaw Channel Autopilot; Classical Design; Continuous Open Loop System; Elliptical Airframe

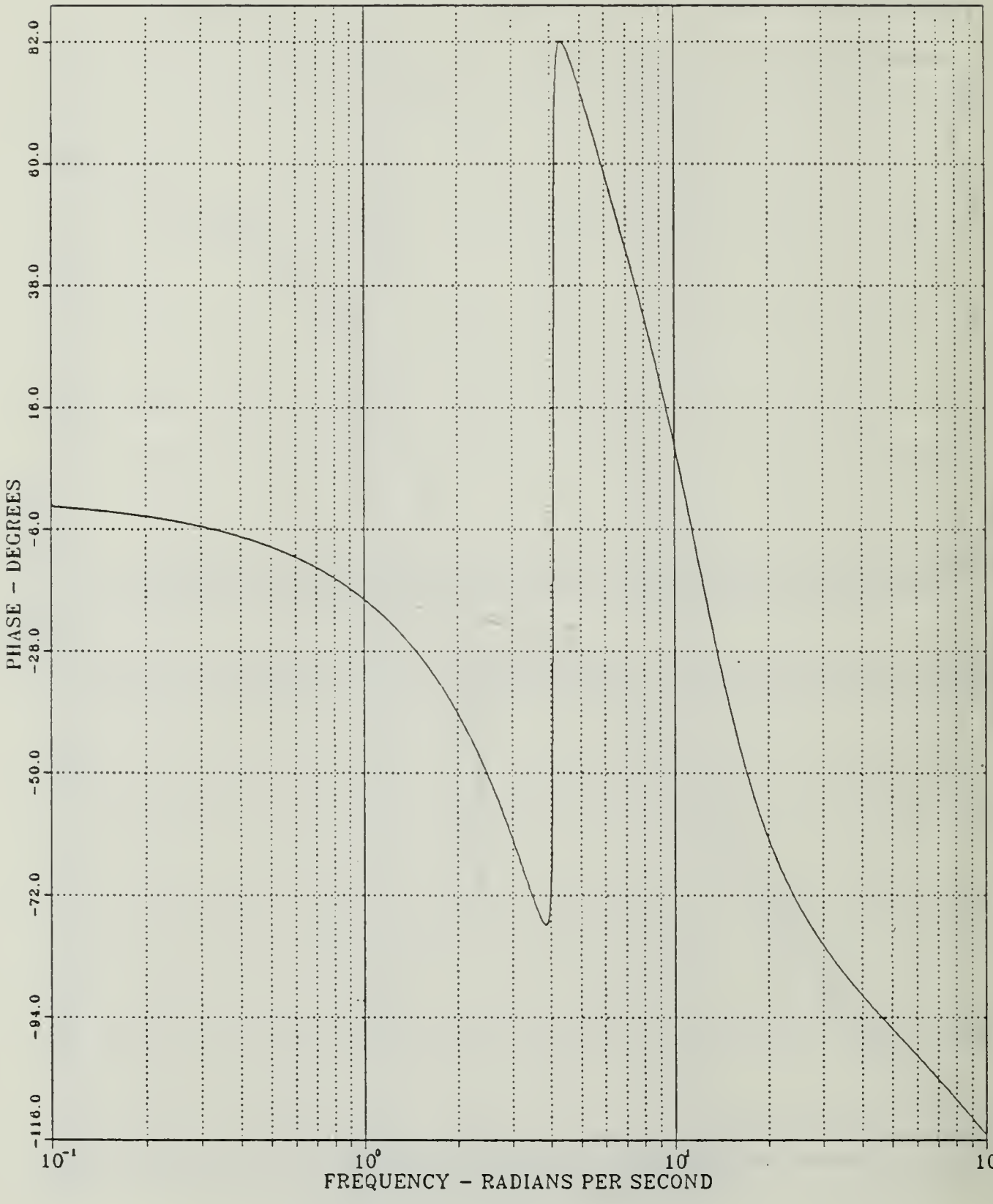

Figure 2.16 Yaw Tail Incidence-Phase vs Frequency; Uncoupled Yaw Channel Autopilot; Classical Design; Continuous Open Loop System; Elliptical Airframe

TABLE II

PHASE CROSSOVER FREQUENCIES AND GAIN MARGINS;
UNCOUPLED YAW CHANNEL AUTOPILOT; CLASSICAL DESIGN;
CONTINUOUS OPEN LOOP SYSTEM; ELLIPTICAL AIRFRAME

	PHASE CROSSOVER FREQUENCY (rad/sec)	GAIN MARGIN (db)
YAW NORMAL ACCELERATION (n_y)	4.2585	37.9099
YAW ANGULAR RATE (r)	10.9162	58.3093
YAW TAIL INCIDENCE (δ_y)	---	---

D. UNCOUPLED ROLL CHANNEL AUTOPILOT FOR CIRCULAR AIRFRAME

The uncoupled roll channel autopilot of a CBTT missile is commanded to roll the missile so as to put the preferred maneuver direction in the direction of the guidance acceleration command. The desired maneuver plane acceleration should be attained as rapidly as the achieved body-fixed pitch acceleration. To accomplish this, the uncoupled roll channel autopilot (i.e., yaw and roll dynamic effects neglected) was designed to have the roll angle time constant equal to the time constant of the normal acceleration achieved by the uncoupled pitch channel autopilot.

A block diagram of the uncoupled roll channel is shown in Figure 2.21. In this diagram both the aerodynamic model and roll control law are involved. The roll control law shown in Figure 2.22 is commanded by roll angle (ϕ_c) and governed by roll angular rate (p) and roll angle (ϕ).

The design and analysis of the uncoupled roll channel autopilot was performed in this section for the stable at zero angle-of-attack circular airframe.

1. Transfer Functions of Aerodynamic Model

The aerodynamic transfer functions of the uncoupled roll channel autopilot obtained from Figure 2.21 are:

a. Transfer Function of Roll Angular Rate:

$$\frac{p}{\delta} = \frac{1}{s} \frac{\bar{q} S d C_{l_{\delta_R}}}{I_{xx}} \delta_R \qquad \text{(II.D.1-1)}$$

TABLE III

PLANT SYSTEM AND INPUT MATRICES; UNCOUPLED YAW CHANNEL AUTOPILOT; CLASSICAL DESIGN; DISCRETE OPEN LOOP SYSTEM; ELLIPTICAL AIRFRAME

A MATRIX 7 ROWS 7 COLUMNS

9.9222048E-01	1.1817730E-02	-2.2307407E-03	-7.6497995E-06	-3.8539979E-03	-2.1943946E-01	-1.3136532E-01
-2.0944947E-01	9.9819665E-01	1.4841173E-04	4.1072105E-07	2.5807553E-04	1.9916791E-02	2.0592592E-02
-1.3299296E-04	-1.3710760E-05	9.9864352E-01	1.2491035E-02	-7.9235026E-05	-6.1222571E-03	-5.3391318E-03
-1.3394357E-02	-3.4729279E-03	-2.2038513E-01	9.9811127E-01	-1.9875062E-02	-1.1264116E+00	-6.7729365E-01
1.4044501E-03	1.4612172E-04	4.1401539E-02	2.5954090E-04	9.5206553E-01	4.7091900E-02	2.7828361E-02
7.1994662E-02	7.7378807E-03	2.5347639E-02	1.5961454E-04	4.2580546E-02	8.9072129E-01	-6.9480232E-02
4.5062902E-02	4.7653181E-03	1.5697141E-02	7.6314008E-05	2.5741467E-02	9.4732584E-01	4.3394452E-02

B MATRIX 7 ROWS 1 COLUMNS

2.2310311E-03
-1.4842727E-04
4.5569141E-05
1.1505695E-02
-4.1419659E-02
-2.5358789E-02
-1.5701517E-02

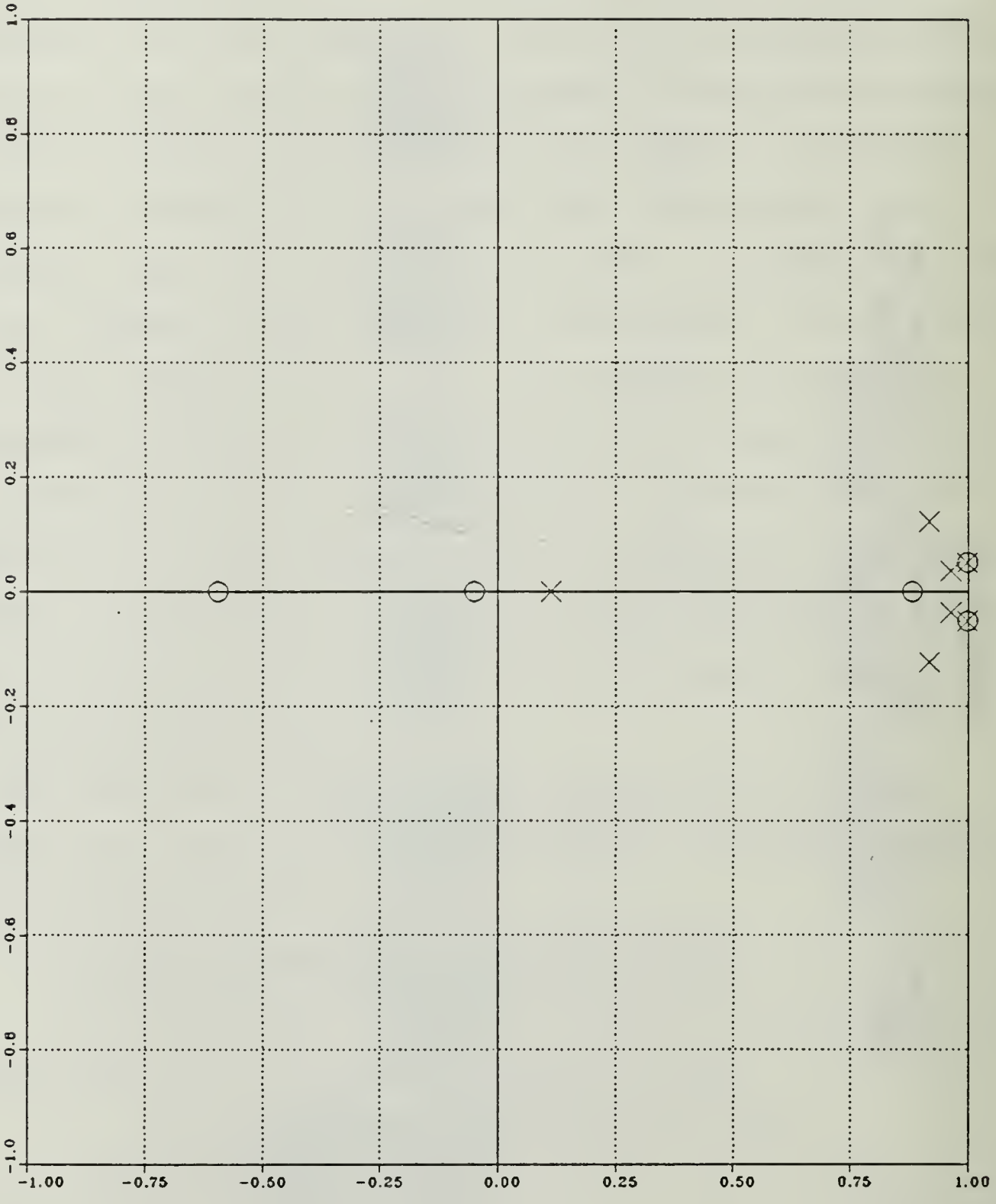

Figure 2.17 Pole-Zero Plot; Uncoupled Yaw Channel Autopilot; Classical Design; Discrete Open Loop System; Elliptical Airframe

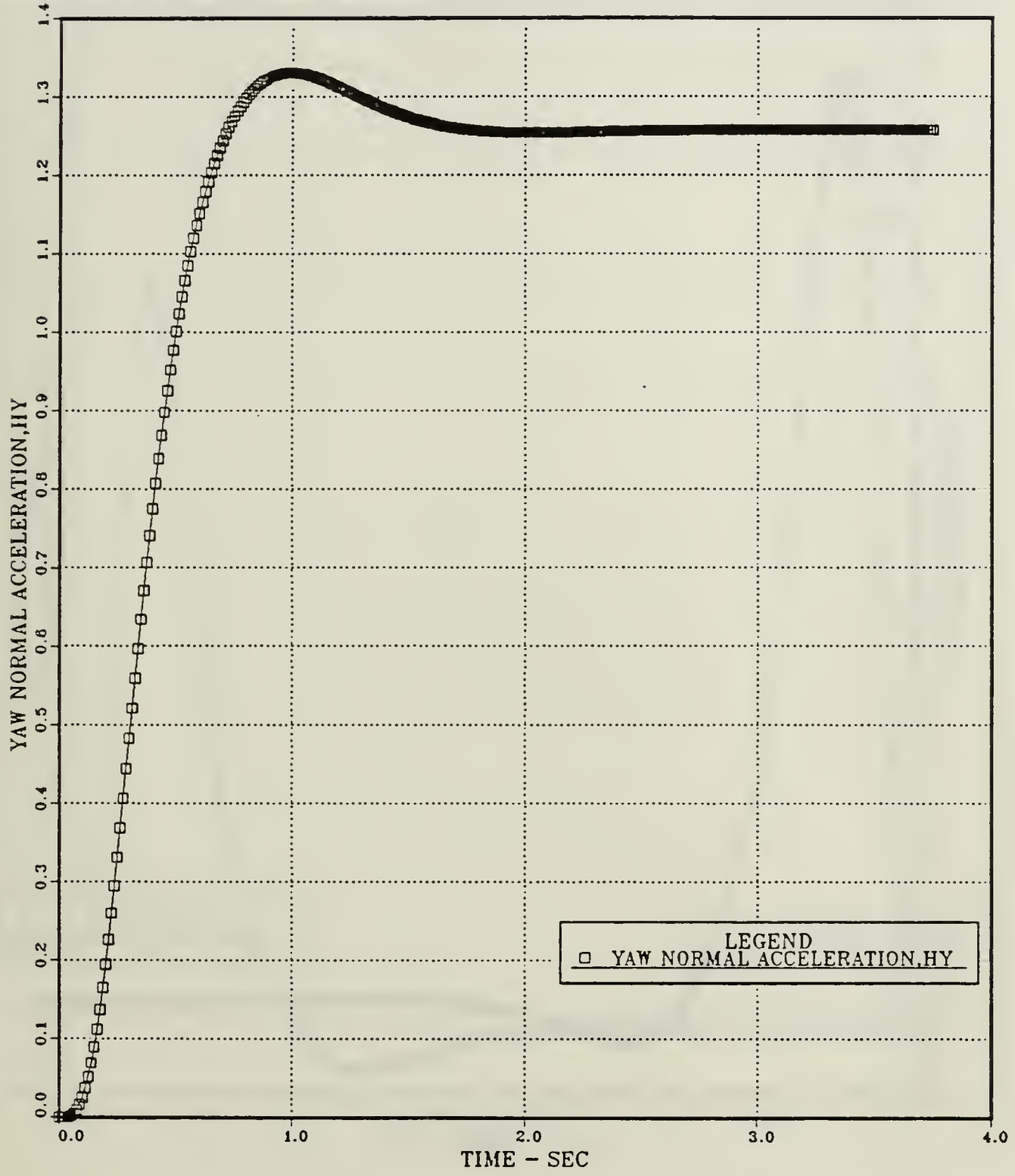

Figure 2.18 Yaw Normal Acceleration vs Time; Uncoupled Yaw Channel Autopilot; Classical Design; Discrete Open Loop System; Elliptical Airframe

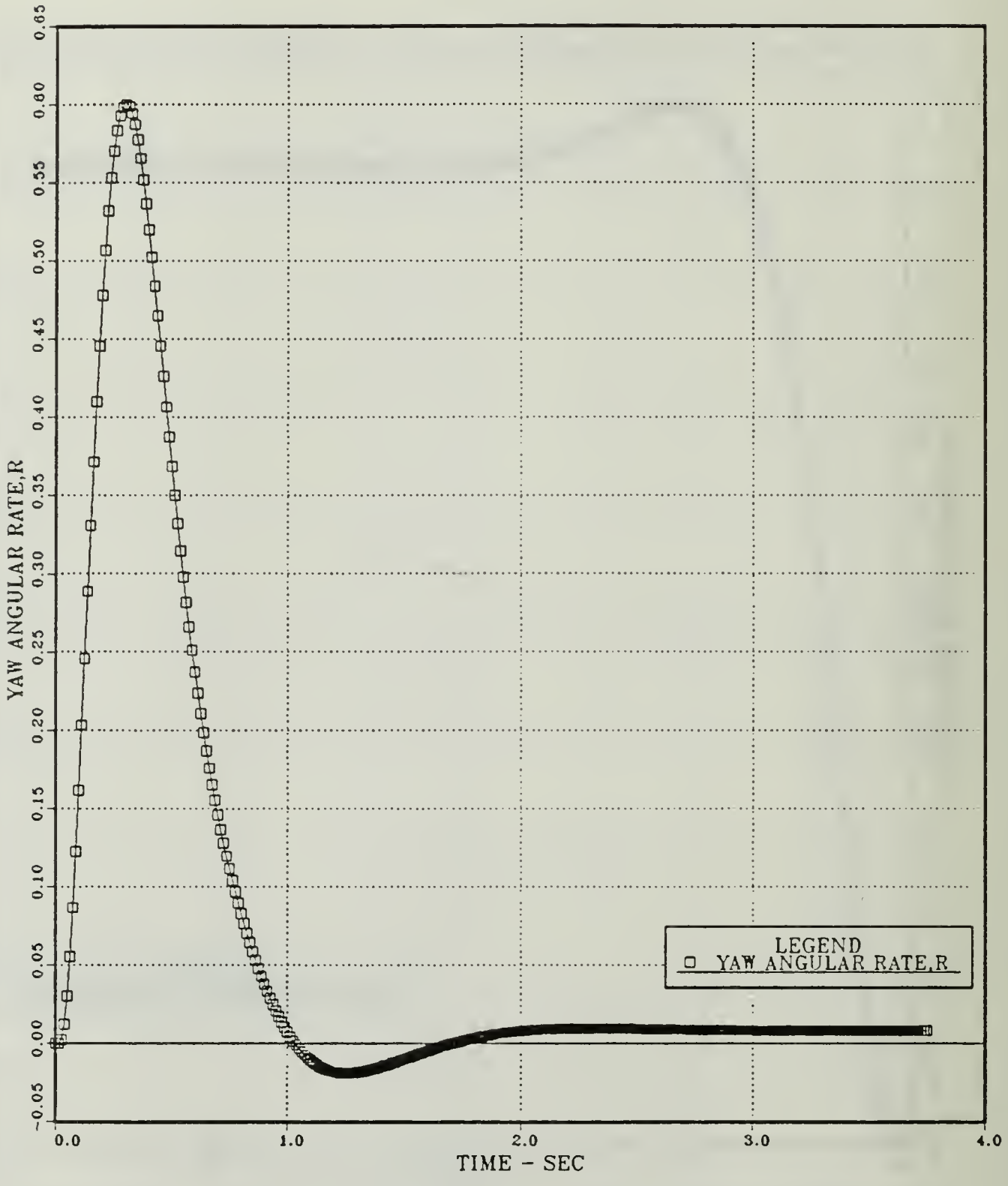

Figure 2.19 Yaw Angular Rate vs Time; Uncoupled Yaw Channel Autopilot; Classical Design; Discrete Open Loop System; Elliptical Airframe

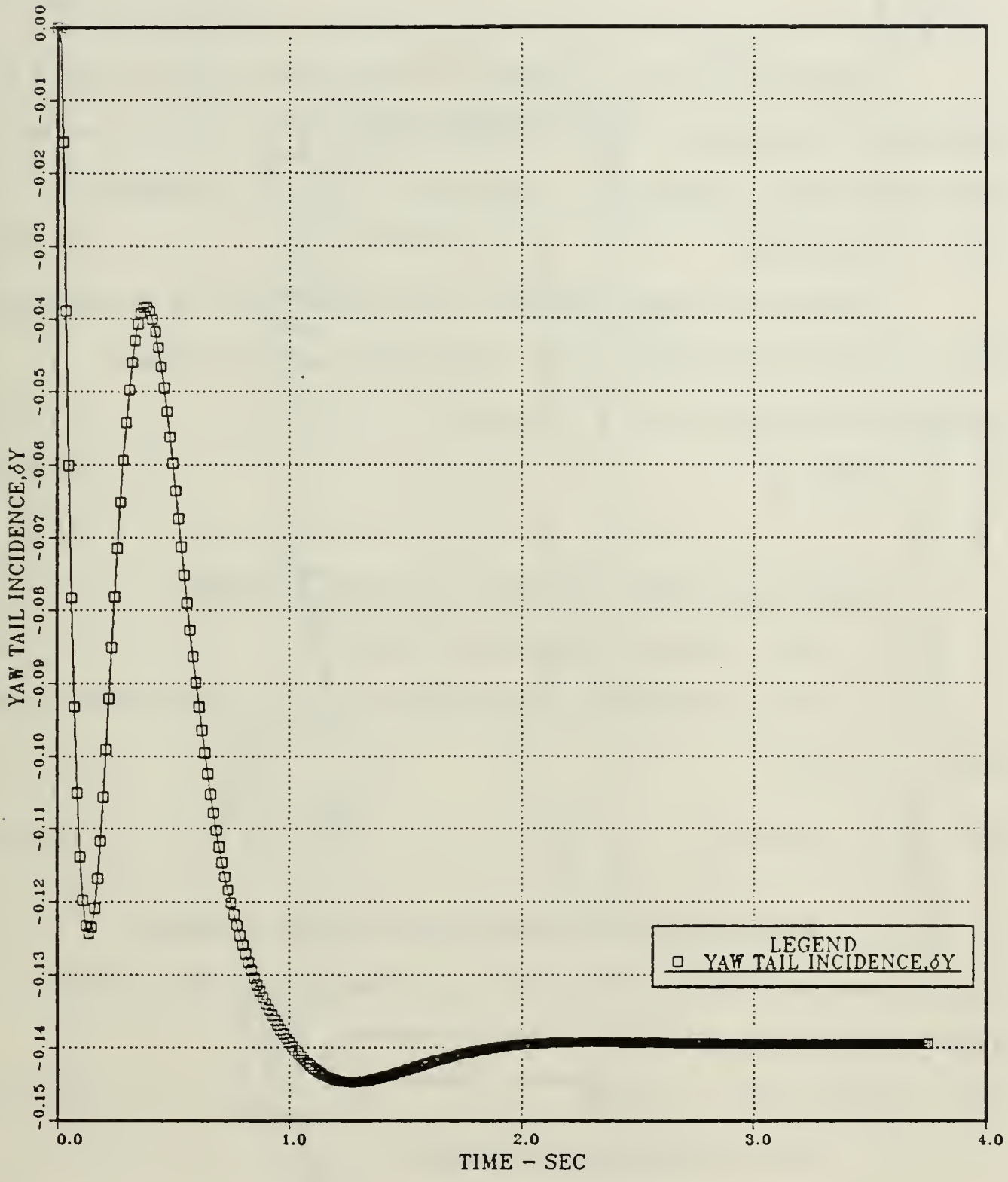

Figure 2.20 Yaw Tail Incidence vs Time; Uncoupled Yaw Channel Autopilot; Classical Design; Discrete Open Loop System; Elliptical Airframe

b. Transfer Function of Roll Angle:

$$\phi = \frac{1}{s} p \qquad \text{(II.D.1-2)}$$

Substituting the values of aerodynamic data (Table VII), linearized aerodynamic derivatives (Table VIII) and geometric and mass properties (Table IX), equation (II.D.1-1) becomes

$$ps = 8.03462\ \bar{\delta}_R \qquad \text{(II.D.1-3)}$$

Applying inverse Laplace transformation to equations (II.D.1-2) and (II.D.1-3), the following set of linear differential equations is obtained:

$$\dot{p} = 8.03462\ \bar{\delta}_R \qquad \text{(II.D.1-4)}$$

$$\dot{\phi} = p \qquad \text{(II.D.1-5)}$$

2. Equations of Roll Control Law and Actuator

a. Roll Angle Compensator Equation

The roll angle compensator equation obtained from Figure 2.22 is:

$$X = \frac{2.2}{\frac{s}{8}+1}(\Phi_c - \Phi) \qquad \text{(II.D.2-1)}$$

Rearranging and applying inverse Laplace transformation (II.D.2-1) turns into the following linear differential equation:

$$\dot{X} = -17.6\Phi - 8X + 17.6\Phi_c \qquad \text{(II.D.2-2)}$$

b. Rate Compensator Equation

The rate compensator equation also obtained from Figure 2.22 is:

$$Y = \frac{0.1506\left(\frac{s}{15}+1\right)}{\left(\frac{s}{5}+1\right)}(X - P) \qquad \text{(II.D.2-3)}$$

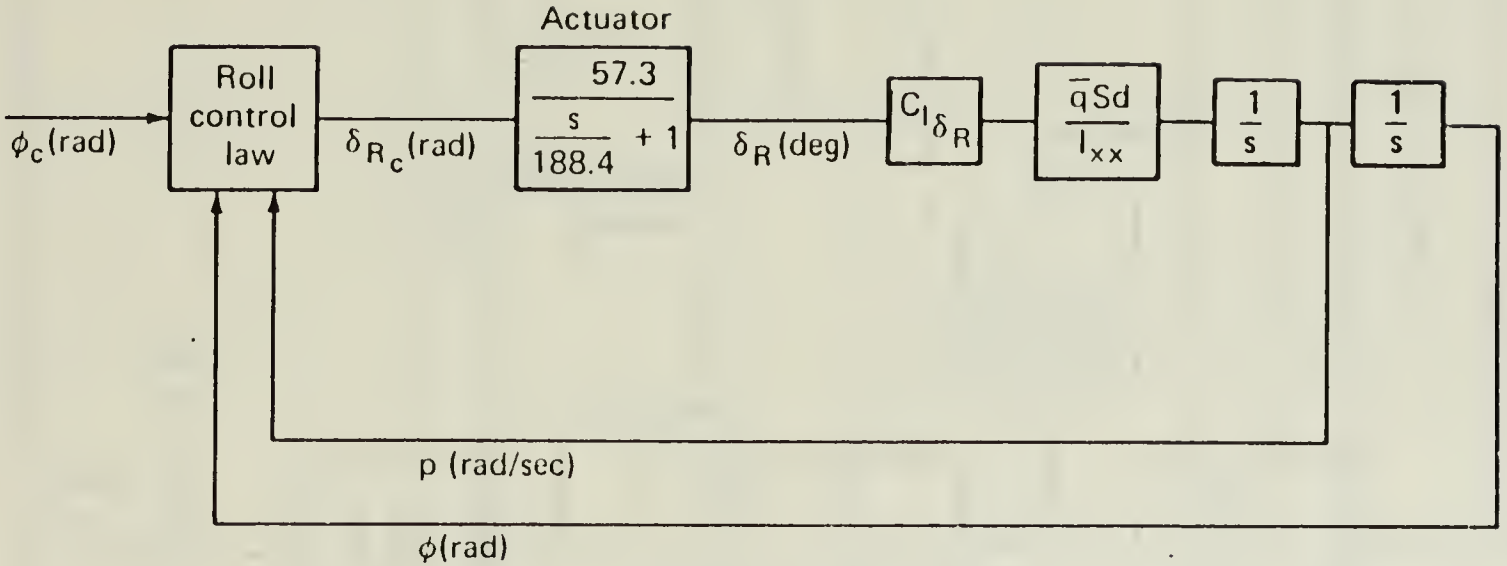

Figure 2.21 Uncoupled Roll Channel

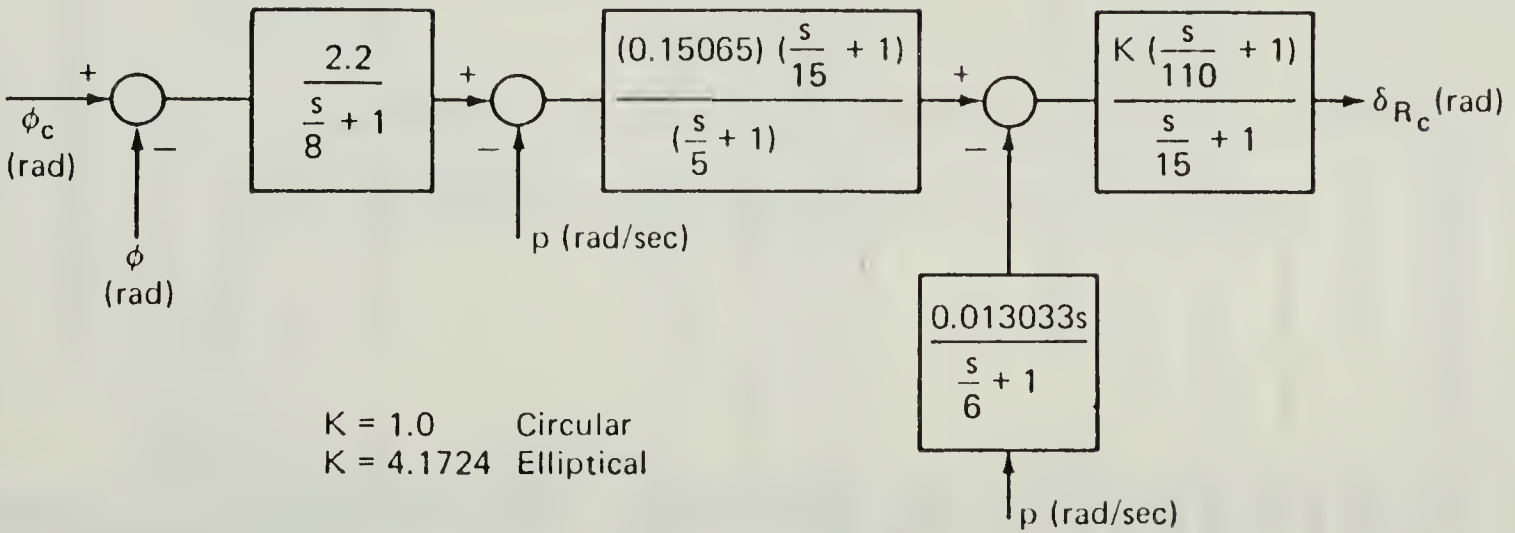

Figure 2.22 Roll Control Law

Rearranging and applying inverse Laplace transformation to (II.D.2-3), it turns into:

$$\dot{Y} + 5Y = 0.0502\dot{X} - 0.0502\dot{p} + 0.75325X - 0.75325p \qquad \text{(II.D.2-4)}$$

Substituting equations (II.D.1-4) and (II.D.2-2) into (II.D.2-4), the last becomes:

$$\dot{Y} = -0.7532p - 0.88352\phi + 0.35165X - 5Y - 0.40334\delta_R + 0.88352\phi_c \qquad \text{(II.D.2-5)}$$

c. Pseudo-Differential Equation

The pseudo-differential equation obtained from Figure 2.22 is:

$$X_1 = \frac{0.013033\,s}{\frac{s}{6}+1}\,p \qquad \text{(II.D.2-6)}$$

Rearranging and applying inverse Laplace transformation to (II.D.2-6), it turns into:

$$\dot{X}_1 = -6X_1 + 0.078198\dot{p} \qquad \text{(II.D.2-7)}$$

Substituting equation (II.D.1-4) into (II.D.2-7), the last becomes:

$$\dot{X}_1 = -6X_1 + 0.628291\,\delta_R \qquad \text{(II.D.2-8)}$$

d. Equation of Actuator Compensator

The equation of actuator compensator obtained from Figure 2.22 is:

$$\delta_{R_c} = \frac{\frac{s}{110}+1}{\frac{s}{15}+1}\,(Y - X_1) \qquad \text{(II.D.2-9)}$$

Rearranging and applying inverse Laplace transformation to (II.D.2-9), it turns into:

$$\dot{\delta}_{R_c} = -15\,\delta_{R_c} + 0.13636\dot{Y} - 0.13636\dot{X}_1 + 15Y - 15X_1 \qquad \text{(II.D.2-10)}$$

Substituting equations (II.D.2-5) and (II.D.2-8) into (II.D.2-10), the last becomes:

$$\dot{\delta}_{R_c} = -0.10271p - 0.2045\phi + 0.04795X + 14.3182Y - 14.1814X_1 - 15\delta_{R_c} - 0.1466\delta_R + 0.2045\phi$$

(III.D.2-11)

e. Actuator Equation

The actuator equation obtained from Figure 2.21 is:

$$\delta_R = \frac{57.3}{\frac{1}{188.4}s+1}\,\delta_{R_c} \qquad \text{(II.D.2-12)}$$

Rearranging and applying inverse Laplace transformation, the last equation turns into:

$$\dot{\delta}_R = 10795.32\delta_{R_c} - 188.4\,\delta_R \qquad \text{(II.D.2-13)}$$

3. Design Approach and Analysis of Continuous System

Utilizing state-space representation, the equations (II.D.1-4), (II.D.1-5), (II.D.2-2), (II.D.2-5), (II.D.2-8), (II.D.2-11), and (II.D.2-13) can be modeled in a seventh-order system of the form $\underline{\dot{x}}=\underline{F}\underline{x}+\underline{G}\underline{u}$. The continuous plant system and input matrices $\underline{F}$ and $\underline{G}$ are shown in Table IV, and the state vector is:

$$X(K) = \begin{bmatrix} p \\ \phi \\ X \\ Y \\ X_1 \\ \delta_{R_c} \\ \delta_R \end{bmatrix} \qquad \text{(II.D.3-1)}$$

where the state variables are:

p : roll angular rate

$\dot{\phi}$: roll angle

X : output of roll angle compensator

Y : output or rate compensator

X : output of pseudo-differentiator

δ_{R_c} : input command in the actuator

δ_R : roll tail incidence

Executing the OPTSYS program, using an input step function which represents "1 gee command" at zero trim angle-of-attack, the pole-zero and time and frequency response plots are obtained.

The pole-zero plot of Figure 2.23 indicates that the continuous open loop system is stable, since the s-plane poles are:

s_1 = -174.785 (roll angular rate) (II.D.3-2)

s_2 = -9.25097+j28.4098 (roll angle) (II.D.3-3)

s_3 = -9.25097-j28.4098 (output of roll angle compensator) (II.D.3-4)

s_4 = -2.46608+j2.71152 (output of rate compensator network) (II.D.3-5)

s_5 = -2.46608-j2.71152 (output of pseudo-differentiator) (II.D.3-6)

s_6 = -8.98209 (input command in the actuator) (II.D.3-7)

s_7 = -5.19932 (roll tail incidence) (II.D.3-8)

The time response plots of the roll angle, angular rate and tail incidence are shown in Figure 2.24 through 2.26. In

TABLE IV

PLANT SYSTEM AND INPUT MATRICES; UNCOUPLED ROLL CHANNEL AUTOPILOT; CLASSICAL DESIGN; CONTINUOUS OPEN LOOP SYSTEM; CIRCULAR AIRFRAME

F MATRIX 7 ROWS 7 COLUMNS

0.0000000E+00	0.0000000E+00	0.0000000E+00	0.0000000E+00	0.0000000E+00	0.0000000E+00	8.0346200E+00
1.0000000E+00	0.0000000E+00	0.0000000E+00	0.0000000E+00	0.0000000E+00	0.0000000E+00	0.0000000E+00
0.0000000E+00	-1.7600000E+01	-8.0000000E+00	0.0000000E+00	0.0000000E+00	0.0000000E+00	0.0000000E+00
-7.5325000E-01	-8.8352000E-01	3.5165000E-01	-5.0000000E+00	0.0000000E+00	0.0000000E+00	-4.0334000E-01
0.0000000E+00	0.0000000E+00	0.0000000E+00	0.0000000E+00	-6.0000000E+00	0.0000000E+00	6.8291000E-01
-1.0271000E-01	-1.2048000E-01	4.7950000E-02	1.4318200E+01	-1.4181840E+01	-1.5000000E+01	-1.4067000E-01
0.0000000E+00	0.0000000E+00	0.0000000E+00	0.0000000E+00	0.0000000E+00	1.0795320E+04	-1.4840000E+02

G MATRIX 7 ROWS 1 COLUMNS

0.0000000E+00
0.0000000E+00
1.7600000E+01
8.8352000E-01
0.0000000E+00
1.2048000E-01
0.0000000E+00

particular, the roll angle time response plot has a 0.55 seconds time constant, 3% overshoot and a steady-state equal to zero. These results are in accordance with the requirements referred in Appendix A, that is a time constant of 0.5 seconds, overshoot less than 10% and zero steady-state roll angle error. All the above three time response plots are identical with those presented in [Ref. 6].

Figures 2.27 through 2.32 show the frequency response plots of the roll angle, angular rate and tail incidence, from which the phase crossover frequencies and gain margins of Table V can be obtained. The positive gain and phase margins of the open loop system ensure the relative stability of the closed loop (controlled) system.

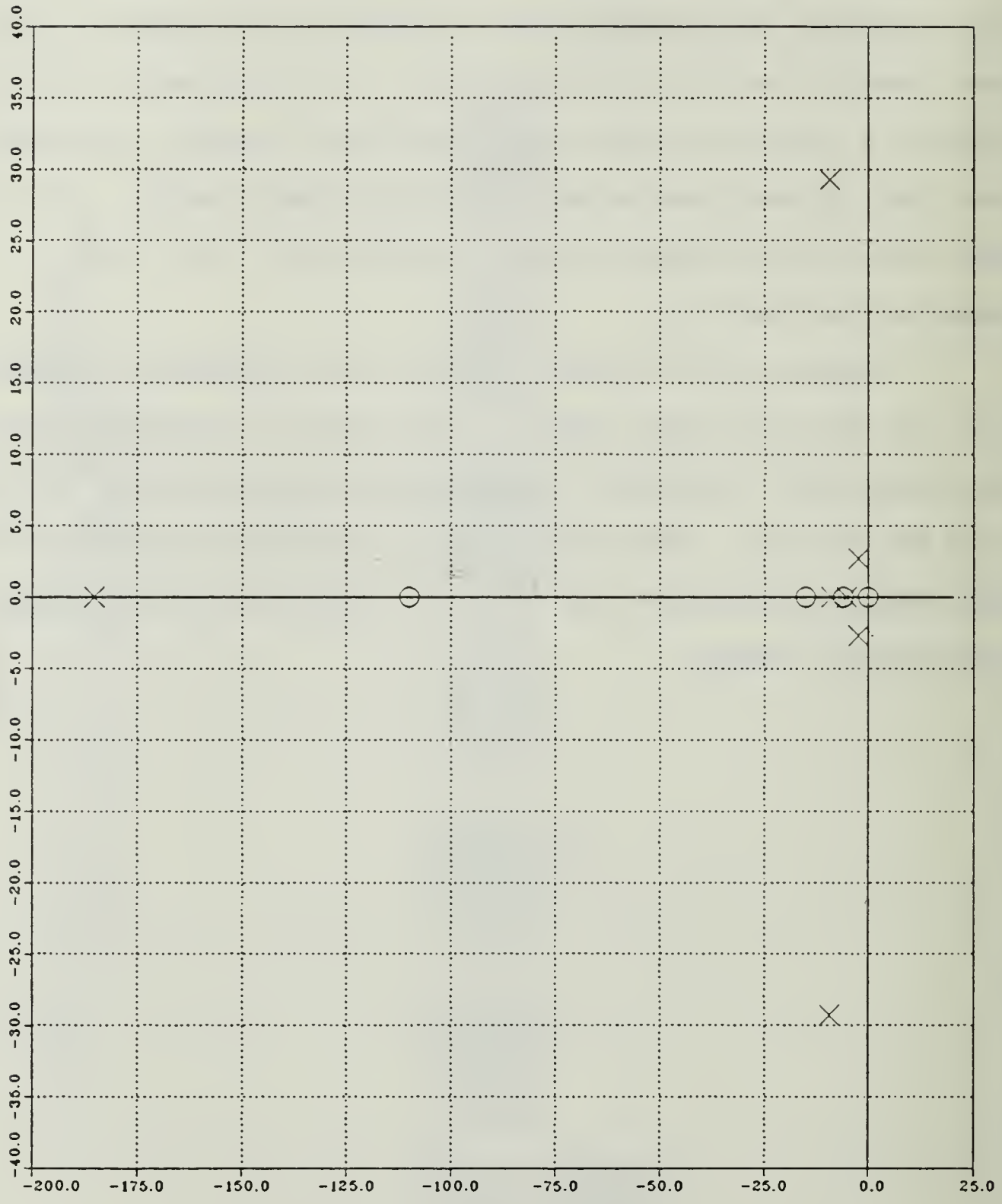

Figure 2.23 Pole-Zero Plot; Uncoupled Roll Channel Autopilot; Classical Design; Continuous Open Loop System; Circular Airframe

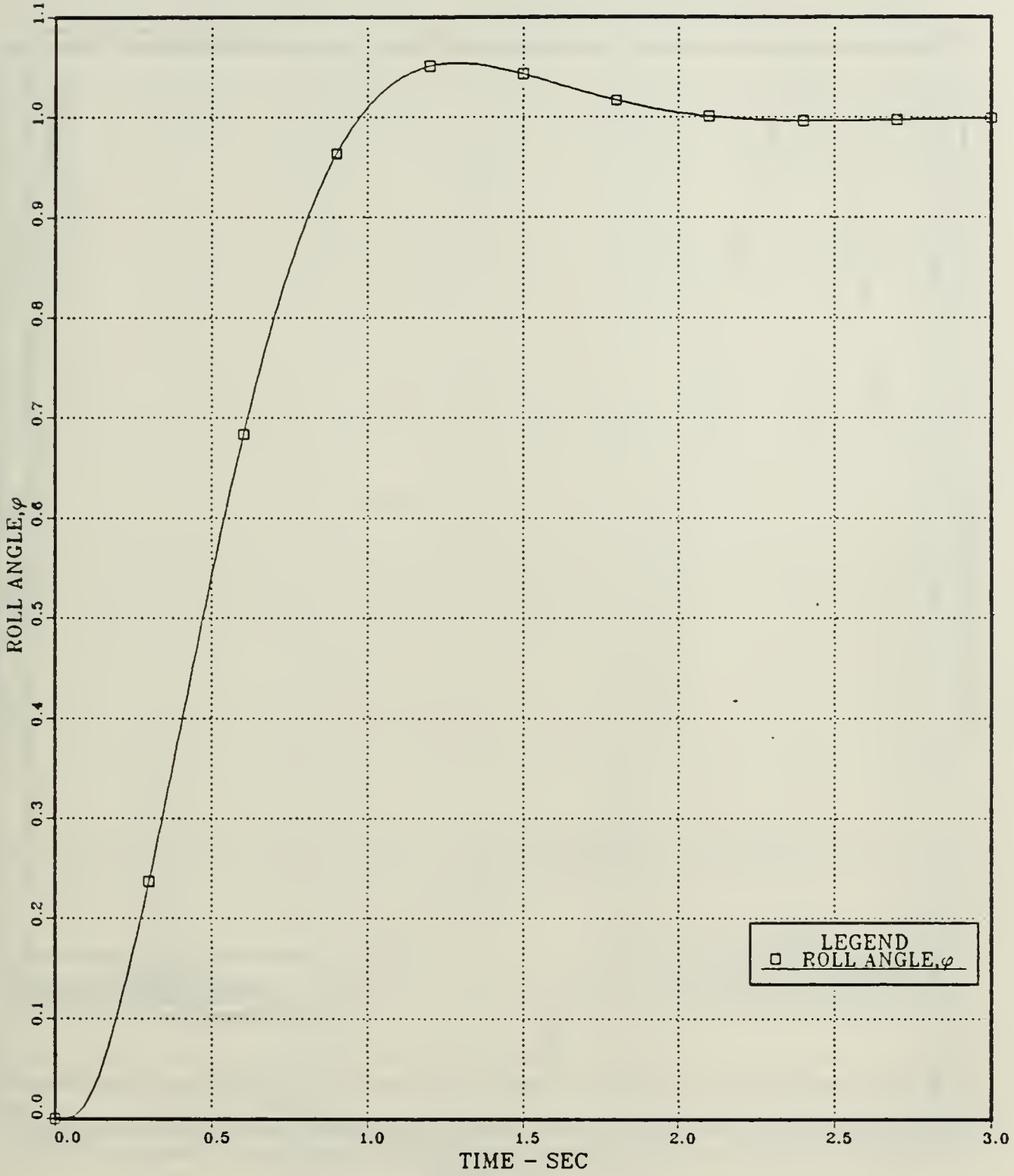

Figure 2.24 Roll Angle vs Time; Uncoupled Roll Channel Autopilot; Classical Design; Continuous Open Loop System; Circular Airframe

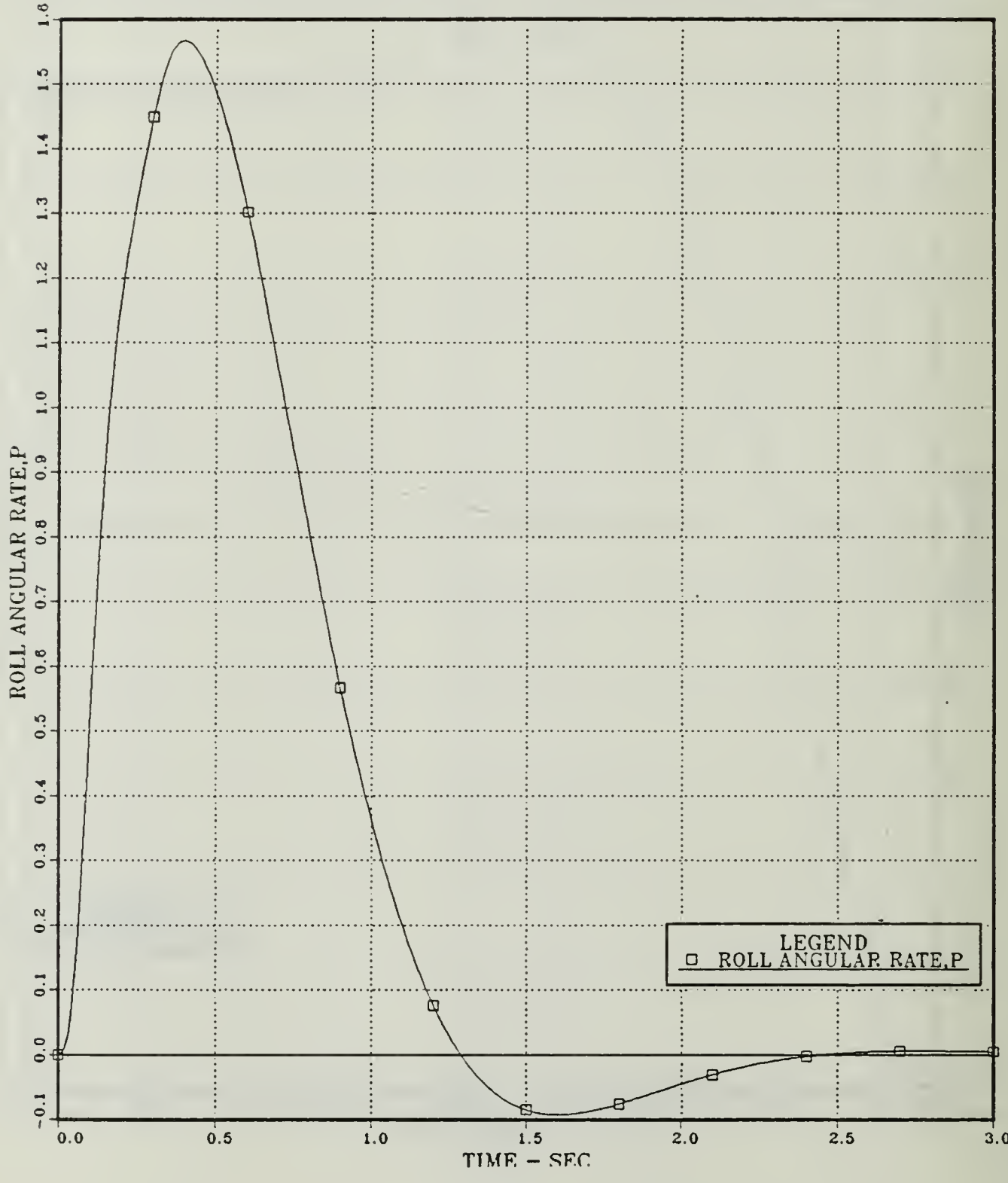

Figure 2.25 Roll Angular Rate vs Time; Uncoupled Roll Channel Autopilot; Classical Design; Continuous Open Loop System; Circular Airframe

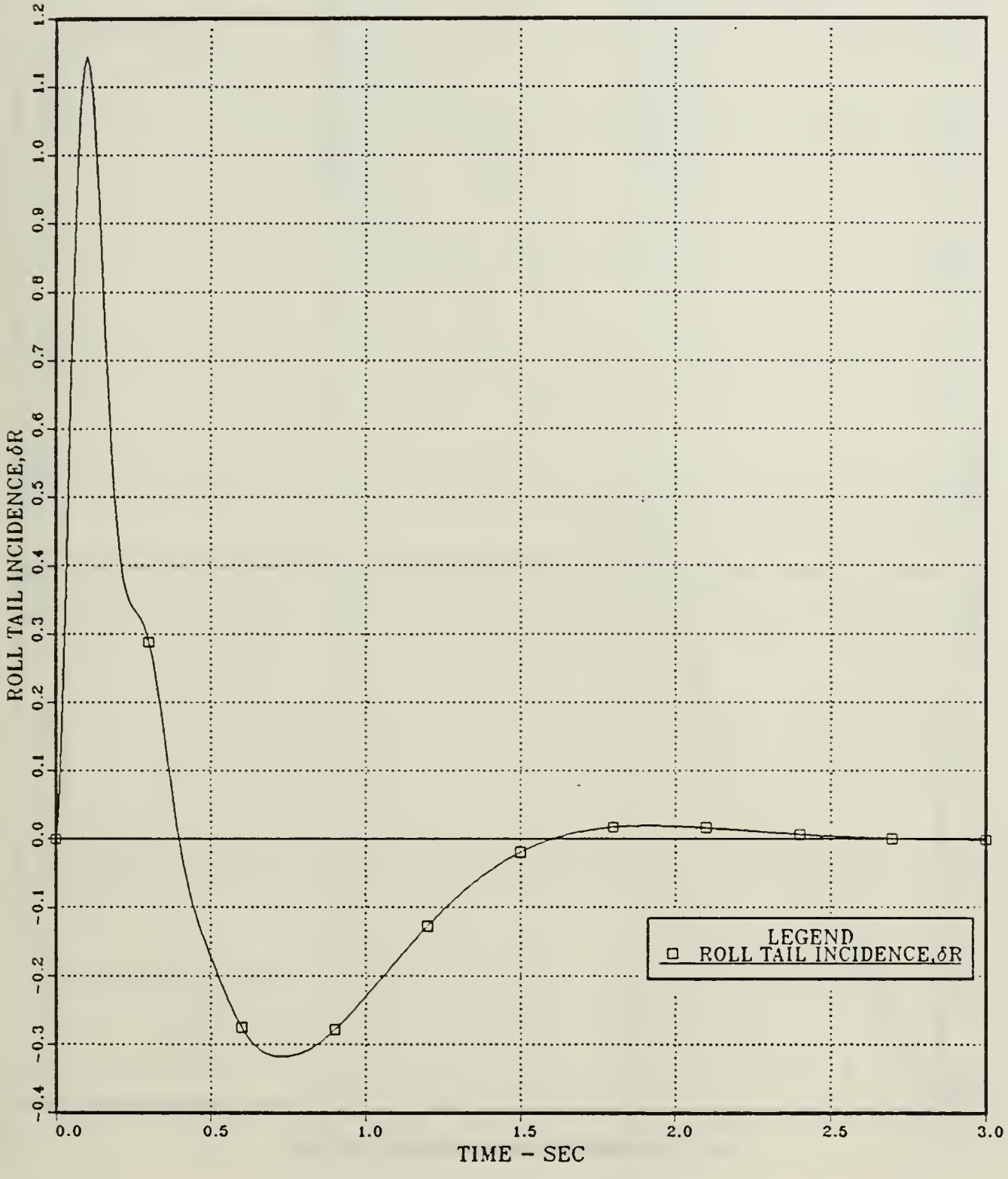

Figure 2.26 Roll Tail Incidence vs Time; Uncoupled Roll Channel Autopilot; Classical Design; Continuous Open Loop System; Circular Airframe

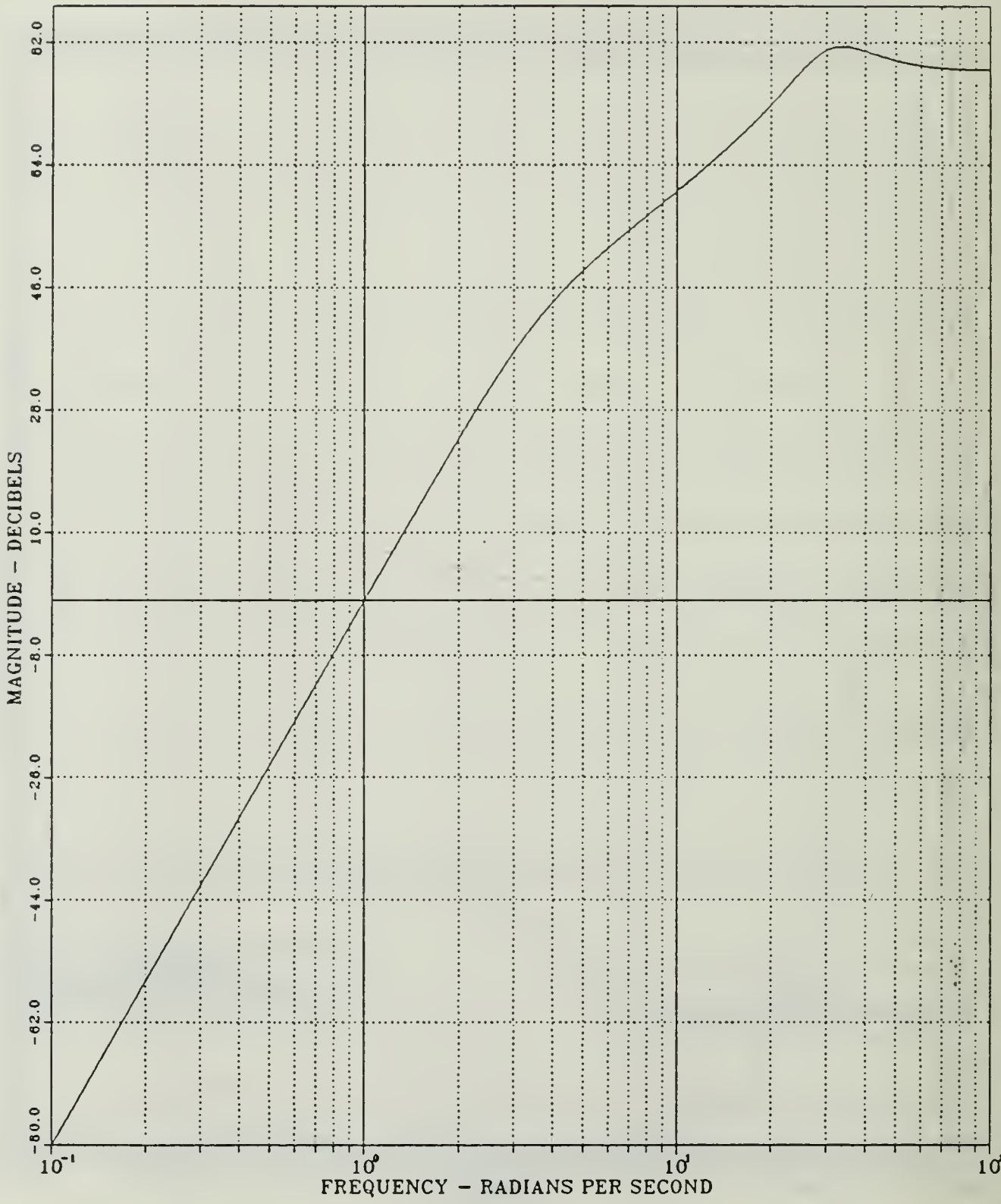

Figure 2.27 Roll Angle-Gain vs Frequency; Uncoupled Roll Channel Autopilot; Classical Design; Continuous Open Loop System; Circular Airframe

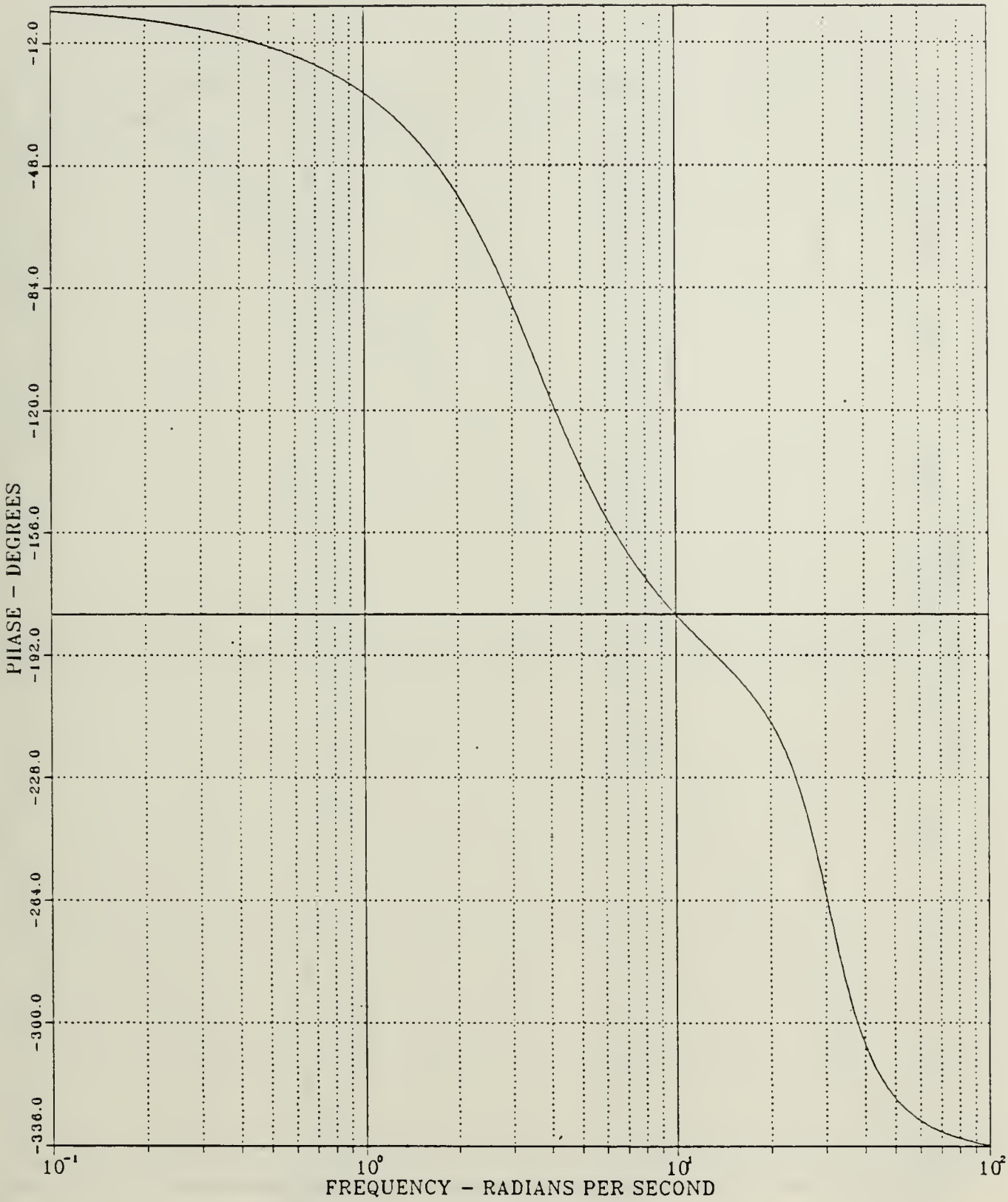

Figure 2.28 Roll Angle-Phase vs Frequency; Uncoupled Roll Channel Autopilot; Classical Design; Continuous Open Loop System; Circular Airframe

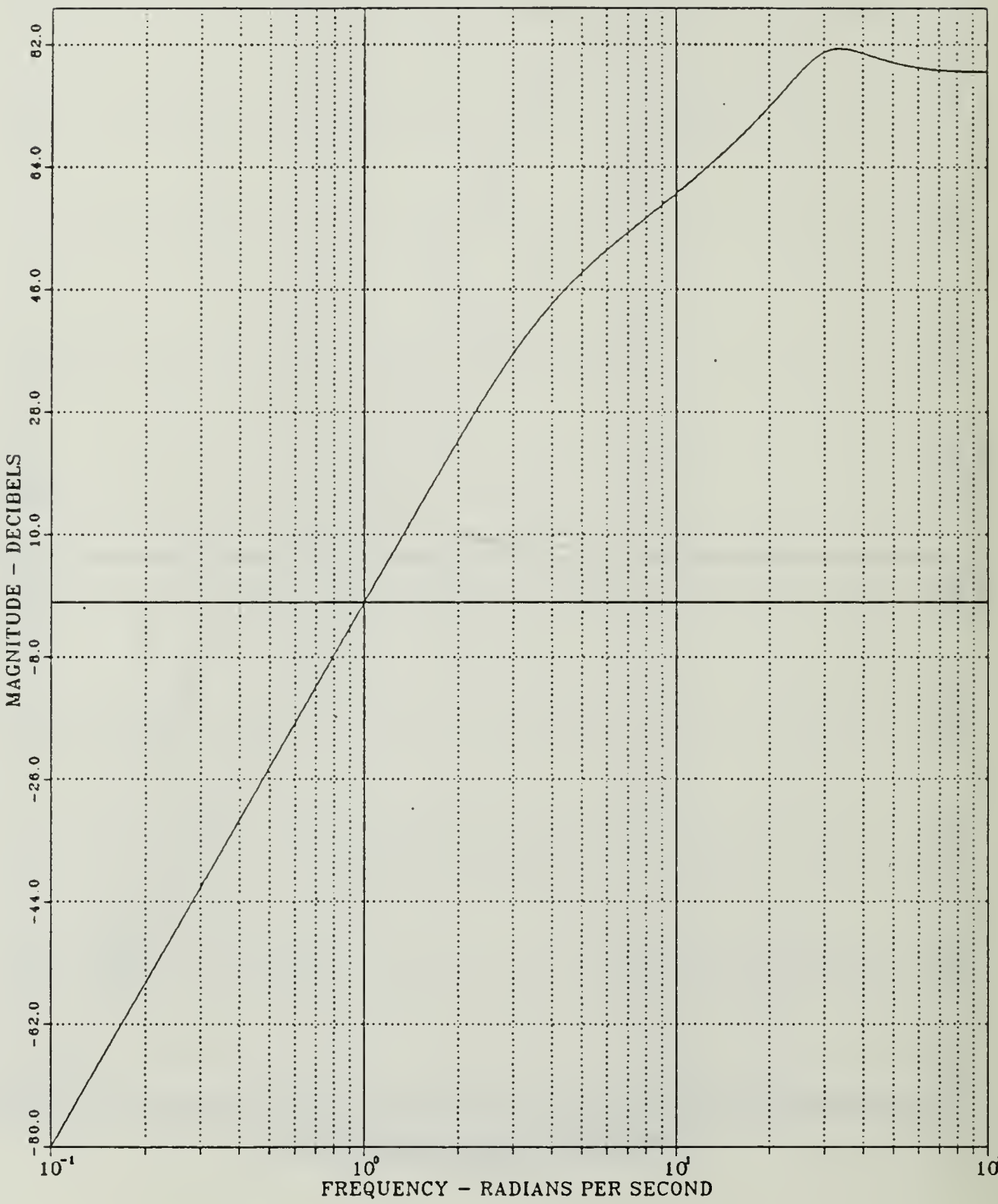

Figure 2.29 Roll Angular Rate-Gain vs Frequency; Uncoupled Roll Channel Autopilot; Classical Design; Continuous Open Loop System Circular Airframe

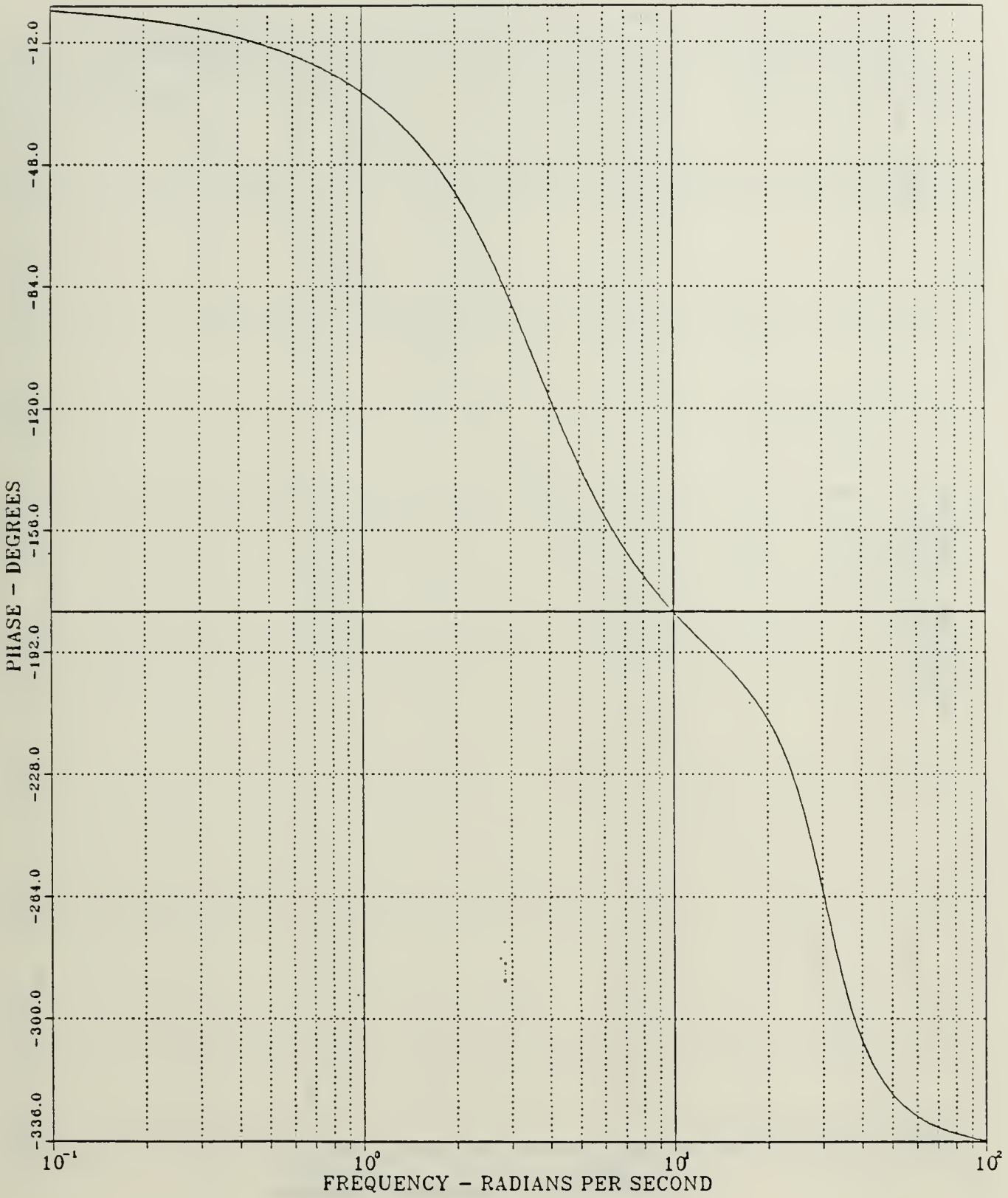

Figure 2.30 Roll Angular Rate-Phase vs Frequency; Uncoupled Roll Channel Autopilot; Classical Design; Continuous Open Loop System; Circular Airframe

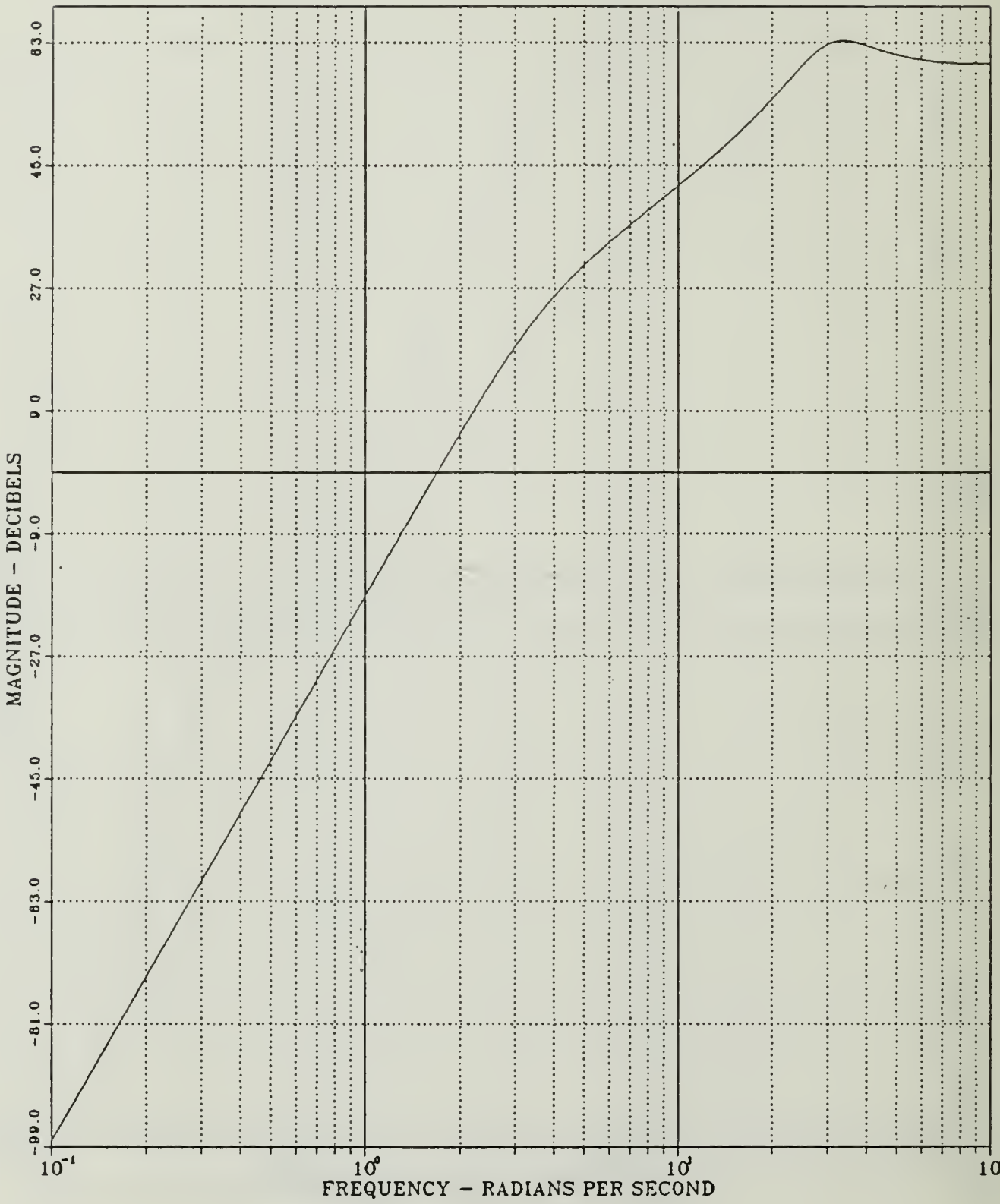

Figure 2.31 Roll Tail Incidence-Gain vs Frequency; Uncoupled Roll Channel Autopilot; Classical Design; Continuous Open Loop System; Circular Airframe

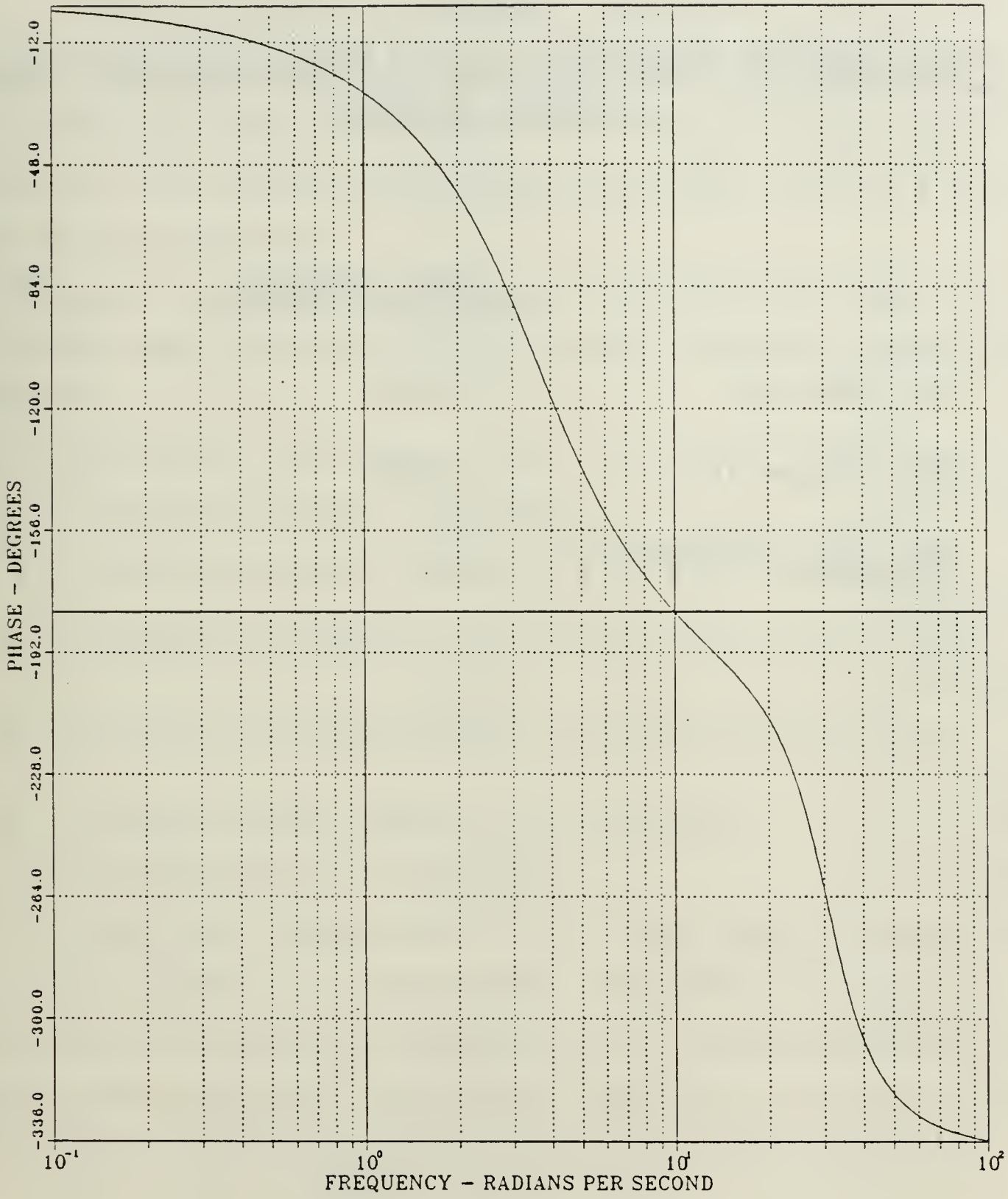

Figure 2.32 Roll Tail Incidence-Phase vs Frequency; Uncoupled Roll Channel Autopilot; Classical Design; Continuous Open Loop System; Circular Airframe

TABLE V

PHASE CROSSOVER FREQUENCIES AND GAIN MARGINS; UNCOUPLED ROLL CHANNEL AUTOPILOT; CLASSICAL DESIGN CONTINUOUS OPEN LOOP SYSTEM; CIRCULAR AIRFRAME

	PHASE CROSSOVER FREQUENCY (rad/sec)	GAIN MARGIN (db)
ROLL ANGLE (Φ)	10.0461	60.2165
ROLL ANGULAR RATE (p)	10.0461	60.2165
ROLL TAIL INCIDENCE (δ_R)	--	--

4. Design Approach and Analysis of Discrete System

Utilizing analog-to-digital conversion by the aid of ORACLS program and for a sample period of 0.0125 seconds, a seventh-order discrete system of the form $\underline{x}(K+1)=\underline{A}\underline{x}(k)+\underline{B}\underline{u}(k)$ is obtained. The discrete plant system and input matrices $\underline{A}$ and $\underline{B}$ are shown in Table VI.

The pole-zero plot of Figure 2.33 indicates that the discrete open loop system is also stable, since the z-plane poles are:

z_1 = 0.0992805 (roll angular rate) (II.D.4-1)

z_2 = 0.835216+j0.309736 (roll angle) (II.D.4-2)

z_3 = 0.835216-j0.309736 (output of roll angle compensator) (II.D.4-3)

z_4 = 0.969087+J0.0328588 (output of rate compensator network) (II.D.4-4)

z_5 = 0.969087-j0.0328588 (output of pseudo-differentiator) (II.D.4-5)

z_6 = 0.893797 (input command in the actuator) (II.D.4-6)

z_7 = 0.937075 (roll tail incidence) (II.D.4-7)

The time response plots of the roll angle, angular rate and tail incidence for the discrete uncoupled roll channel are presented in Figures 2.34 through 2.36. A close observation of these plots indicates that they are identical with those of the continuous classical system found in the previous section.

TABLE VI

PLANT SYSTEM AND INPUT MATRICES; UNCOUPLED ROLL CHANNEL AUTOPILOT; CLASSICAL DESIGN; DISCRETE OPEN LOOP SYSTEM; CIRCULAR AIRFRAME

A MATRIX 7 ROWS 7 COLUMNS

9.9773902E-01	-2.7010847E-03	1.0244796E-03	2.2682988E-01	-2.2389762E-01	3.2276943E+00	3.6703040E-02
1.2492613E-02	9.9999121E-01	3.3634249E-06	7.9208540E-04	-7.8245738E-04	1.6118668E-02	3.2138596E-04
-1.3299605E-03	-2.0935729E-01	9.0483727E-01	-3.6880414E-05	3.6449595E-05	-9.6590785E-04	-2.6905169E-05
-9.0777845E-03	-1.1024102E-02	3.9997348E-03	9.2763173E-01	1.1629342E-02	-1.7003703E-01	-2.0014363E-03
-1.8846421E-04	-2.2516572E-04	8.5385117E-05	1.8882113E-02	9.0910577E-01	2.6628472E-01	2.9604195E-03
-1.9074329E-03	-2.3073854E-03	8.4579262E-04	1.5273552E-01	-1.5030342E-01	7.4549779E-01	-1.1703192E-03
-6.2862481E-02	-7.5586771E-02	2.8170138E-02	5.6107793E+00	-5.5299587E+00	4.3288394E+01	5.0179261E-02

B MATRIX 7 ROWS 1 COLUMNS

2.7010847E-03
8.7921592E-06
2.0935729E-01
1.1024102E-02
2.2516572E-04
2.3073854E-03
7.5586771E-02

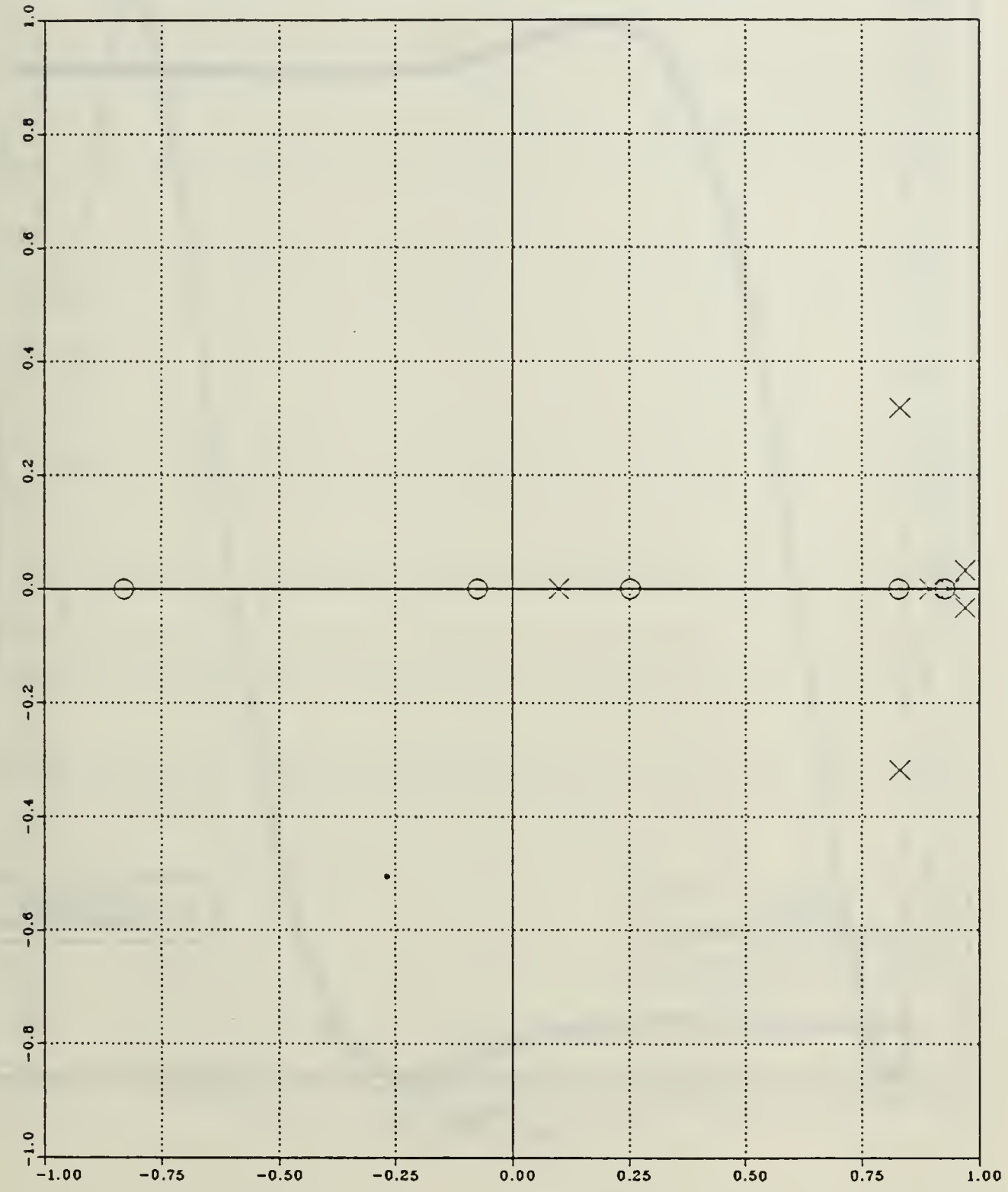

Figure 2.33 Pole-Zero Plot; Uncoupled Roll Channel; Classical Design; Discrete Open Loop System; Circular Airframe

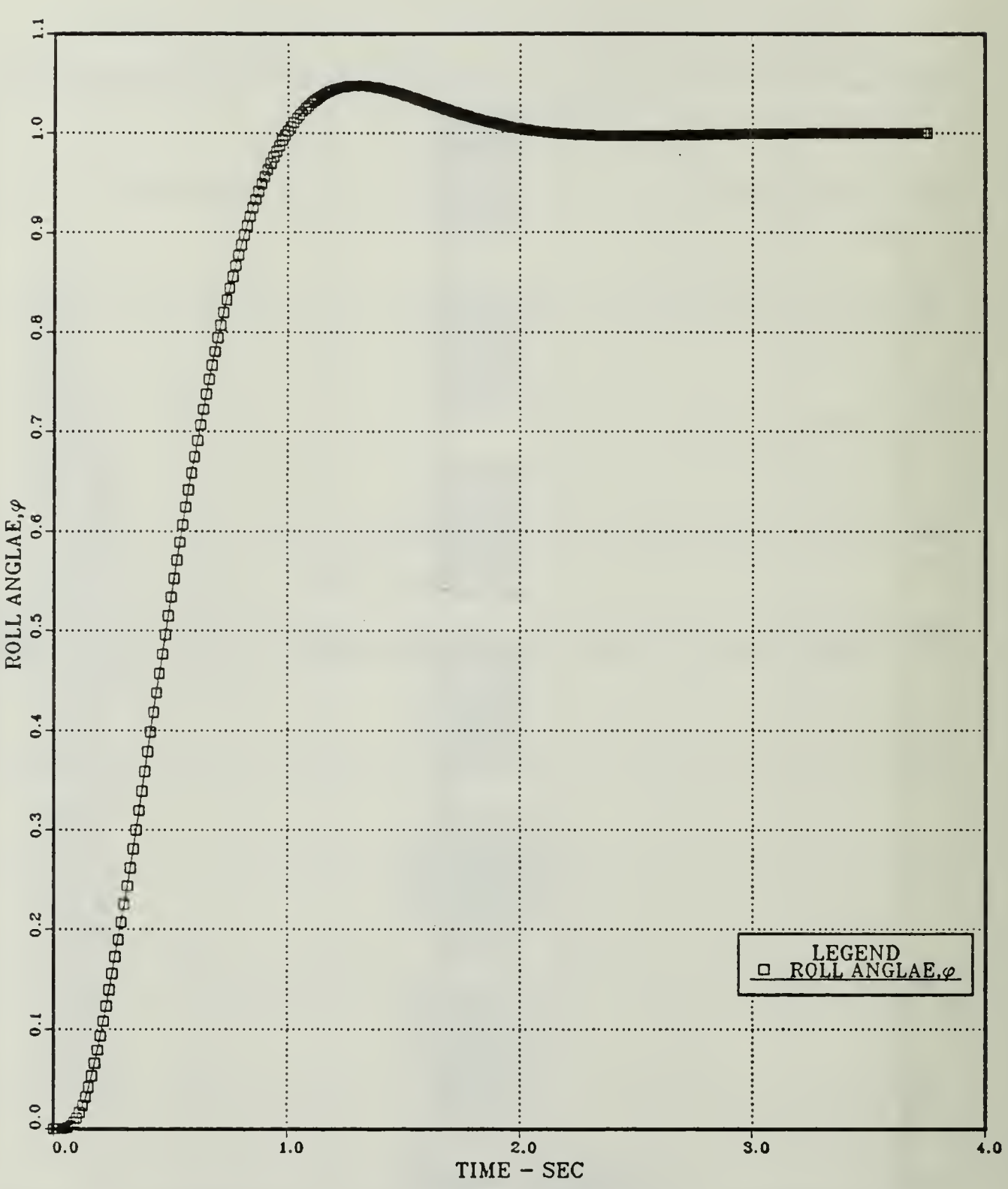

Figure 2.34 Roll Angle vs Time; Uncoupled Roll Channel Autopilot; Classical Design; Discrete Open Loop System;

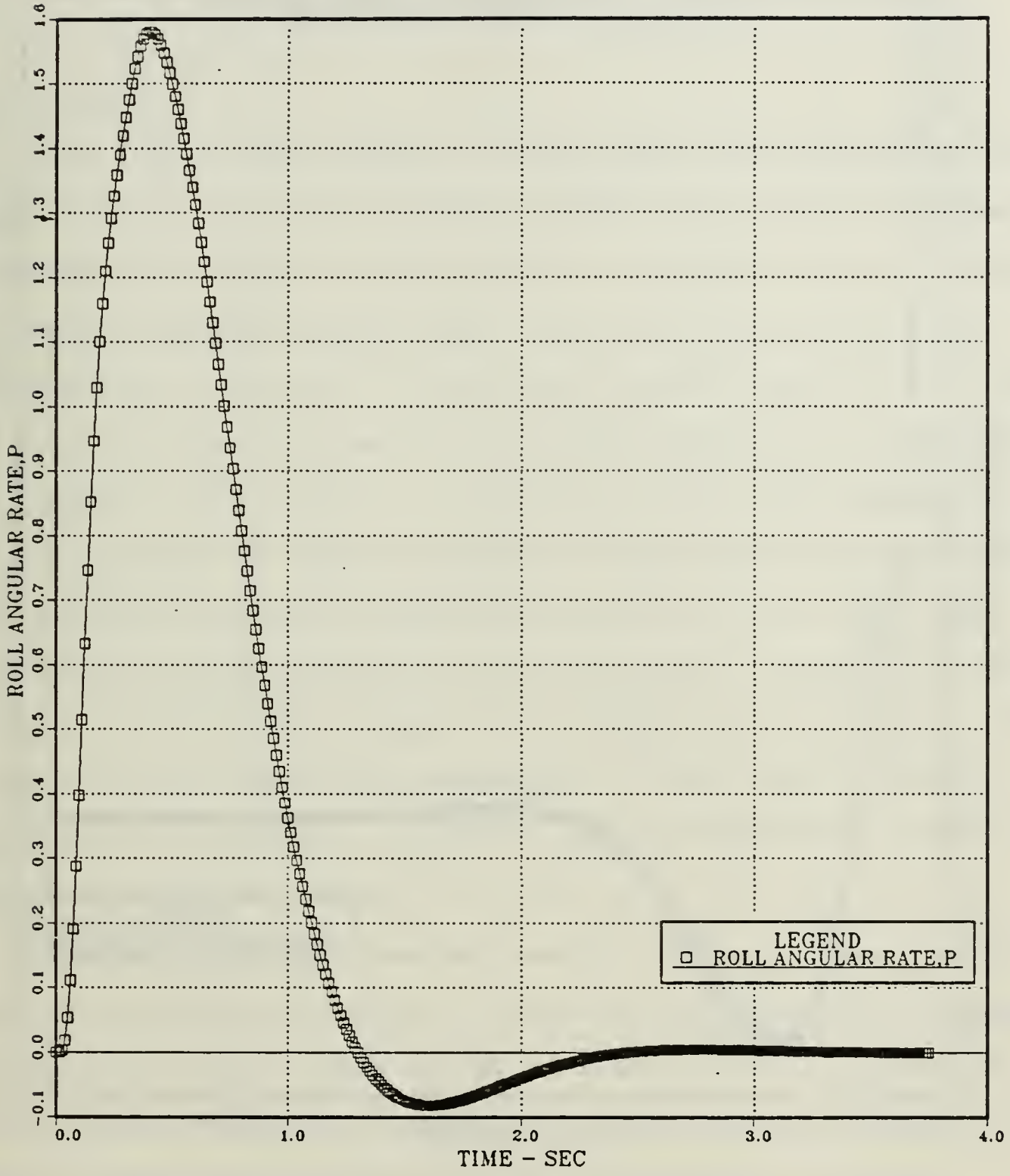

Figure 2.35 Roll Angular Rate vs Time; Uncoupled Roll Channel Autopilot; Classical Design; Discrete Open Loop System; Circular Airframe

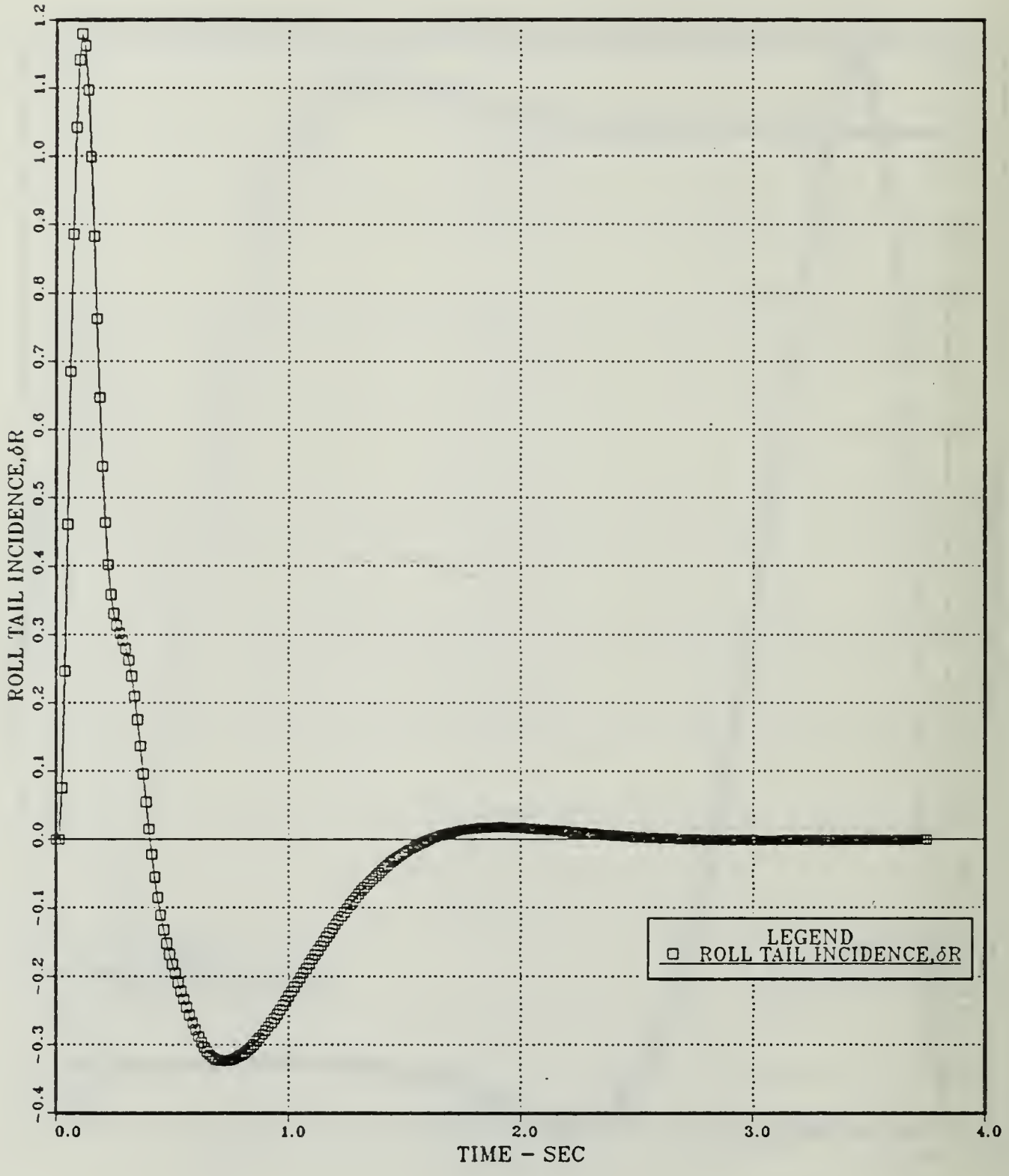

Figure 2.36 Roll Tail Incidence vs Time; Uncoupled Roll Channel Autopilot; Classical Design; Discrete Open Loop System; Circular Airframe

III. MODERN CONTROL DESIGN AND ANALYSIS OF LINEAR UNCOUPLED LATERAL AUTOPILOTS

A. GENERAL

The task of this chapter is the design and analysis of the same discrete uncoupled lateral channel autopilots discussed in the previous chapter, using different techniques which are based on modern control formulation. The difference in the two approaches is entirely in the design method since the end result, a set of difference equations providing control, is identical.

Modern control theory is contrasted with the classical control theory in that the former is applicable to multi-input-multi-output systems, which may be linear or nonlinear time-invariant or time-varying, while the latter is applicable only to linear time-invariant single-input-single-output systems. Also, modern control theory is essentially a time-domain approach, while the conventional classical control theory is a complex frequency-domain approach.

System design in classical control theory is based on trial-and-error procedures which, in general, will not yield optimal control systems. System design in modern control theory, on the other hand, enables the design of optimal control systems of great complexity and good accuracy with respect to given performance indexes. In addition, design in modern control theory can be carried out for a class of inputs instead of

specific input function, such as the impulse, step or sinusoidal functions and can also include initial conditions.

One of the most attractive features of modern control design method is that the procedure consists of two independent steps. One step assumes that all the system states are available for feedback purposes. In general, even if this is not a practical enough assumption since it needs a large number of sensors, it is usually adopted in order to accomplish the first design step, namely the control-law. The remaining step is the design of an estimator which estimates the entire state vector, given measurements of portion of the state provided by the system output equation. The final control algorithm consists of the control-law and estimator combined, where the control-law calculations are based on the estimated states rather than the actual states. This substitution is reasonable and the combined design can give closed loop characteristics which are unchanged from those assumed in designing the control-law and estimator separately.

B. DISCRETE STATE-FEEDBACK DESIGN

Considering the following discrete control system:

$$\underline{X}(K+1) = \underline{A}\underline{x}(k) + \underline{B}\underline{u}(k) \qquad \text{(III.B.1-1)}$$

$$\underline{Y}(k) = \underline{H}\underline{x}(k) \qquad \text{(III.B.1-2)}$$

the control-law design is also referred to as state-feedback design since it is simply the feedback of a linear combination of all the system states, that is:

$$\underline{u}(k) = \underline{F}\underline{x}(k) \qquad \text{(III.B.1-3)}$$

where $\underline{F}$: control-law gain vector

Thus, the characteristic equation of the controlled (closed loop) system is:

$$\det (z\underline{I}-\underline{A}+\underline{B}\underline{F}) = 0 \qquad \text{(III.B.1-4)}$$

The discrete state-feedback design, providing that the system is controllable, consists then of finding the control-law gain vector F so that the roots of (III.B.1-4) are in desirable locations.

A program logic for computing the control-law gain vector via the Ackermann's formula is given in Appendix E [Ref. 9]. Utilizing this control algorithm a Fortran program was written (Appendix F) which has as inputs the sample period, the discrete plant system and control input matrices, the s-plane poles and provides as output the control-law gain vector.

1. Uncoupled Yaw Channel for Elliptical Airframe

a. Control-Law Gain Vector

Executing the Ackermann Fortran program described in Appendix F with inputs:

(1) Sample period of 0.0125 seconds

(2) Discrete plant system and control input matrices $\underline{A}$ and $\underline{B}$ of Table III

(3) S-plane poles defined in equations (II.C.3-2) through (II.C.3-8)

the following control-law gain vector for the elliptical airframe of the uncoupled yaw channel is obtained:

$$\underline{F}=[-1.0195\ -0.109\ -0.3492\ 0.0393\ -0.6152\ 32.4775\ -31.0868] \qquad \text{(III.B.1-5)}$$

b. Design Approach and Analysis

The discrete state-feedback designed yaw autopilot can be found by introducing the control-law gain vector of (II.B.1-5) into the original system.

The pole-zero plot of Figure 3.1 indicates that the discrete closed lop system is stable, since the z-plane closed loop poles are:

z_1 = 0.46461 (yaw angular rate) (III.B.1-6)

z_2 = 0.898888+j0.137039 (III.B.1-7)

z_3 = 0.898888-j0.137039 (yaw normal acceleration) (III.B.1-8)

z_4 = 0.998423+j0.051078 (III.B.1-9)

z_5 = 0.998423-j0.0510789 (output of acceleration compensator network) (III.B.1-10)

z_6 = 0.962974+j0.0358712 (input command in the actuator) (III.B.1-11)

z_7 = 0.962974-j0.0358712 (yaw tail incidence) (III.B.1-12)

The time response plots of the yaw normal acceleration, angular rate and tail incidence are presented in Figures 3.2 through 3.4. A close observation of the above pole-zero and time response plots for the discrete yaw state-feedback design indicates that they are identical with those of the discrete classical design found in the previous chapter.

c. Simplified Design

The discrete state-feedback designed autopilot of the previous section can be simplified by reducing the returning gain loops. This can be accomplished by placing zeros into appropriate elements of the control-law gain vector:

$\underline{F}$=[-1.0195 -0.109 -0.3492 0 -0.6152 32.4775 -31.0868] (III.B.1-13)

The pole-zero and time response plots of the resulting simplified state-feedback yaw autopilot, shown in Figures 3.5 through 3.8, do not present significant differences from the corresponding plots of the discrete classical design apart from the overshoot which was slightly increased. The discrete closed loop system is again stable, since the z-plane closed loop poles are:

z_1 = 0.467984)III.B.1-14)

z_2 = 0.891328+j0.126019 (III.B.1-15)

z_3 = 0.891328-j0.126019 (III.B.1-16)

z_4 = 0.998422+j0.0510788 (III.B.1-17)

z_5 = 0.998422-j0.0510788 (III.B.1.18)

z_6 = 0.969075+j0.0429695 (III.B.1-19)

z_7 = 0.969075-j0.0429695 (III.B.1-20)

2. Uncoupled Roll Channel for Circular Airframe

a. Control-Law Gain Vector

Following the same procedure as in the yaw channel case apart from the use of discrete matrices $\underline{A}$ and $\underline{B}$ from Table III and s-plane poles from (II.D.3-2) through (II.D.3-8), the control-law gain vector for the circular airframe roll channel was found to be:

$\underline{F}$=[0 0.0004 0 0.0178 -0.0179 -1.499 0.0023] (III.B.2-1)

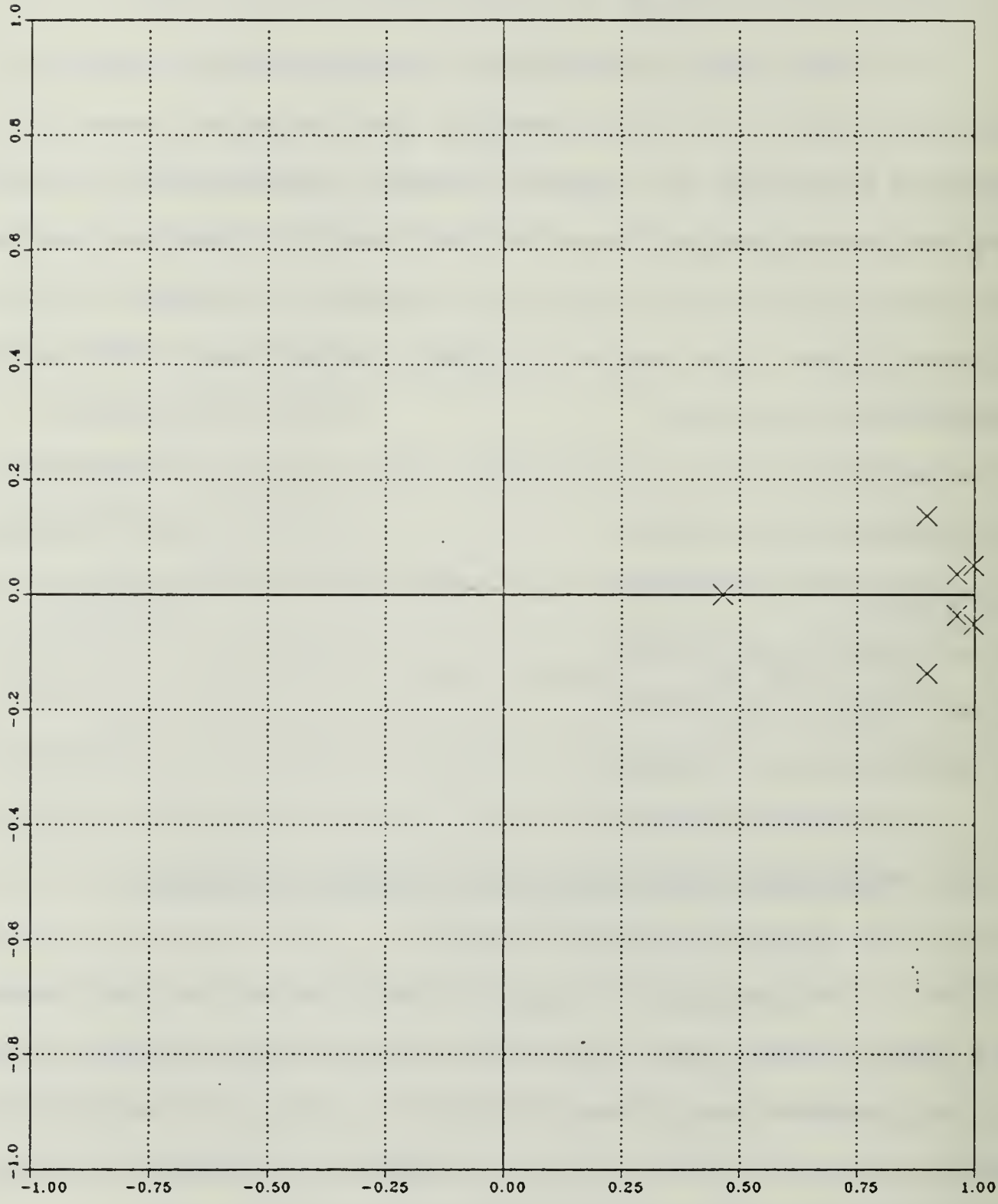

Figure 3.1 Pole-Zero Plot; Uncoupled Yaw Channel Autopilot; State-Feedback Design; Discrete Closed Loop System; Elliptical Airframe

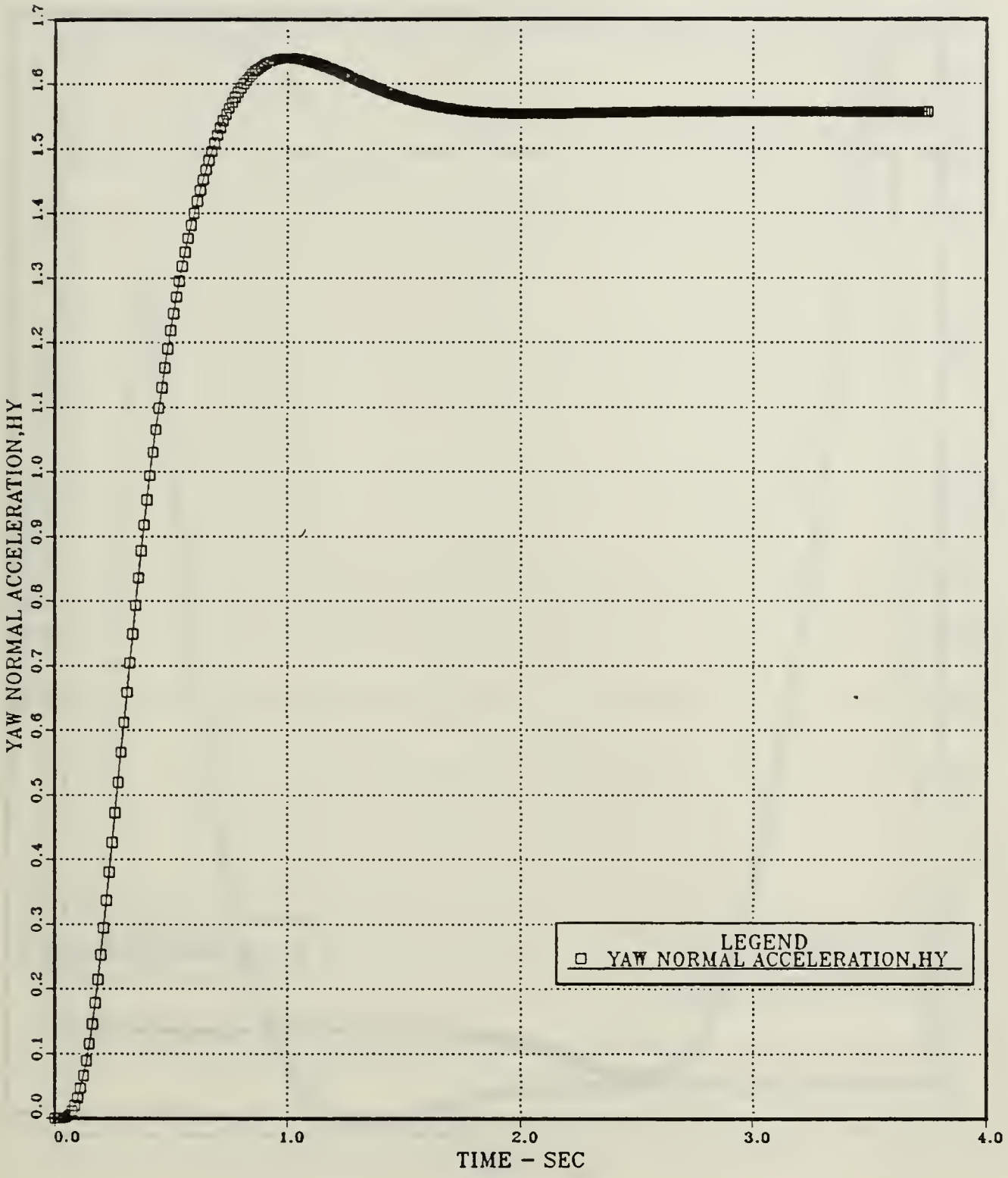

Figure 3.2 Yaw Normal Acceleration vs Time; Uncoupled Yaw Channel Autopilot; State-Feedback Design; Discrete Closed Loop System; Elliptical Airframe

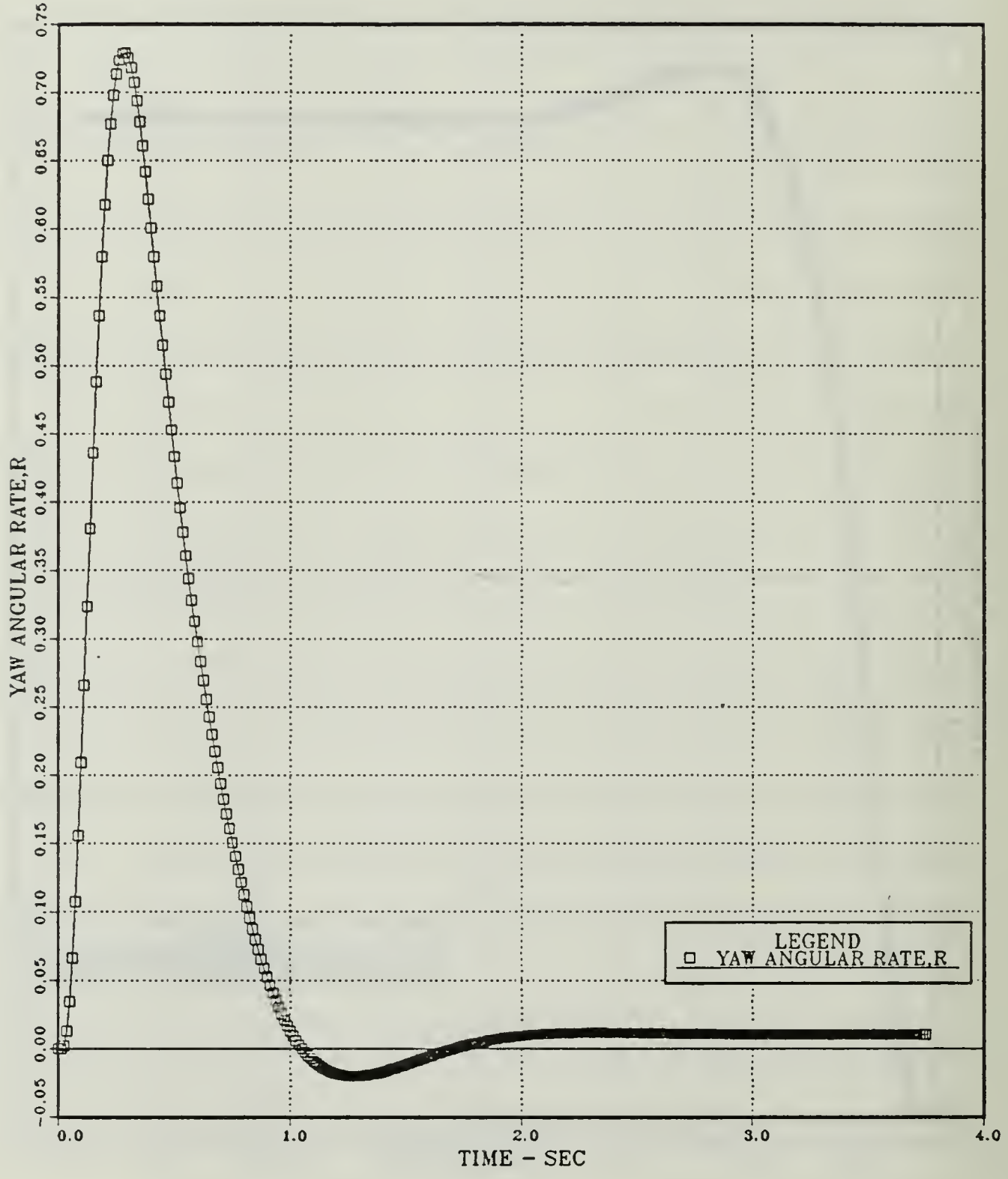

Figure 3.3 Yaw Angular Rate vs Time; Uncoupled Yaw Channel Autopilot; State-Feedback Design; Discrete Closed Loop System; Elliptical Airframe

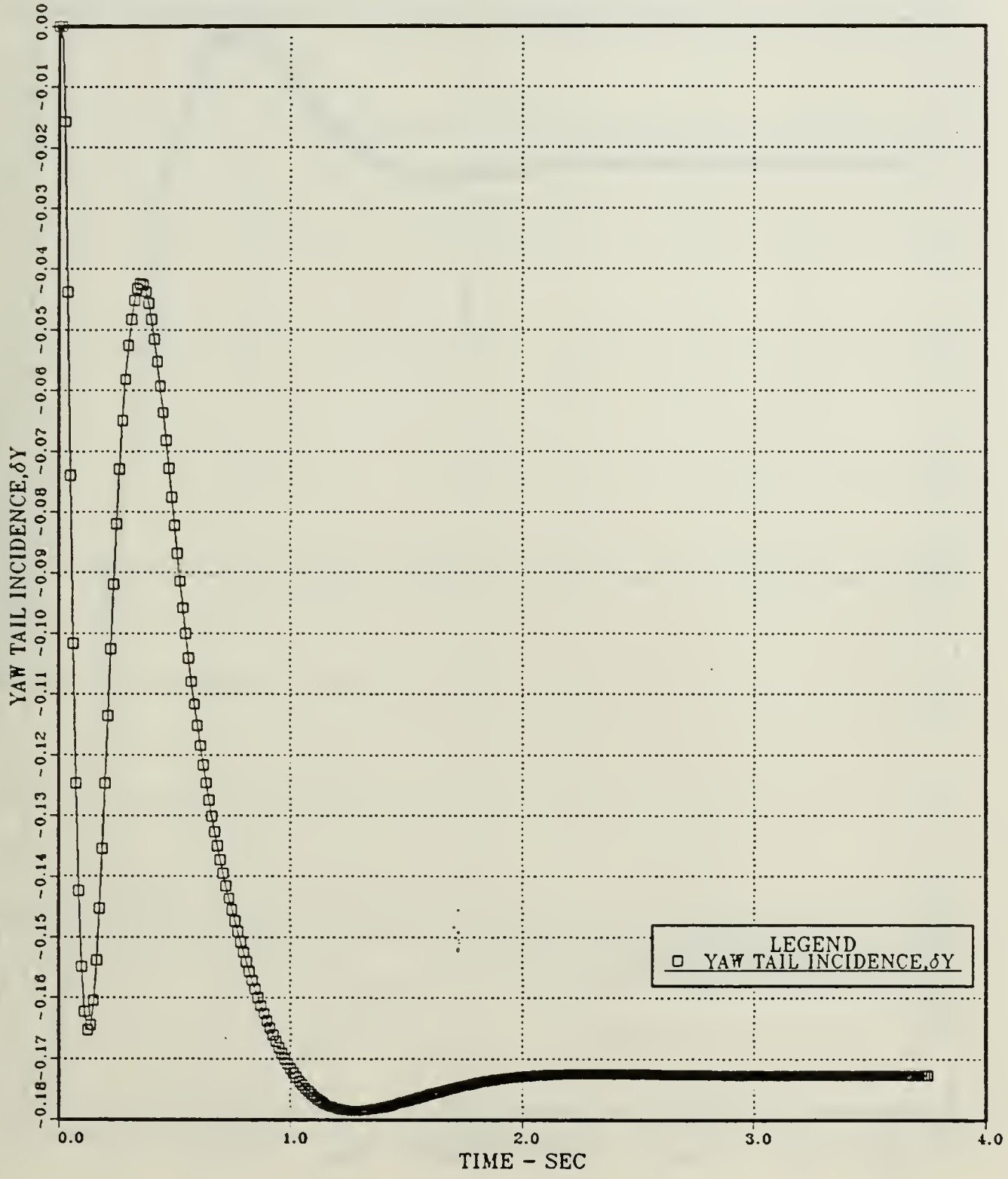

Figure 3.4 Yaw Tail Incidence vs Time; Uncoupled Yaw Channel Autopilot; State-Feedback Design; Discrete Closed Loop System; Elliptical Airframe

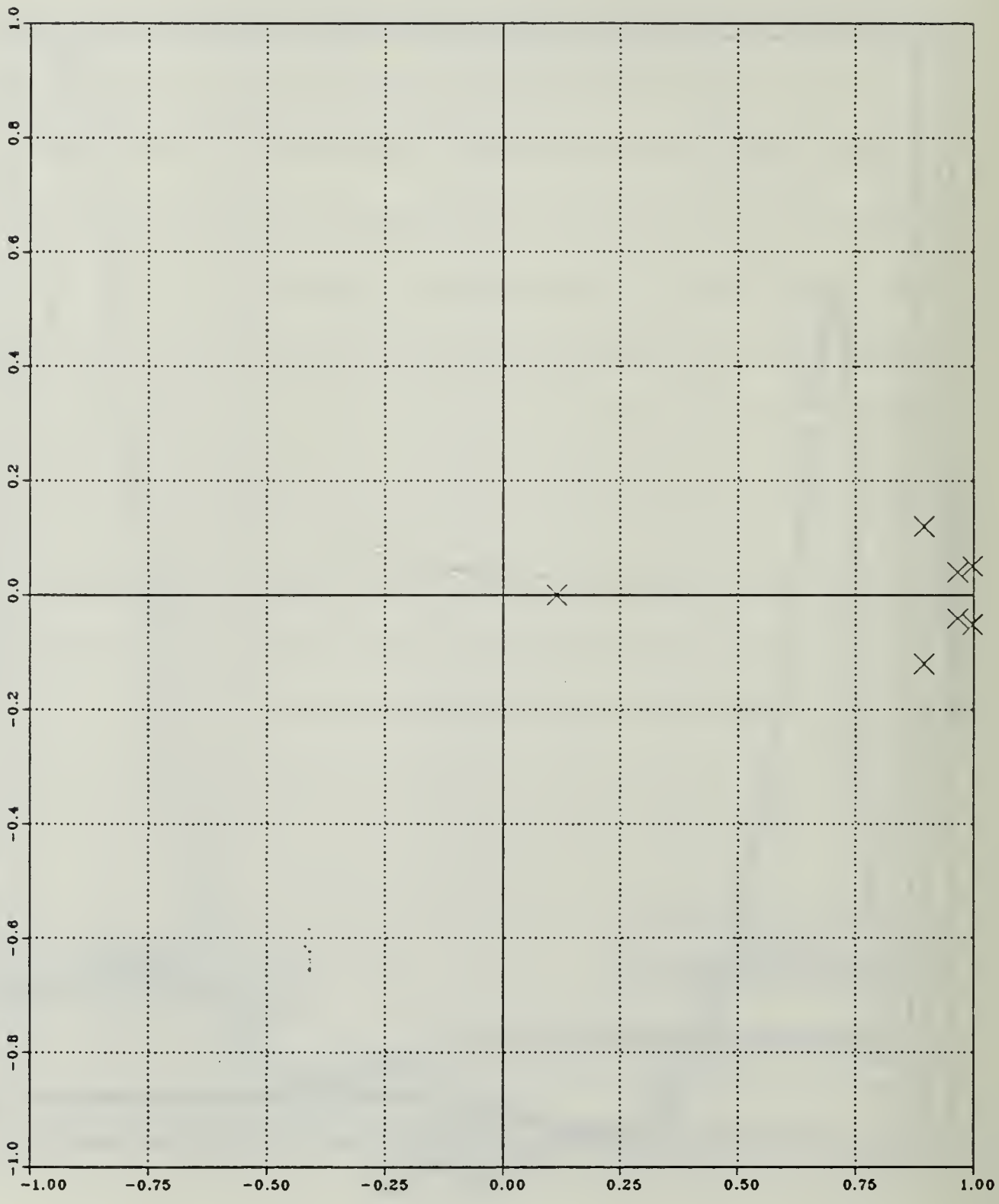

Figure 3.5 Pole-Zero Plot; Uncoupled Yaw Channel Autopilot; Simplified State-Feedback Design; Discrete Closed Loop System; Elliptical Airframe

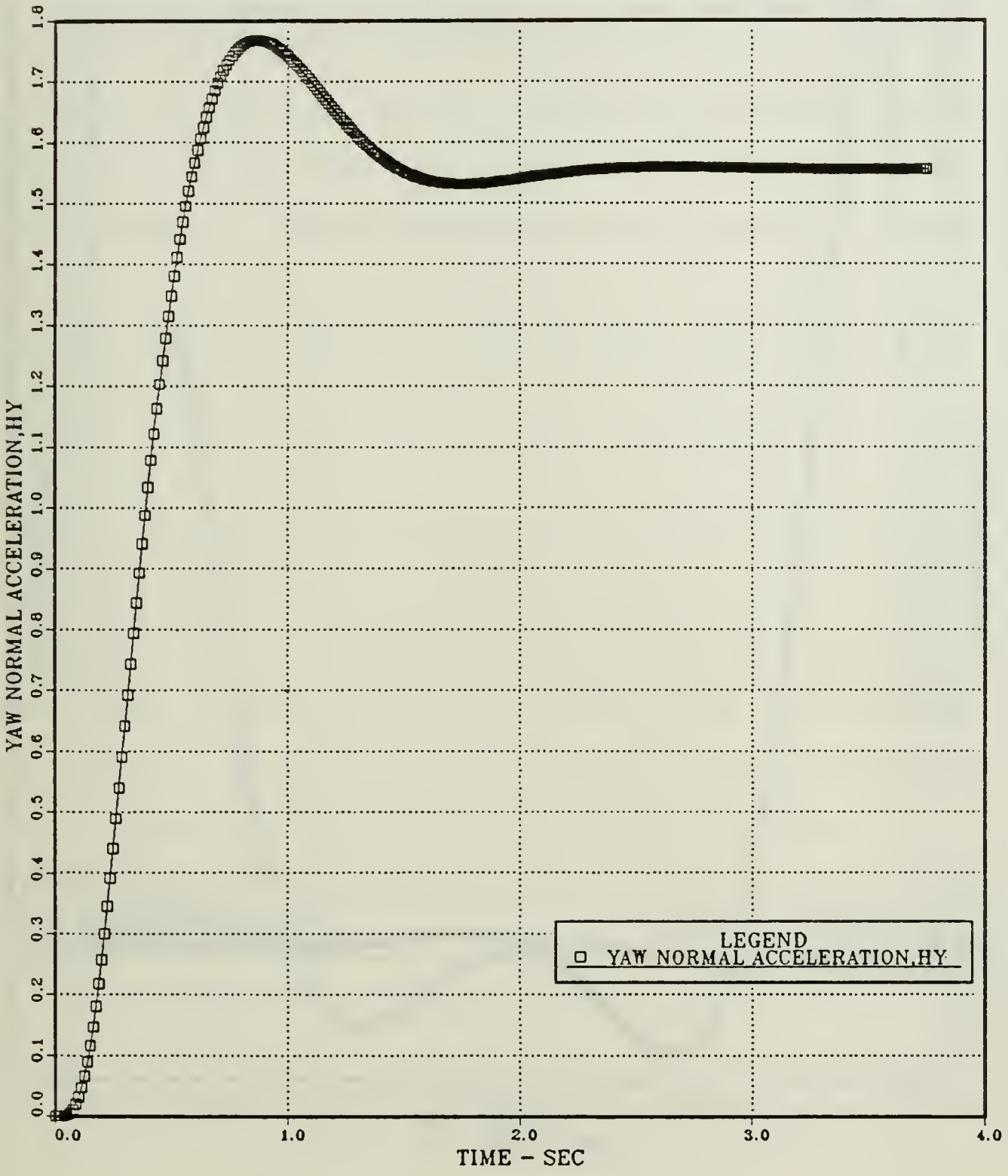

Figure 3.6 Yaw Normal Acceleration vs Time; Uncoupled Yaw Channel Autopilot; Simplified State-Feedback Design; Discrete Closed Loop System; Elliptical Airframe

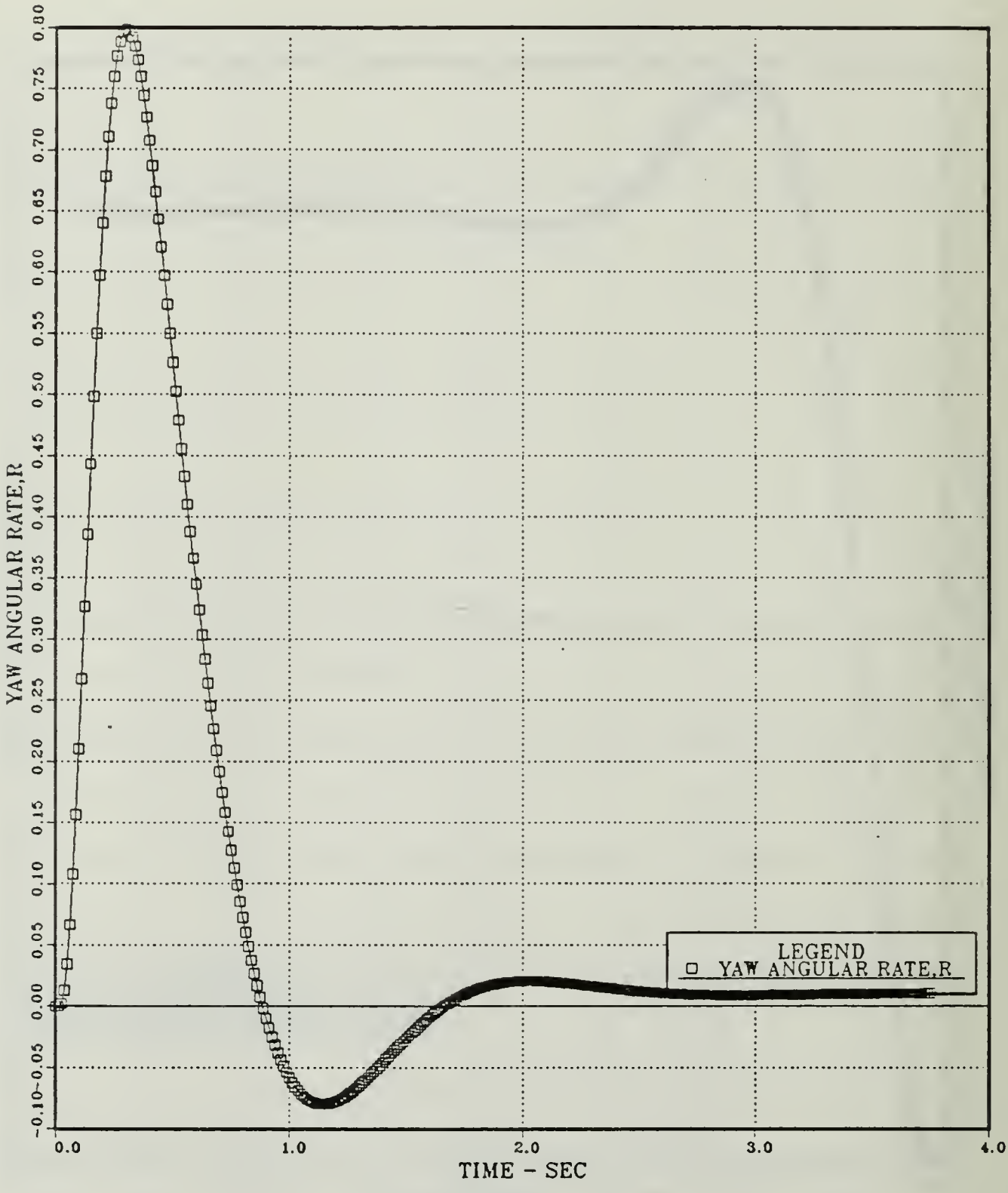

Figure 3.7 Yaw Angular Rate vs Time; Uncoupled Yaw Channel Autopilot; Simplified State-Feedback Design; Discrete Closed Loop System; Elliptical Airframe

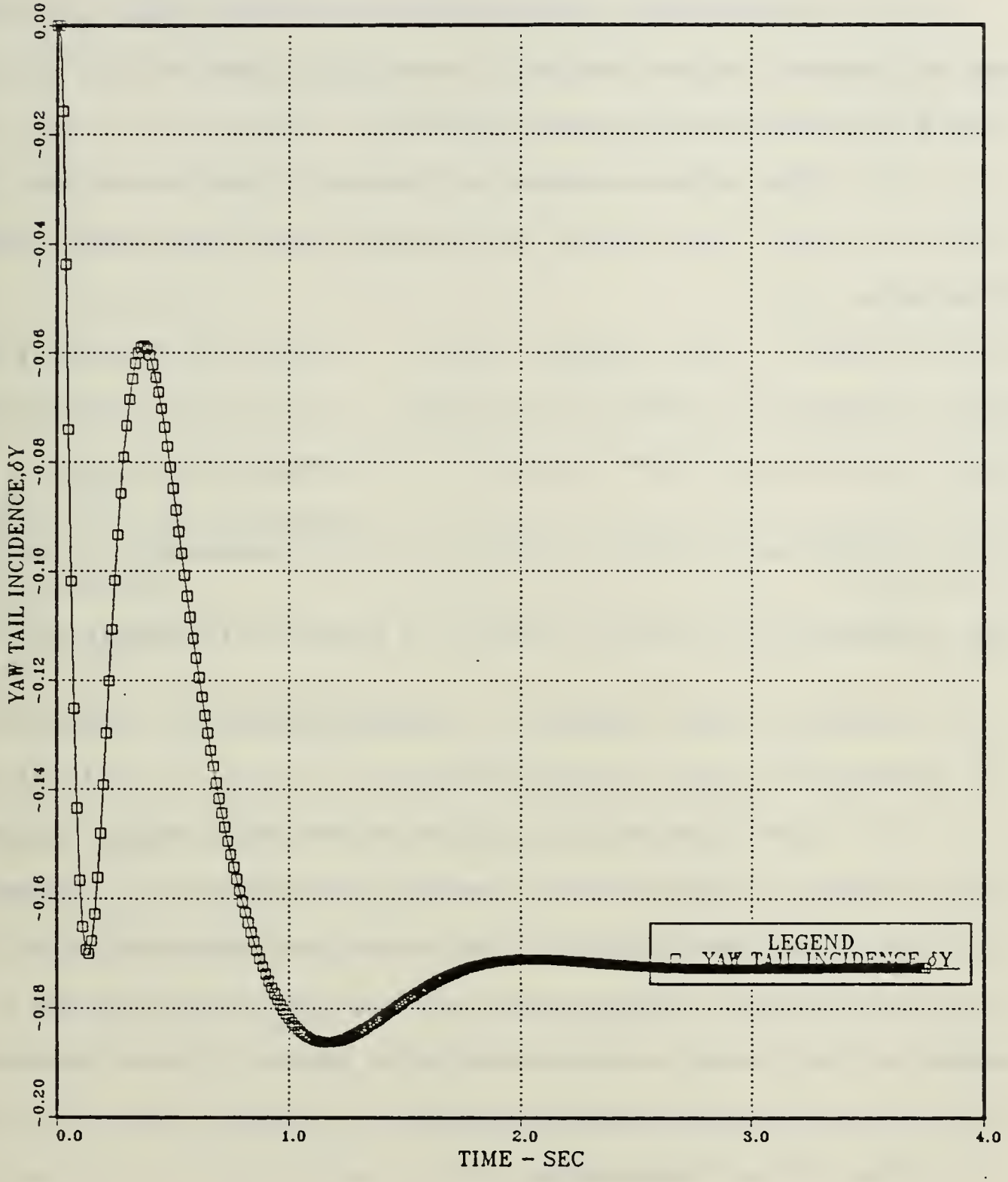

Figure 3.8 Yaw Tail Incidence vs Time; Uncoupled Yaw Channel Autopilot; Simplified State-Feedback Design; Discrete Closed Loop System; Elliptical Airframe

b. Design Approach and Analysis

The discrete state-feedback designed roll autopilot can be found by introducing the control-law gain vector of (III.B.2-1) into the original system.

The pole-zero plot of Figure 3.9 indicates that the discrete closed loop system is stable, since the z-plane closed loop poles are:

z_1 = 0.0989714 (roll angular rate) (III.B.2-2)

z_2 = 0.832909+j0.315088 (roll angle) (III.B.2-3)

z_3 = 0.832909-j0.315088 (output of roll angle compensator) (III.B.2-4)

z_4 = 0.969236+j0.0333773 (output of rate compensator network) (III.B.2-5)

z_5 = 0.969236-j0.0333773 (output of pseudo-differentiator) (III.B.2-6)

z_6 = 0.896583 (input command in the actuator) (III.B.2-7)

z_7 = 0.938233 (roll tail incidence) (III.B.2-8)

The time response plots of the roll angle, angular rate and tail incidence are presented in Figures 3.10 through 3.12. A close observation of the above pole-zero and time response plots for the discrete roll state-feedback design indicates that they are identical with those of the discrete classical design found in the previous chapter.

c. Simplified Design

The state-feedback roll designed autopilot can be simplified by reducing the returning gain loops as follows:

$\underline{F}$=[0 0 0 0.178 -0.0179 -1.499 0] (III.B.2-9)

The pole-zero and time response plots of the resulting simplified state-feedback roll autopilot, shown in Figures 3.13 through 3.16, do not present significant differences from the corresponding plots of the discrete classical design. The discrete closed loop system is again stable, since the z-plane closed loop poles are:

$z_1 = 0.0992745$ (III.B.2-10)

$z_2 = 0.836632+j0.305719$ (III.B.2-11)

$z_3 = 0.836632-j0.305719$ (III.B.2-12)

$z_4 = 0.967647+j0.0334948$ (III.B.2-13)

$z_5 = 0.967647-j0.0334948$ (III.B.2-14)

$z_6 = 0.895937$ (III.B.2-15)

$z_7 = 0.938256$ (III.B.2-16)

C. DISCRETE ESTIMATOR DESIGN

The state-feedback design discussed in the last section assumed that all system states were available for feedback purposes. Since the state vector is not always accessible to direct measurement, an estimator is going to be introduced in this section as an additional dynamic design in order to implement control to the original system. The estimator design method consists mainly of determining algorithms which will reconstruct all the states, given measurements of a portion of them.

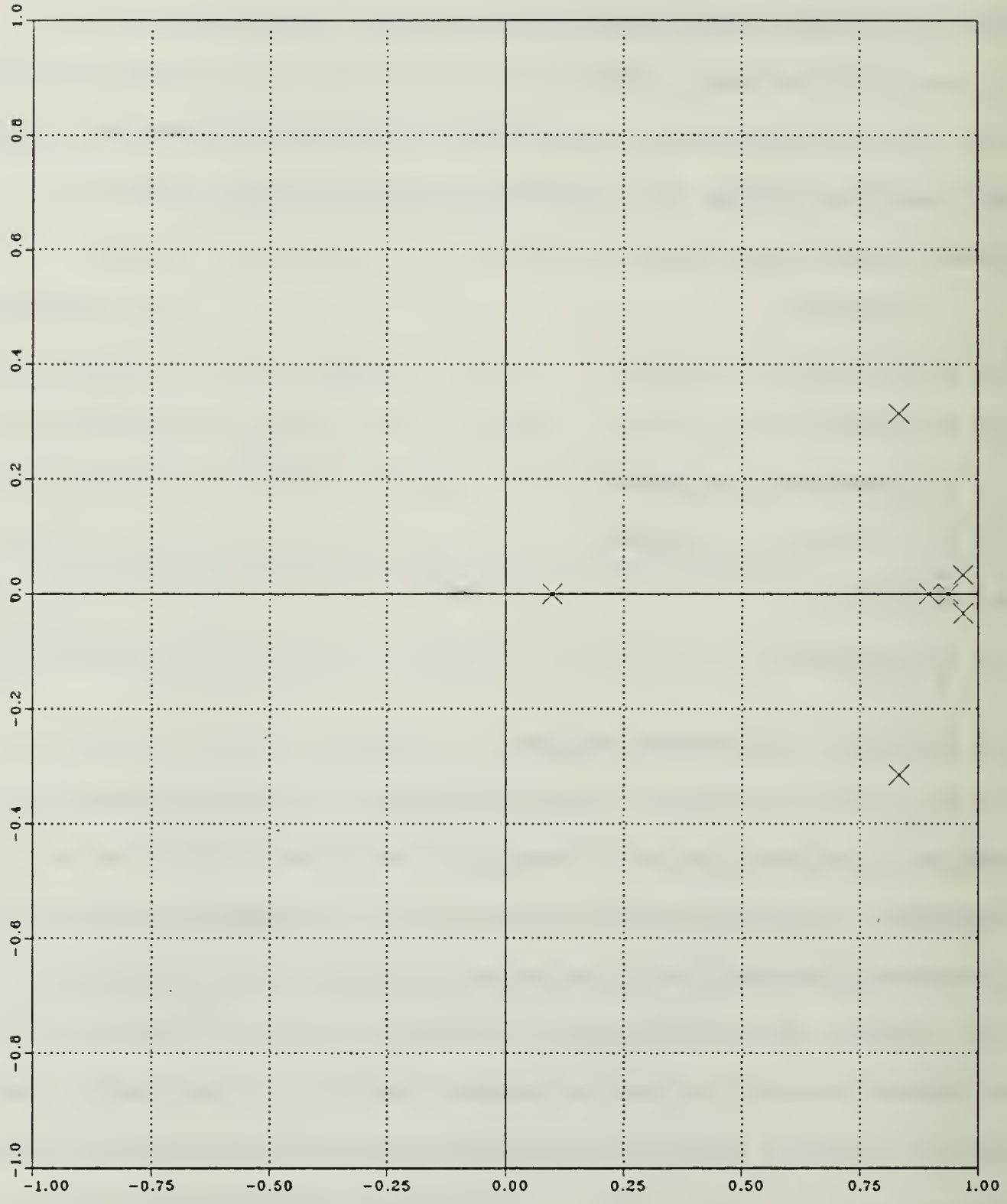

Figure 3.9 Pole-Zero Plot; Uncoupled Roll Channel Autopilot; State-Feedback Design; Discrete Closed Loop System; Circular Airframe

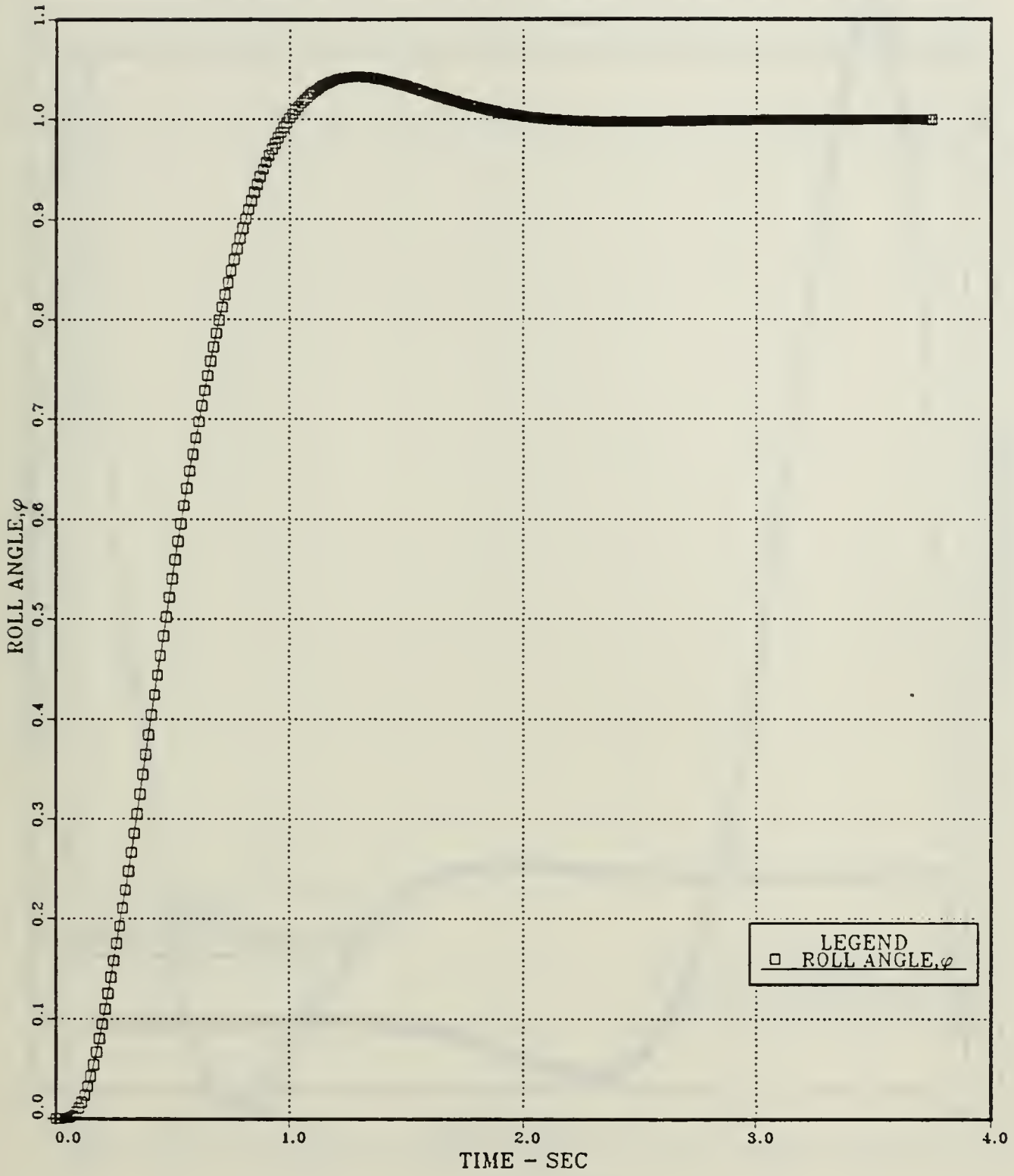

Figure 3.10 Roll Angle vs Time; Uncoupled Roll Channel Autopilot; State-Feedback Design; Discrete Closed Loop System; Circular Airframe

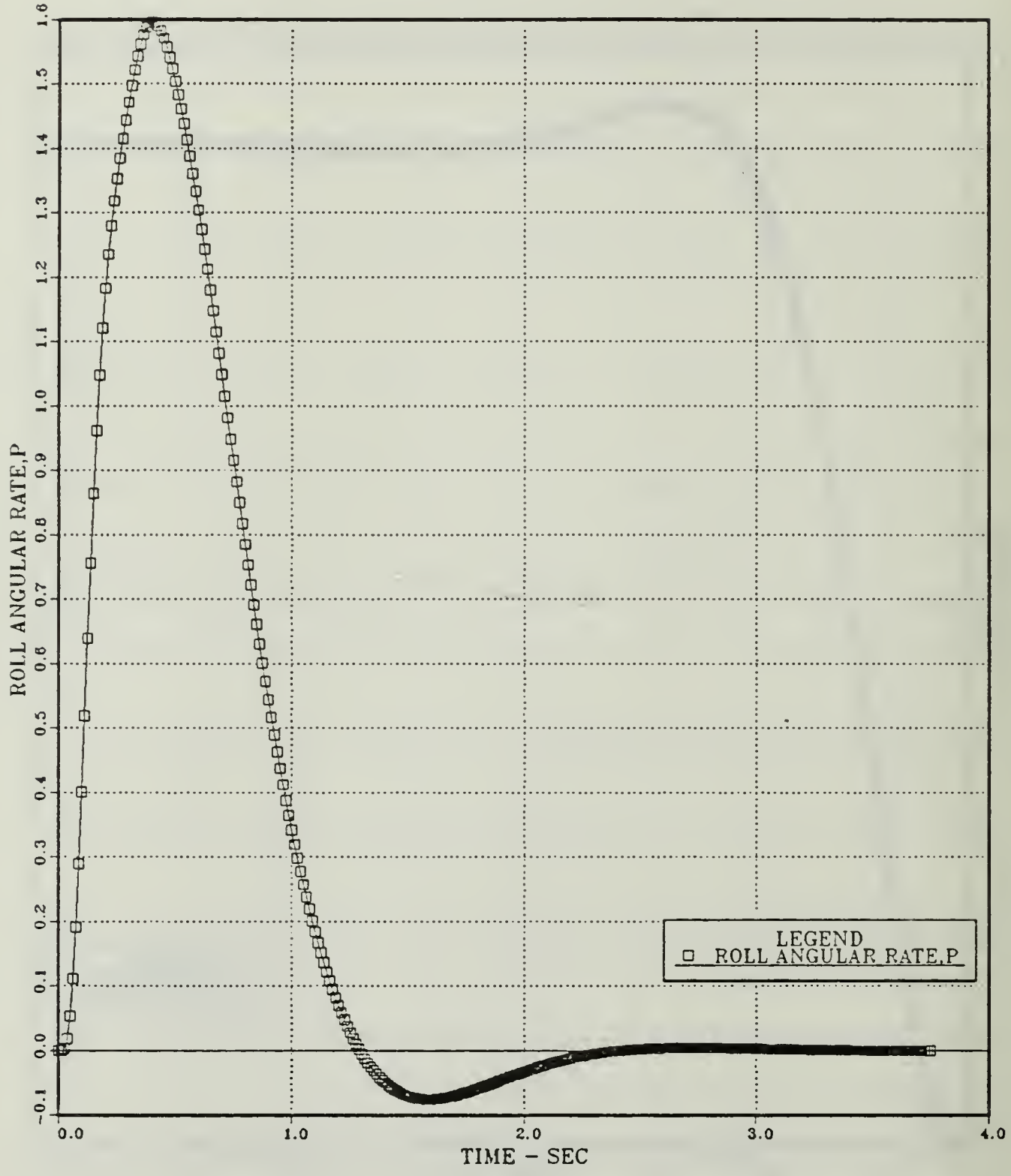

Figure 3.11 Roll Angular Rate vs Time; Uncoupled Roll Channel Autopilot; State-Feedback Design; Discrete Closed Loop System; Circular Airframe

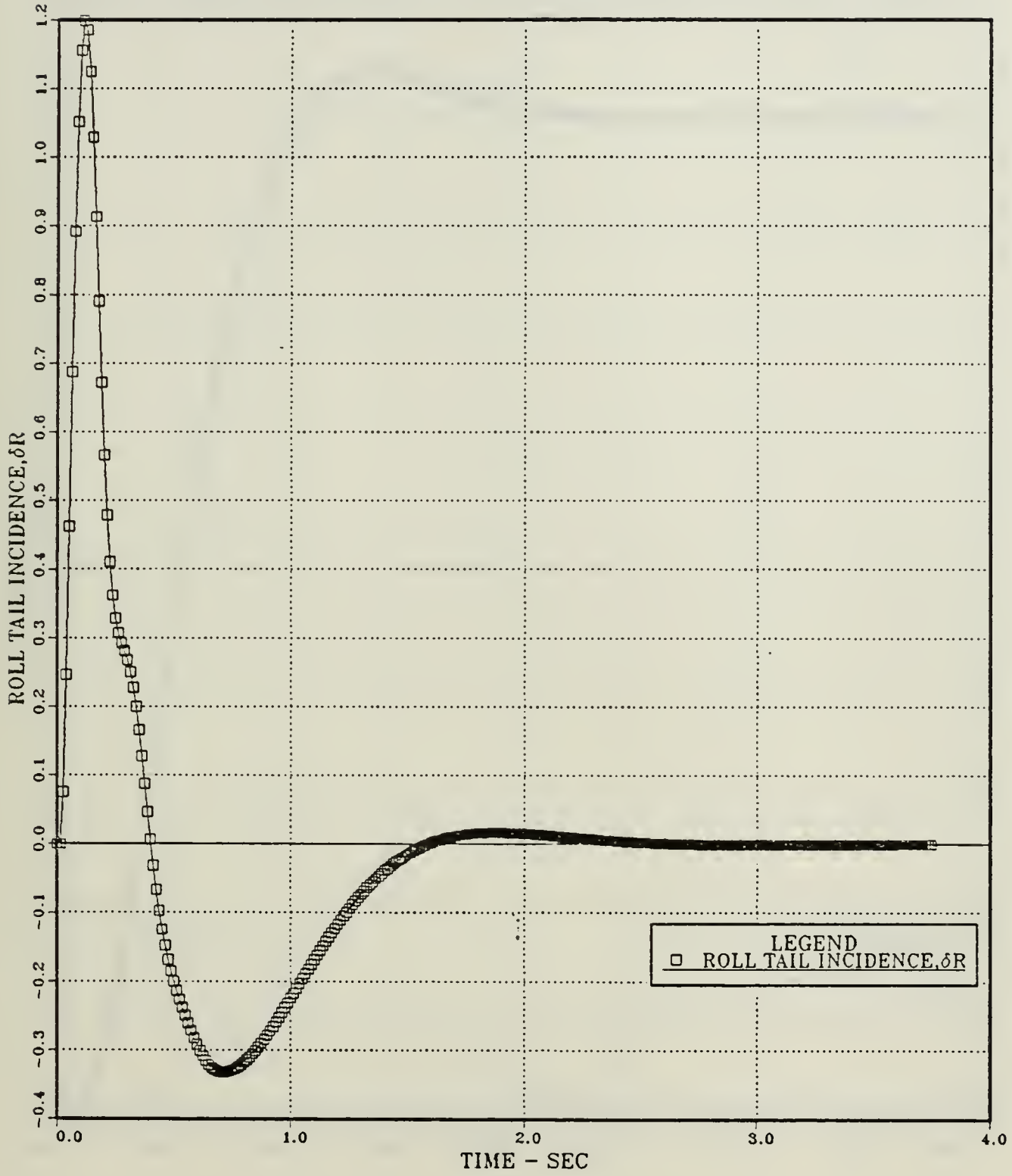

Figure 3.12 Roll Tail Incidence vs Time; Uncoupled Roll Channel Autopilot; State-Feedback Design; Discrete Closed Loop System; Circular Airframe

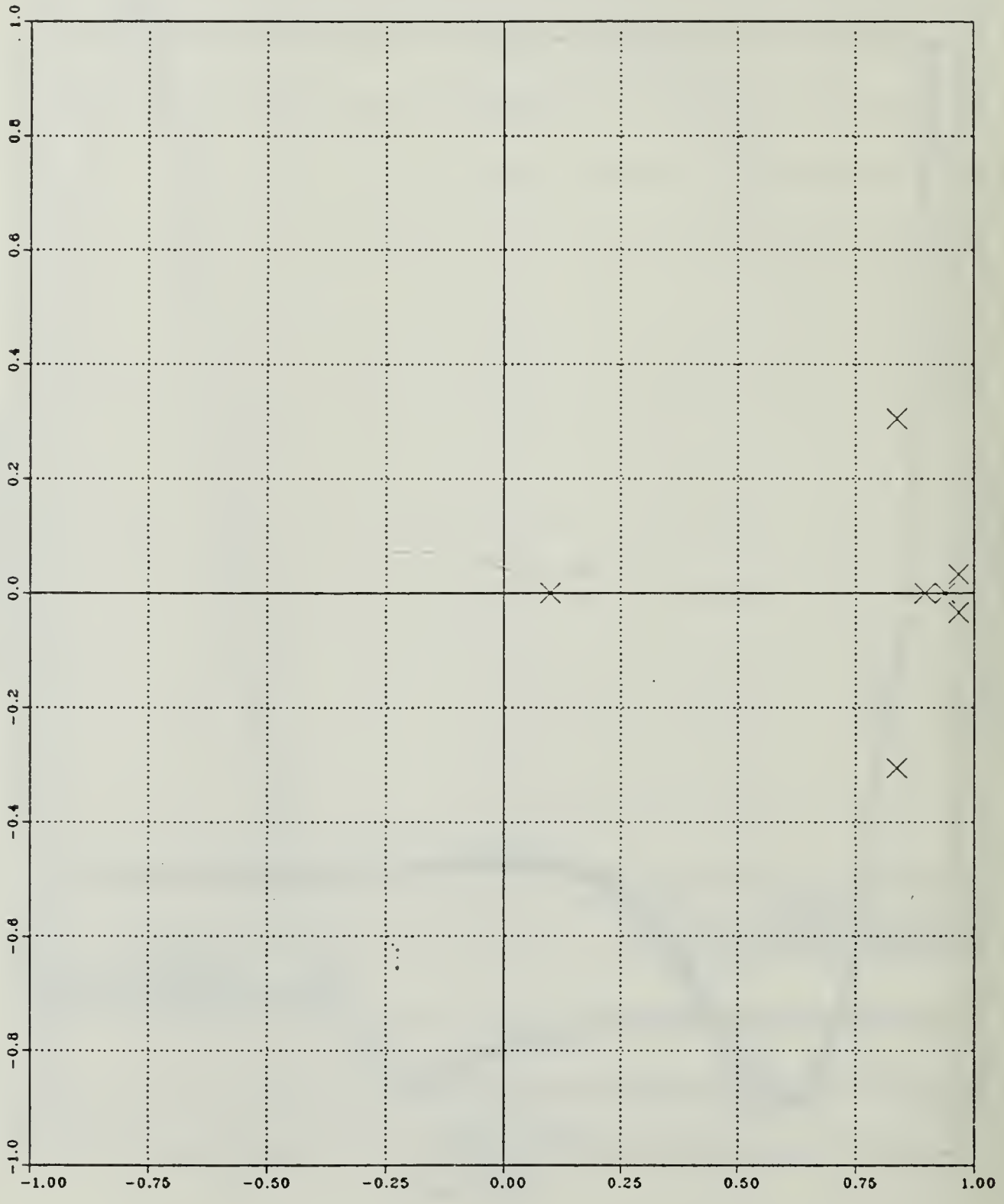

Figure 3.13 Pole-Zero Plot; Uncoupled Roll Channel Autopilot; Simplified State-Feedback Design; Discrete Closed Loop System; Circular Airframe

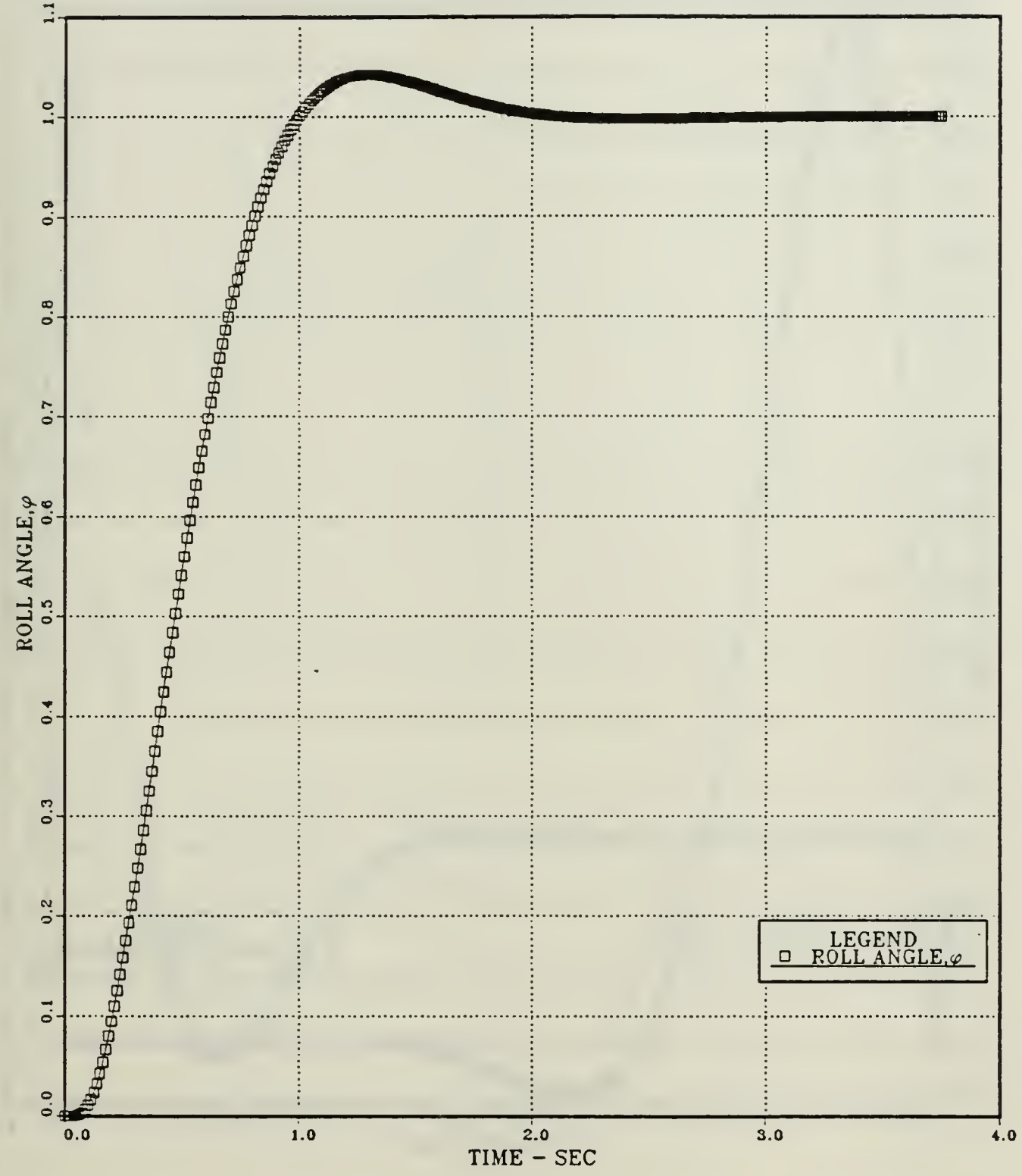

Figure 3.14 Roll Angle vs Time; Uncoupled Roll Channel Autopilot; Simplified State-Feedback Design; Discrete Closed Loop System; Circular Airframe

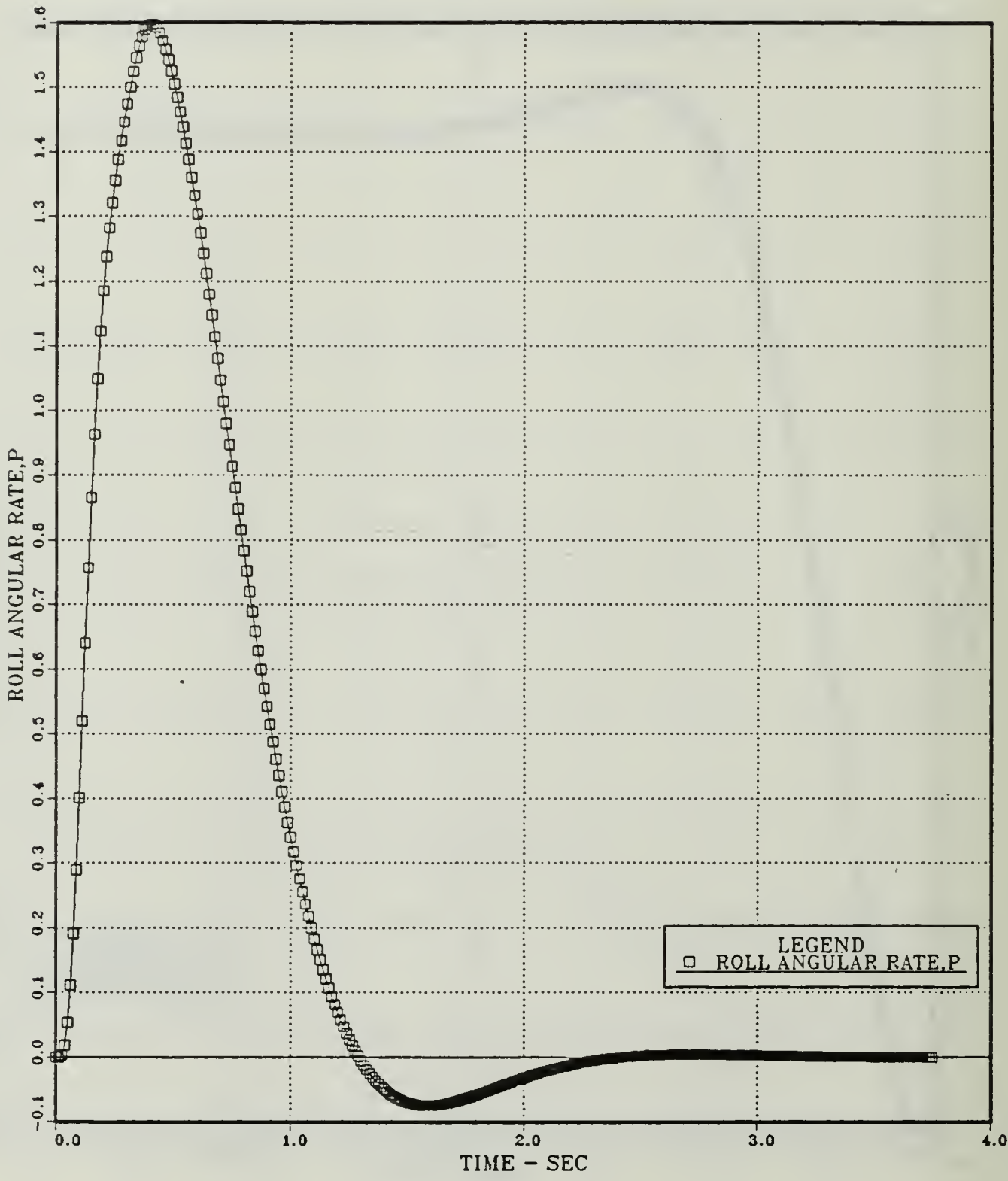

Figure 3.15 Roll Angular Rate vs Time; Uncoupled Roll Channel Autopilot; Simplified State-Feedback Design; Discrete Closed Loop System; Circular Airframe

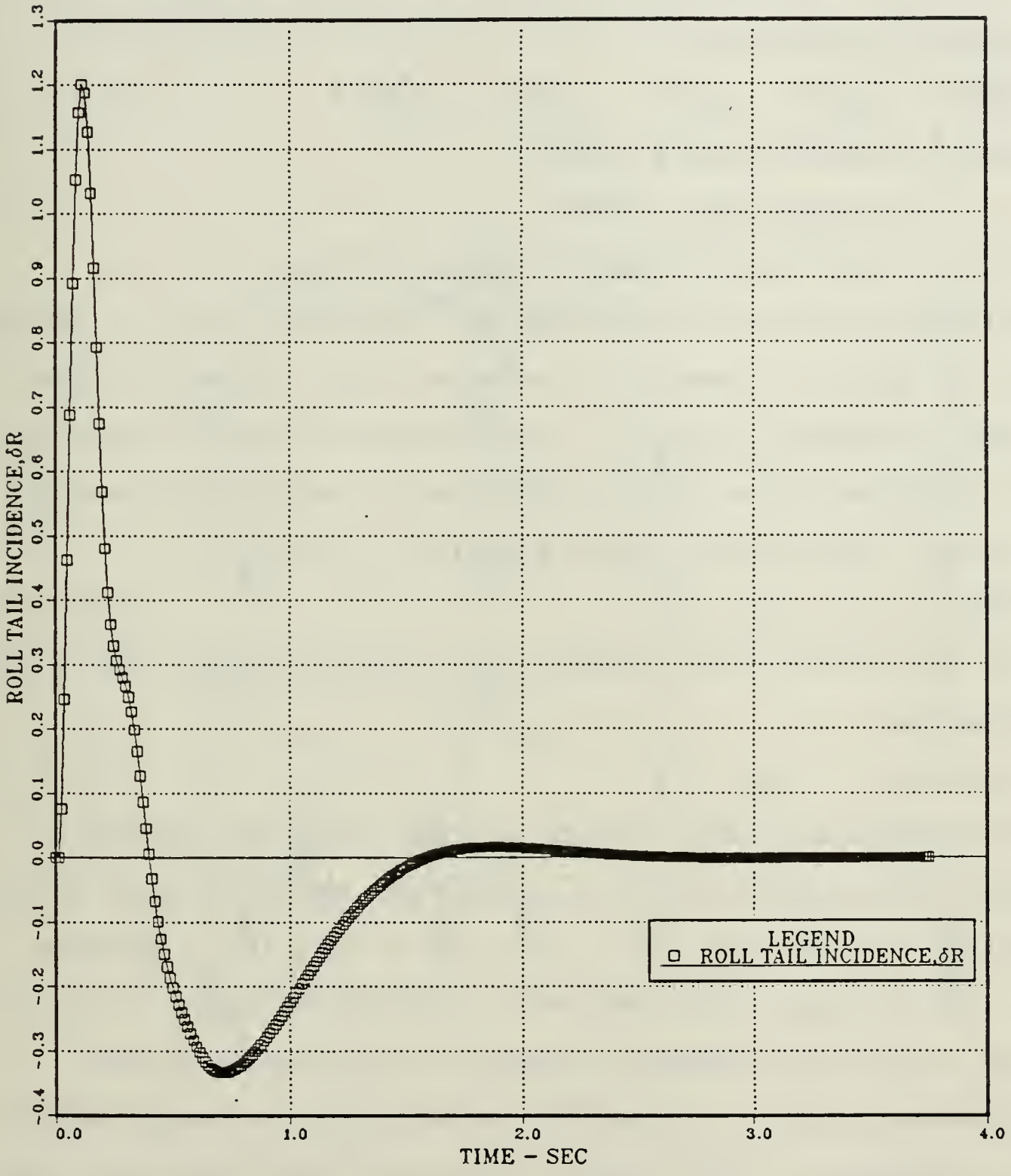

Figure 3.16 Roll Tail Incidence vs Time; Uncoupled Roll Channel Autopilot; Simplified State-Feedback Design; Discrete Closed Loop System; Circular Airframe

Considering the same as in the state-feedback case discrete control system, a prediction estimator defined by the following equation is introduced:

$$\underline{\hat{x}}(K+1) = \underline{A}\underline{\hat{x}}(k) + \underline{B}\underline{u}(k) + \underline{K}[\underline{y}(k) - \underline{H}\underline{\hat{x}}(k)] \qquad \text{(III.C.1-1)}$$

where $\underline{\hat{x}}$: estimate state vector

$\underline{K}$: estimate gain vector

In this closed loop estimator, shown in Figure 3.17, the difference between the measured and estimated output is fed back and the model is constantly corrected with this error signal which is defined as $\underline{\tilde{x}}=\underline{x}-\underline{\hat{x}}$. The difference equation describing the behavior of the error is obtained by subtracting equation from the actual plant output equation (II.B.1-2):

$$\underline{\tilde{x}}(K+1) = [\underline{A} - \underline{K}\underline{H}]\ \underline{\tilde{x}}(k) \qquad \text{(III.C.1-2)}$$

Thus the characteristic equation of the controlled (closed loop) system is:

$$\det\ (z\underline{I} - \underline{A} + \underline{K}\underline{H}) = 0 \qquad \text{(III.C.1-3)}$$

The discrete estimator design, providing that the system is observable, consists then of finding the estimator gain vector $\underline{K}$ so that the roots of (III.C.1-3) are at desirable locations.

The estimator gain vector can be obtained again, as in the case of the state-feedback design, by application of the Ackermann program of Appendix F with inputs the sample period, the transposes of the discrete plant and output matrices, and faster s-plane poles from those of the continuous system.

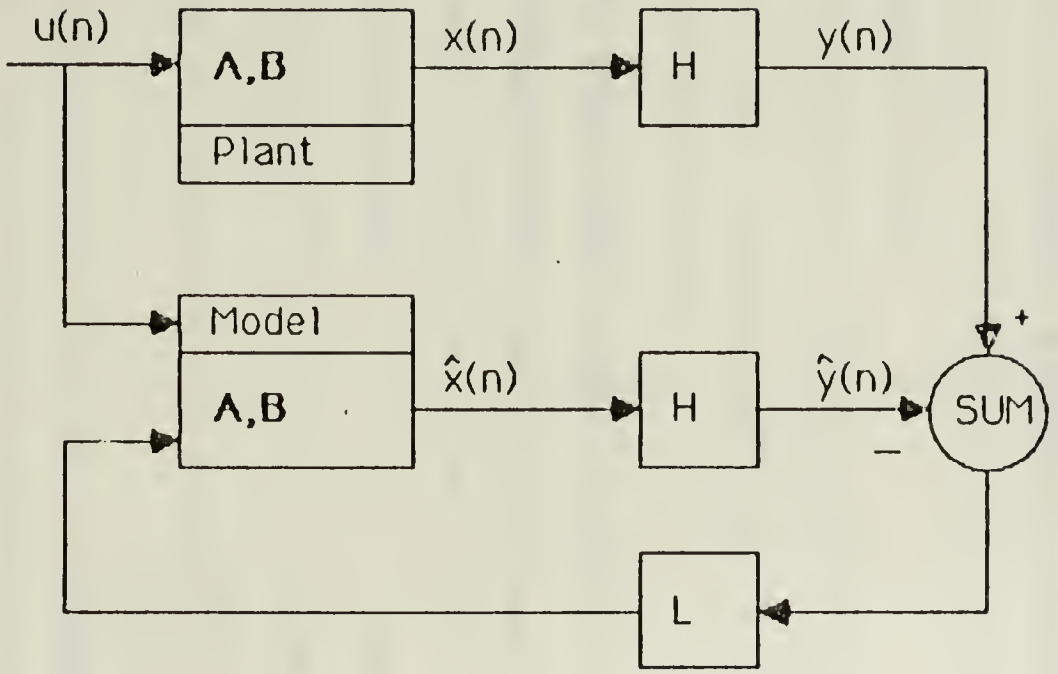

Figure 3.17 Discrete Closed Loop Estimator

1. Uncoupled Yaw Channel for Elliptical Airframe

a. Estimator Gain Vector

Executing the Ackermann Fortran program (Appendix F) with inputs:

(1) Sample period of 0.0125 seconds

(2) The transposes of the discrete yaw system plant and output matrices, that is $\underline{A}^T$ and $\underline{H}_1^T$, where:

$$\underline{H}_1^T = \begin{bmatrix} 1 \\ 0 \\ 0 \\ 0 \\ 0 \\ 0 \\ 0 \end{bmatrix} \qquad \text{(III.C.1-4)}$$

(3) S-plane poles slightly faster than those of the continuous open loop system, that is with more negative real parts:

$s_1 = -174.386$ (III.C.1-5)

$s_2 = -6.1142+j10.6396$ (III.C.1-6)

$s_3 = -6.1142-j10.6396$ (III.C.1-7)

$s_4 = -0.0227475+j4.08919$ (III.C.1-8)

$s_5 = -0.0227475-j4.08919$ (III.C.1-9)

$s_6 = -2.9396+j2.99929$ (III.C.1-10)

$s_7 = -2.9396-j2.99929$ (III.C.1-11)

the transpose of the estimator gain vector for the elliptical airframe of the uncoupled yaw channel is calculated as output, from which the following $\underline{K}$ is obtained:

$$\underline{K} = \begin{bmatrix} -0.0034 \\ 0.0008 \\ -0.0003 \\ -0.0177 \\ 0.0005 \\ -0.0017 \\ -0.0240 \end{bmatrix} \qquad \text{(III.C.1-12)}$$

b. Design Approach and Analysis

The discrete estimator designed yaw autopilot can be found by introducing the estimator gain vector of (III.C.1-12) into the original system.

The pole-zero plot of Figure 3.18 indicates that the discrete closed loop system is stable, since the z-plane closed loop poles were found to be:

z_1 = 0.117115 (yaw angular rate) (III.C.1-13)

z_2 = 0.918174+j0.122926 (III.C.1-14)

z_3 = 0.918174-j0.122926 (yaw normal acceleration) (III.C.1-15)

z_4 = 0.998399+j0.0510958 (III.C.1-16)

z_5 = 0.998399-j0.0510958 (output of acceleration compensator network) (III.C.1-17)

z_6 = 0.963249+j0.0361306 (input command in the actuator) (III.C.1-18)

z_7 = 0.963249-j0.0361306 (yaw tail incidence) (III.C.1-19)

The time response plots of the yaw normal acceleration, angular rate and tail incidence are presented in Figures 3.19 through 3.21. A close observation of the above pole-zero and time response plots of the discrete yaw estimator design indicates that they are very close to those of the discrete classical design found in the previous chapter.

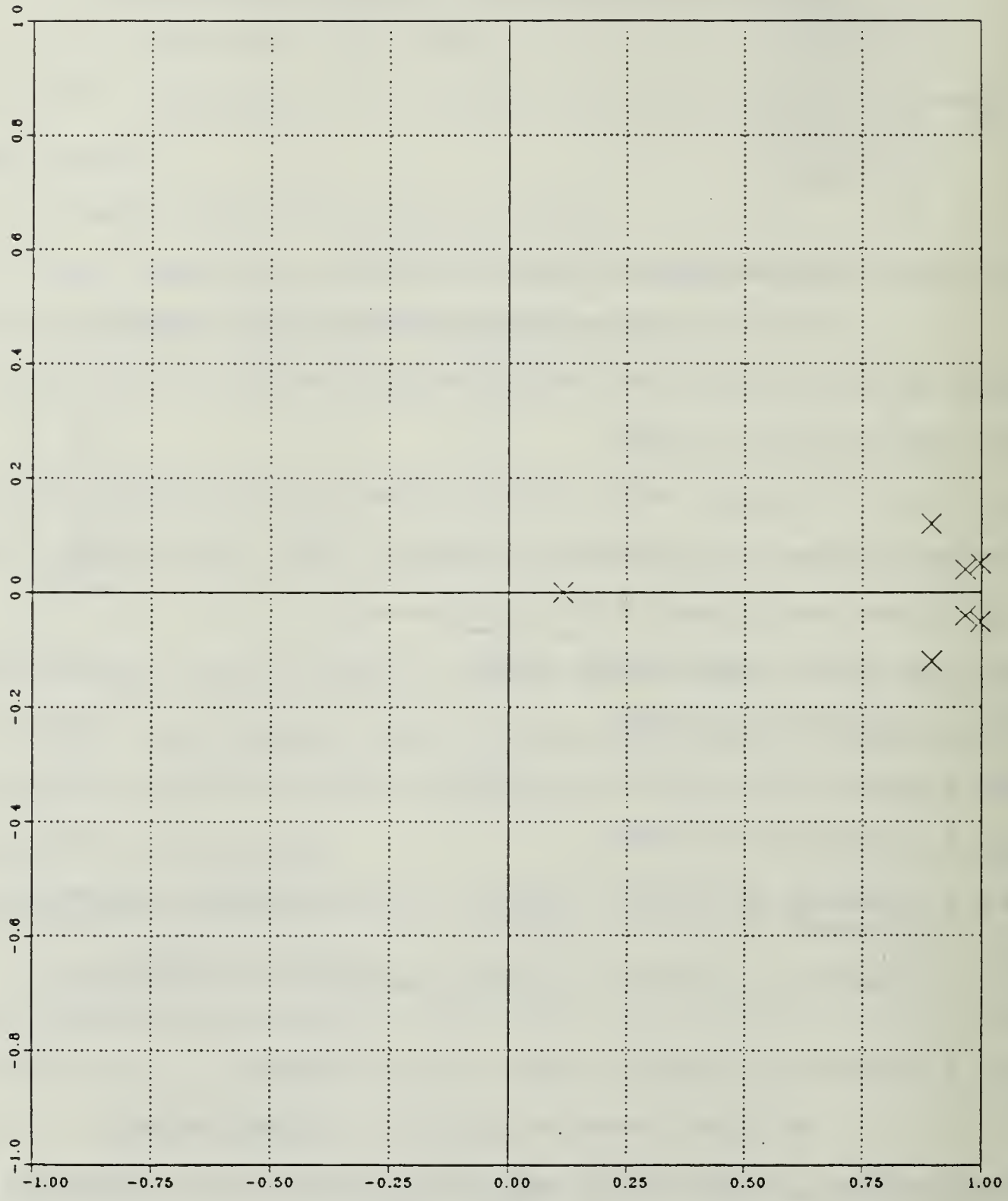

Figure 3.18 Pole-Zero Plot; Uncoupled Yaw Channel Autopilot; Estimator Design; Discrete Closed Loop System; Elliptical Airframe

c. Simplified Design

The discrete estimator designed autopilot of the previous section can be simplified by reducing the returning gain loops. This can be accomplished by placing zeros into appropriate elements of the estimator gain vector:

$$\underline{K} = \begin{bmatrix} -0.0034 \\ 0 \\ 0 \\ -0.0177 \\ 0 \\ -0.0017 \\ -0.0240 \end{bmatrix} \qquad \text{(III.C.1-20)}$$

The pole-zero and time response plots of the resulting simplified estimator yaw autopilot, shown in Figures 3.22 through 3.25, do not present significant differences from the corresponding plots of the discrete classical design, apart from the overshoot which was slightly increased. The discrete closed loop system is again stable, since the z-plane closed loop poles are:

$z_1 = 0.117117$ (III.C.1-21)

$z_2 = 0.918434+j0.122898$ (III.C.1-22)

$z_3 = 0.918434-j0.122898$ (III.C.1-23)

$z_4 = 0.998422+j0.0510954$ (III.C.1-24)

$z_5 = 0.998422-j0.0510954$ (III.C.1-25)

$z_6 = 0.962965+j0.0357874$ (III.C.1-26)

$z_7 = 0.962965-j0.0357874$ (III.C.1-27)

2. Uncoupled Roll Channel for Circular Airframe

a. Estimator Gain Vector

Following the same procedure as in the yaw channel case apart from the use of:

(1) The transpose of the discrete roll system plant matrix

(2) S-Plane poles slightly faster than those of the continuous open loop roll system, that is:

$$S_1 = -184.795 \qquad \text{(III.C.2-1)}$$

$$S_2 = -9.26097+j28.4098 \qquad \text{(III.C.2-2)}$$

$$S_3 = -9.26097-j28.4098 \qquad \text{(III.C.2-3)}$$

$$S_4 = -2.47608+j2.71152 \qquad \text{(III.C.2-4)}$$

$$S_5 = -2.47608-j2.71152 \qquad \text{(III.C.2-5)}$$

$$S_6 = -8.99209 \qquad \text{(III.C.2-6)}$$

$$S_7 = -5.20032 \qquad \text{(III.C.2-7)}$$

the estimator gain vector for the circular airframe roll channel is obtained:

$$\underline{K} = \begin{bmatrix} 0.004 \\ 0 \\ 0 \\ -0.0002 \\ 0.0003 \\ 0 \\ -0.0492 \end{bmatrix} \qquad \text{(III.C.2-8)}$$

b. Design Approach and Analysis

The discrete estimator designed roll autopilot can be found by introducing the estimator gain vector of (III.C.2-8) into the original system.

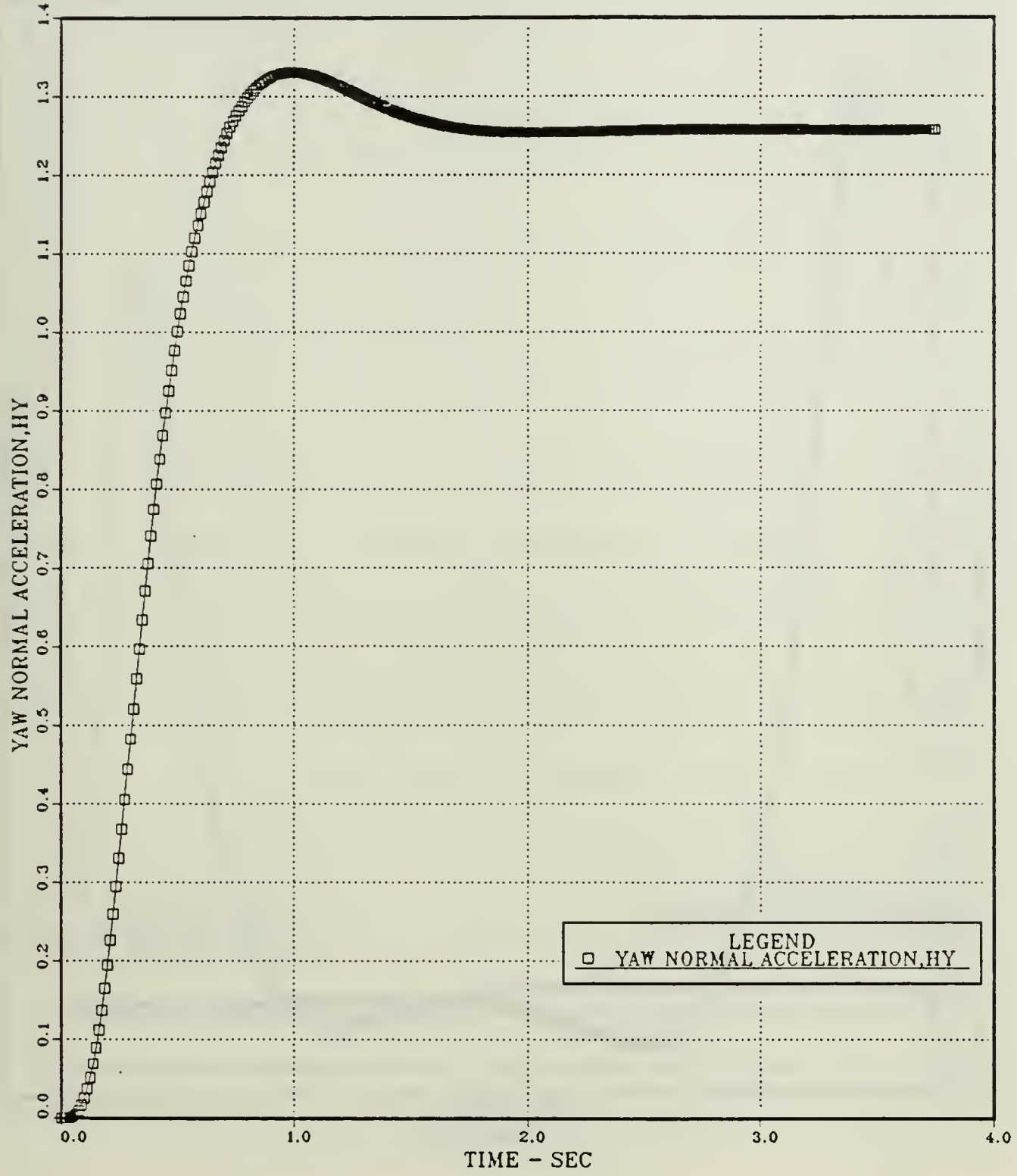

Figure 3.19 Yaw Normal Acceleration vs Time; Uncoupled Yaw Channel Autopilot; Estimator Design; Discrete Closed Loop System; Elliptical Airframe

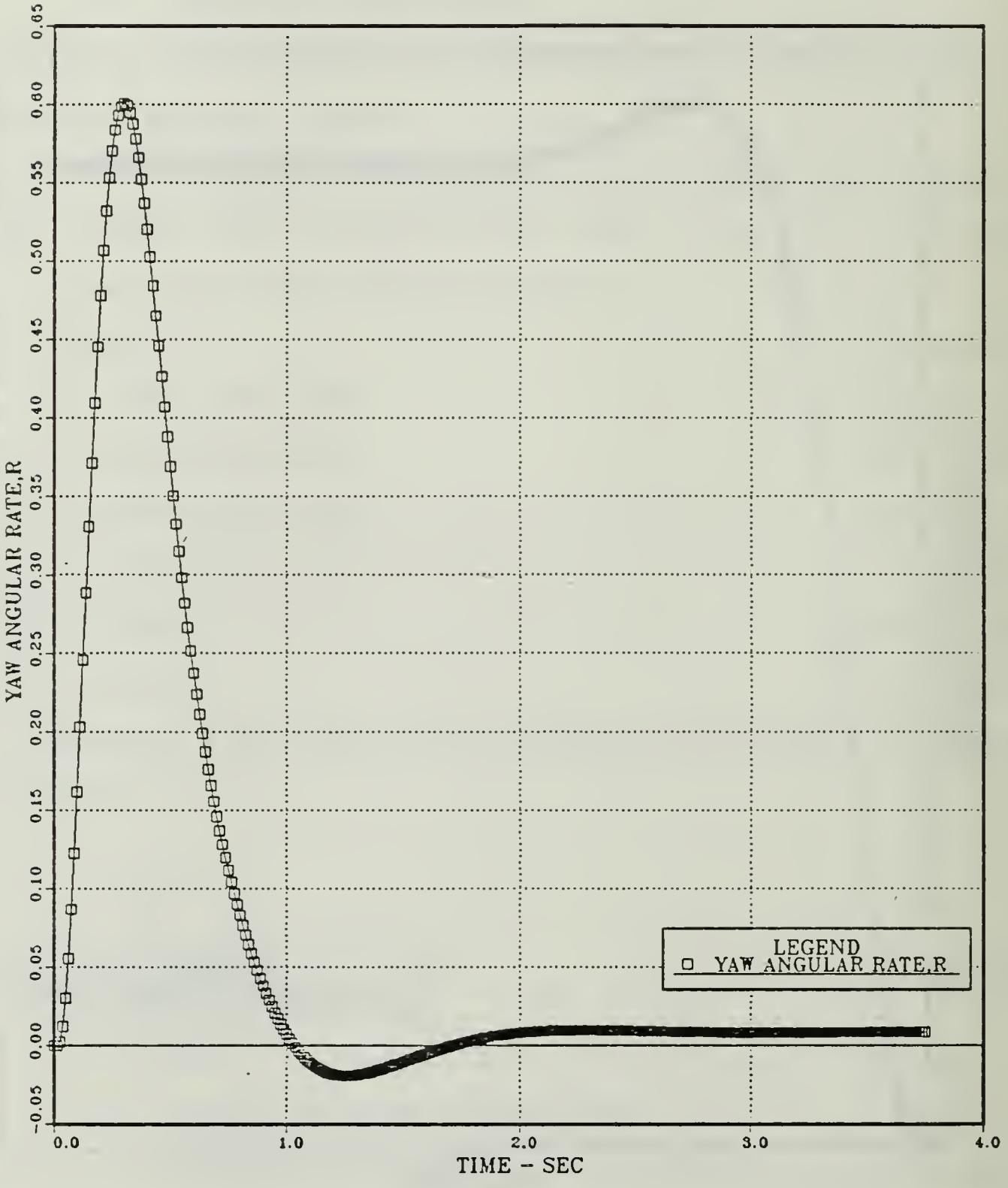

Figure 3.20 Yaw Angular Rate vs Time; Uncoupled Yaw Channel Autopilot; Estimator Design; Discrete Closed Loop System; Elliptical Airframe

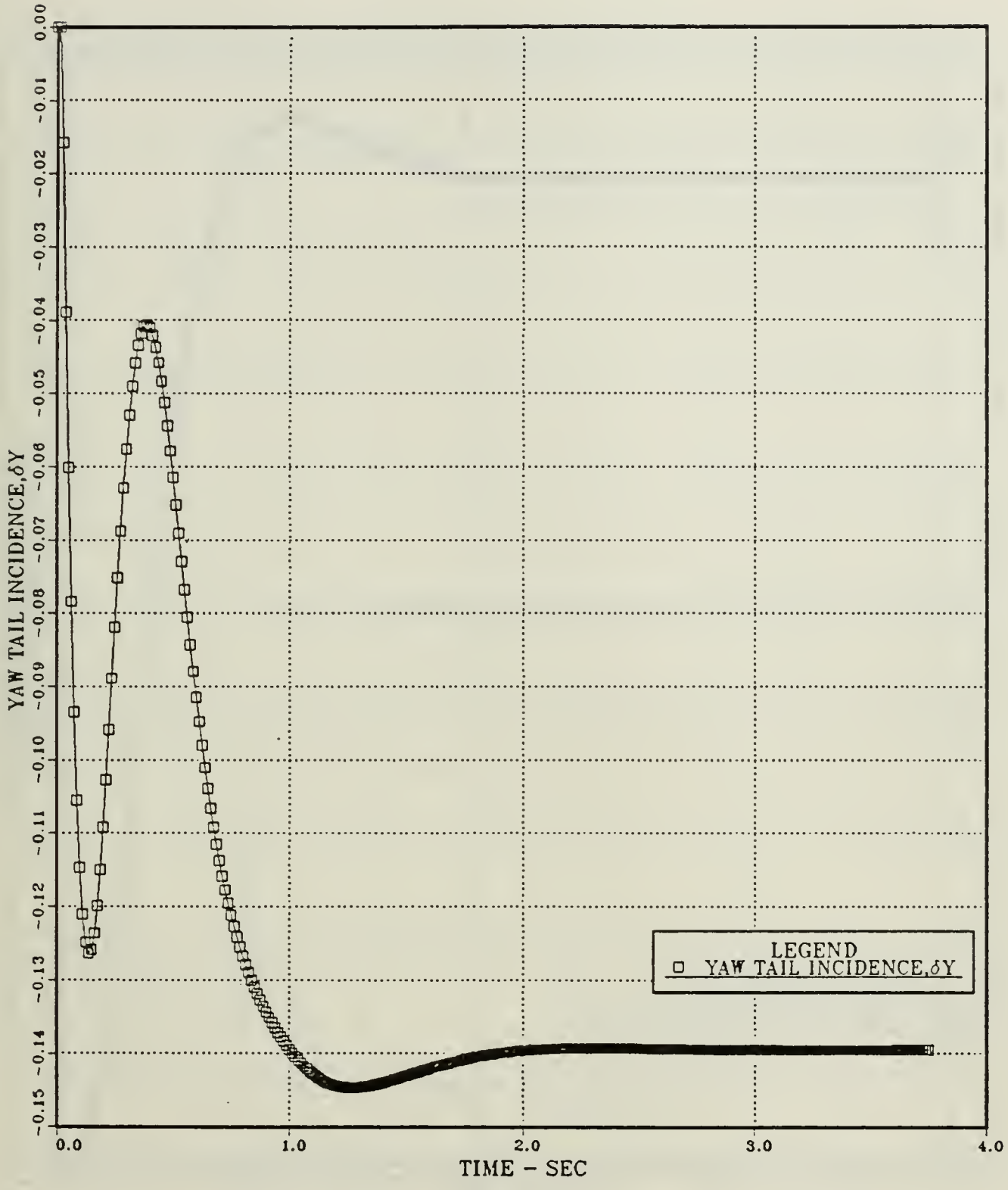

Figure 3.21 Yaw Tail Incidence vs Time; Uncoupled Yaw Channel Autopilot; Estimator Design; Discrete Closed Loop System; Elliptical Airframe

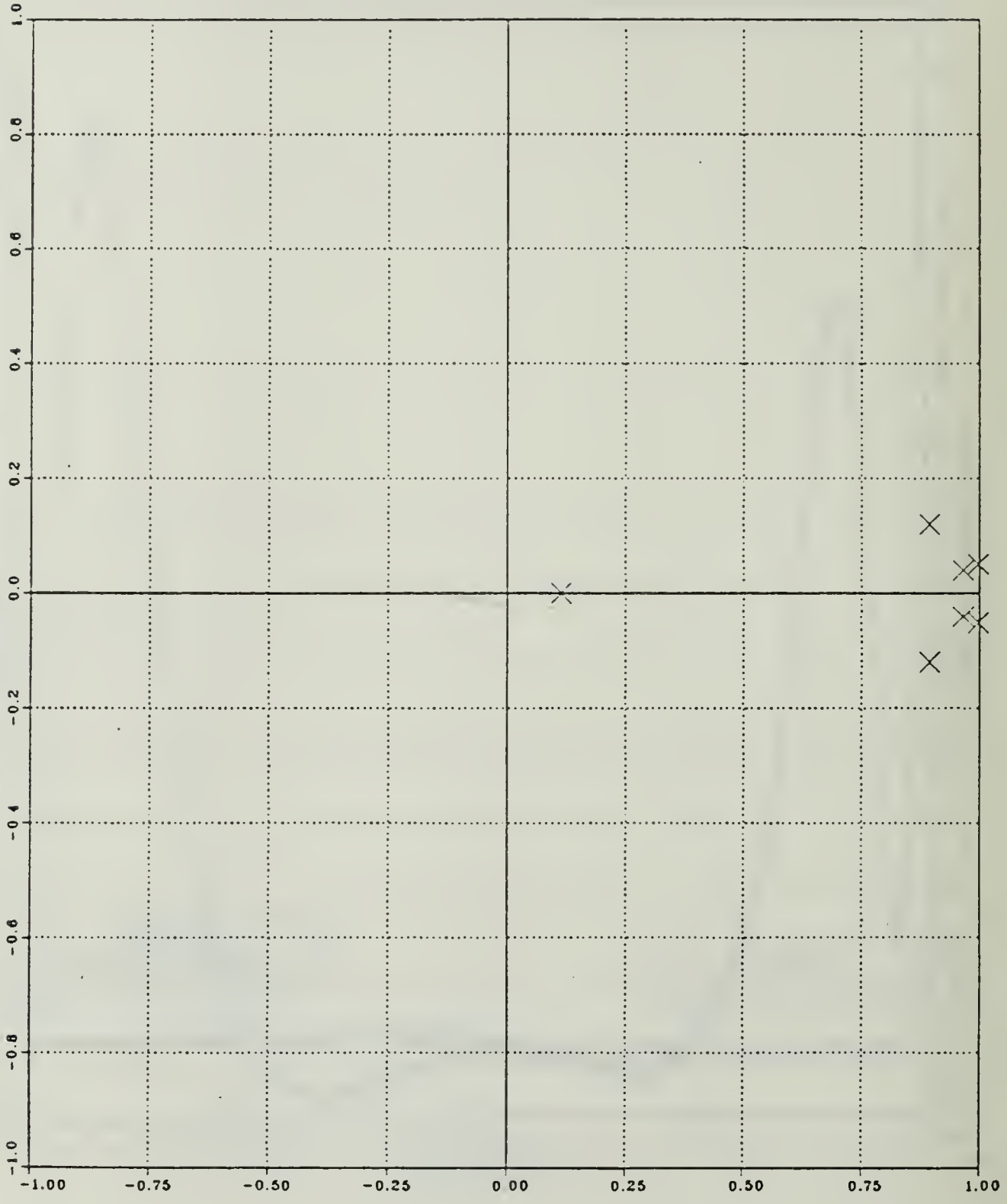

Figure 3.22 Pole-Zero Plot; Uncoupled Yaw Channel Autopilot; Simplified Estimator Design; Discrete Closed Loop System; Elliptical Airframe

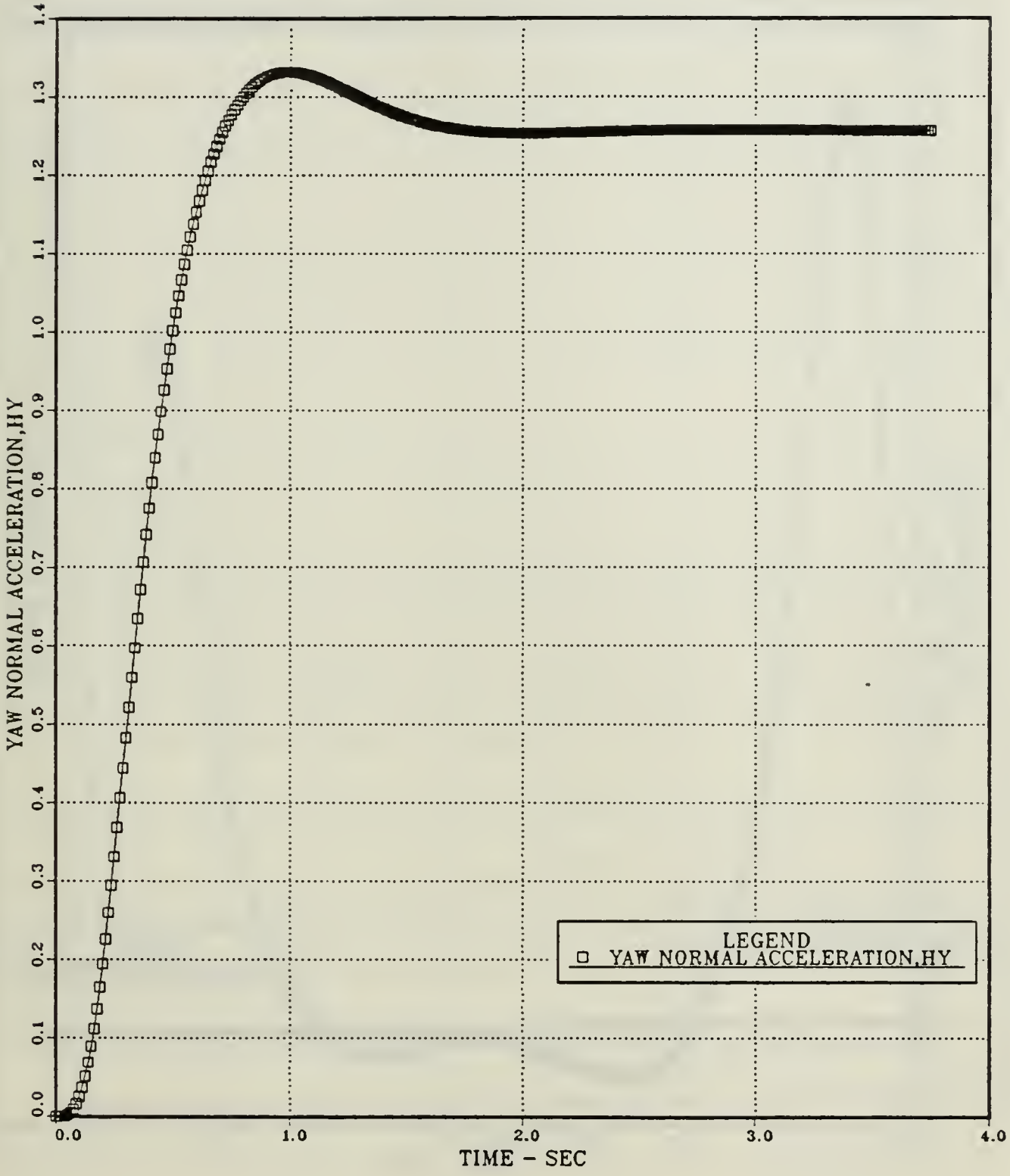

Figure 3.23 Yaw Normal Acceleration vs Time; Uncoupled Yaw Channel Autopilot; Simplified Estimator Design; Discrete Closed Loop System; Elliptical Airframe

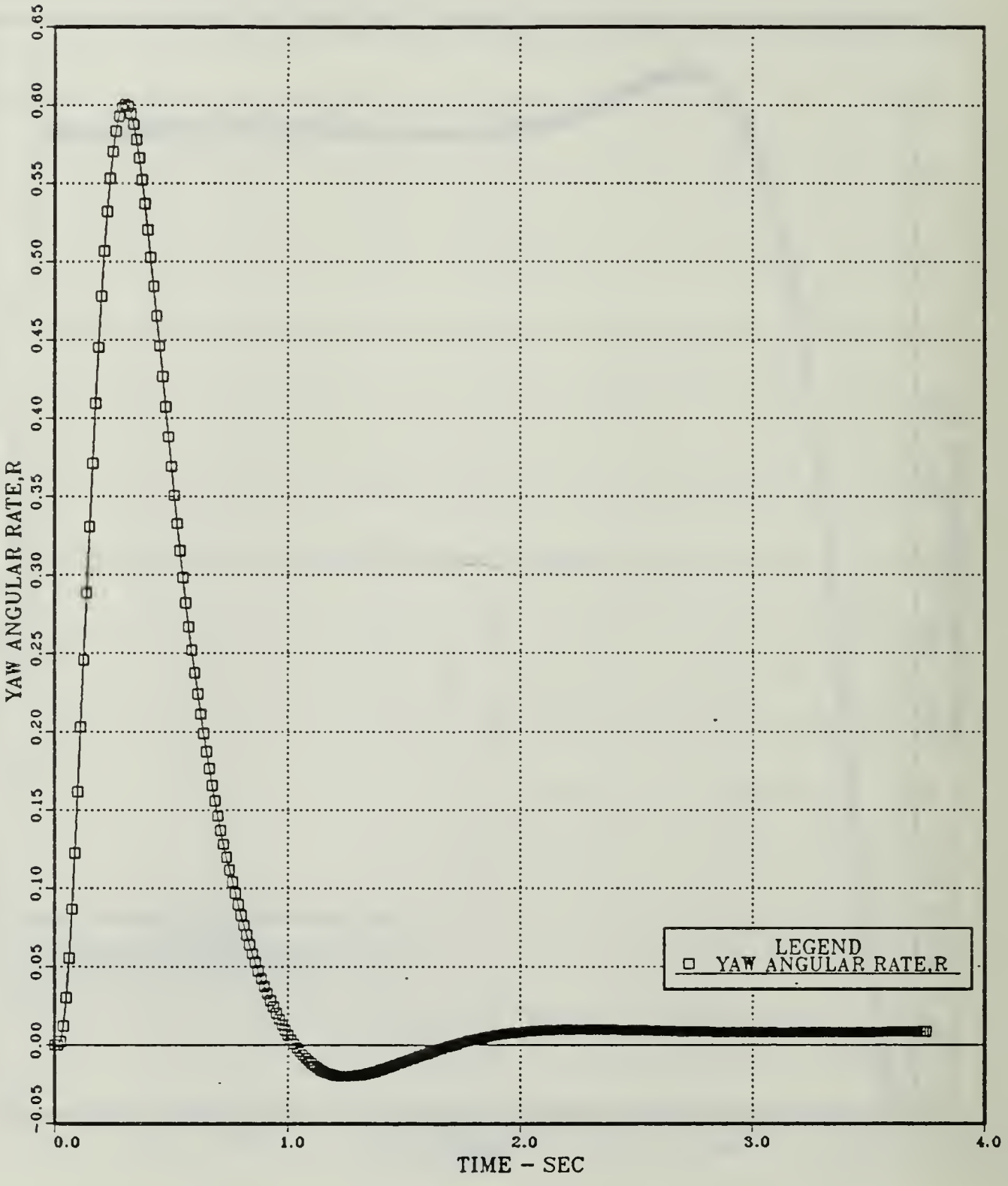

Figure 3.24 Yaw Angular Rate vs Time; Uncoupled Yaw Channel Autopilot; Simplified Estimator Design; Discrete Closed Loop System; Elliptical Airframe

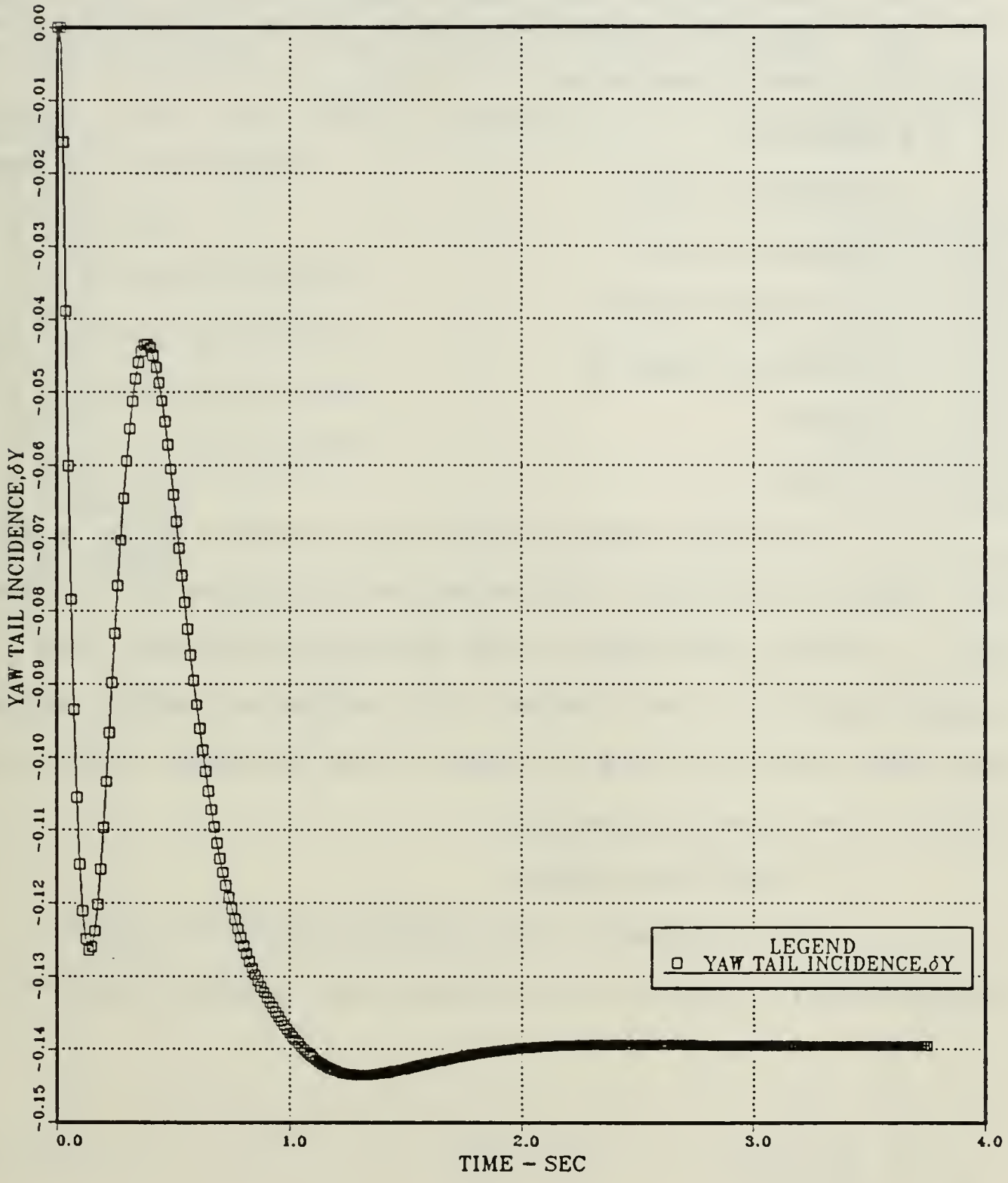

Figure 3.25 Yaw Tail Incidence vs Time; Uncoupled Yaw Channel Autopilot; Simplified Estimator Design; Discrete Closed Loop System; Elliptical Airframe

The pole-zero plot of Figure 3.26 indicates that the discrete closed loop system is stable, since the z-plane closed loop poles were found to be:

$z_1 = 0.0967149$ (III.C.2-9)

$z_2 = 0.830876+j0.31913$ (III.C.2-10)

$z_3 = 0.830876-j0.31913$ (III.C.2-11)

$z_4 = 0.970259+j0.0325175$ (III.C.2-13)

$z_5 = 0.970259-j0.0325179$ (III.C.2-14)

$z_6 = 0.894774$ (III.C.2-15)

$z_7 = 0.937225$ (III.C.2-16)

The time response plots of the roll angle, angular rate and tail incidence are presented in Figures 3.27 through 3.29. A close observation of the above pole-zero and time response plots for the discrete roll estimator design indicates that they are very close to those of the discrete classical design found in the previous chapter.

c. Simplified Design

The estimator roll designed autopilot can be simplified by reducing the returning gain loops as follows:

$$\underline{K} = \begin{bmatrix} 0 \\ 0 \\ 0 \\ 0.0178 \\ -0.0179 \\ -1.499 \\ 0 \end{bmatrix} \quad \text{(III.C.2-17)}$$

The pole and time response plots of the resulting simplified estimator roll autopilot, shown in Figures 3.30

through 3.33, do not present significant differences from the corresponding plots of the discrete classical design. The discrete closed loop system is again stable, since the z-plane closed loop poles are:

$z_1 = 0.0992745$ (III.C.2-18)

$z_2 = 0.836632+j0.305719$ (III.C.2-19)

$z_3 = 0.836632-j0.305719$ (III.C.2-20)

$z_4 = 0.967647+j0.0334948$ (III.C.2-21)

$z_5 = 0.967647-j0.0334948$ (III.C.2-22)

$z_6 = 0.895937$ (III.C.2-23)

$z_7 = 0.938256$ (III.C.2-24)

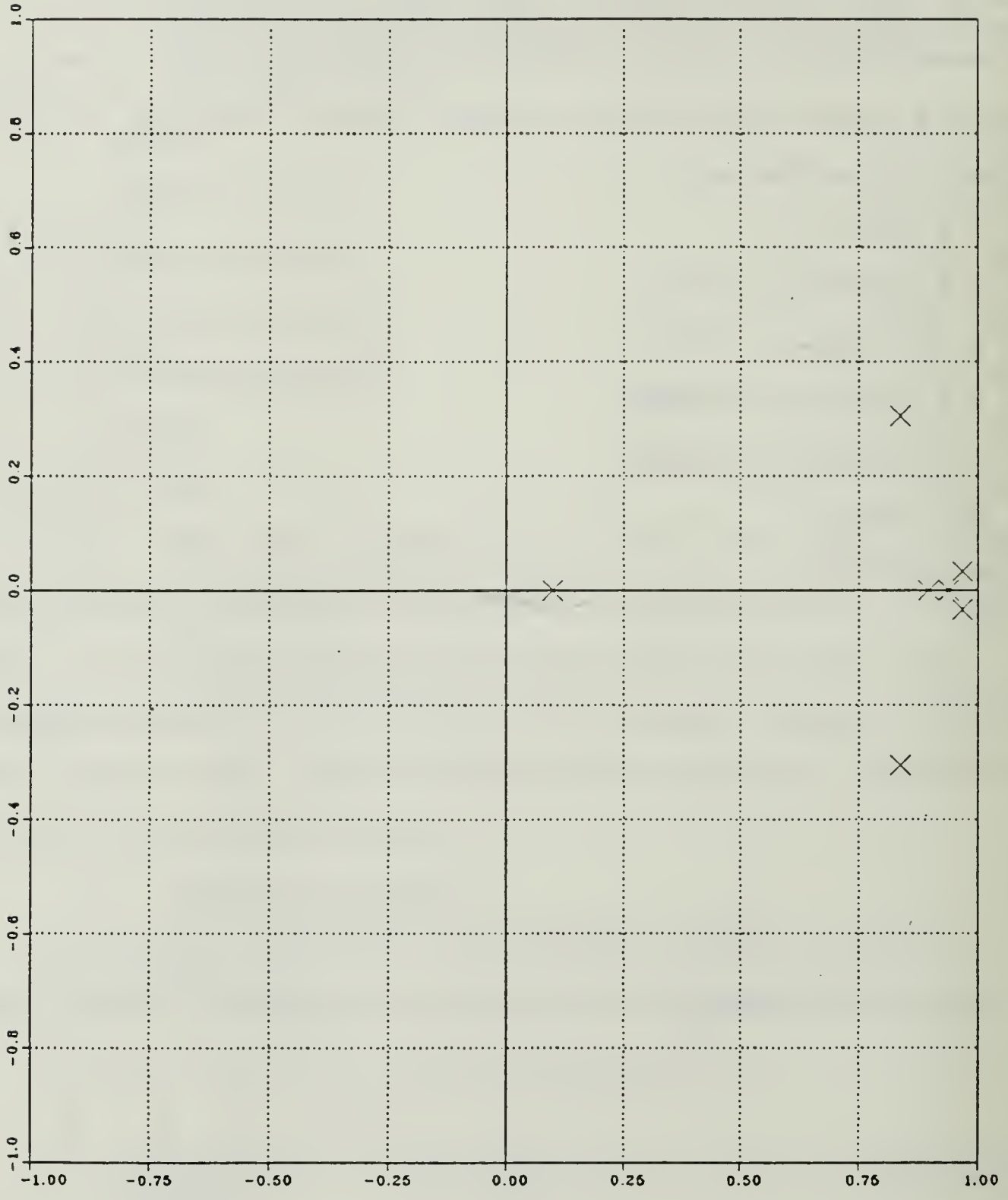

Figure 3.26 Pole-Zero Plot; Uncoupled Roll Channel Autopilot; Estimator Design; Discrete Closed Loop System; Circular Airframe

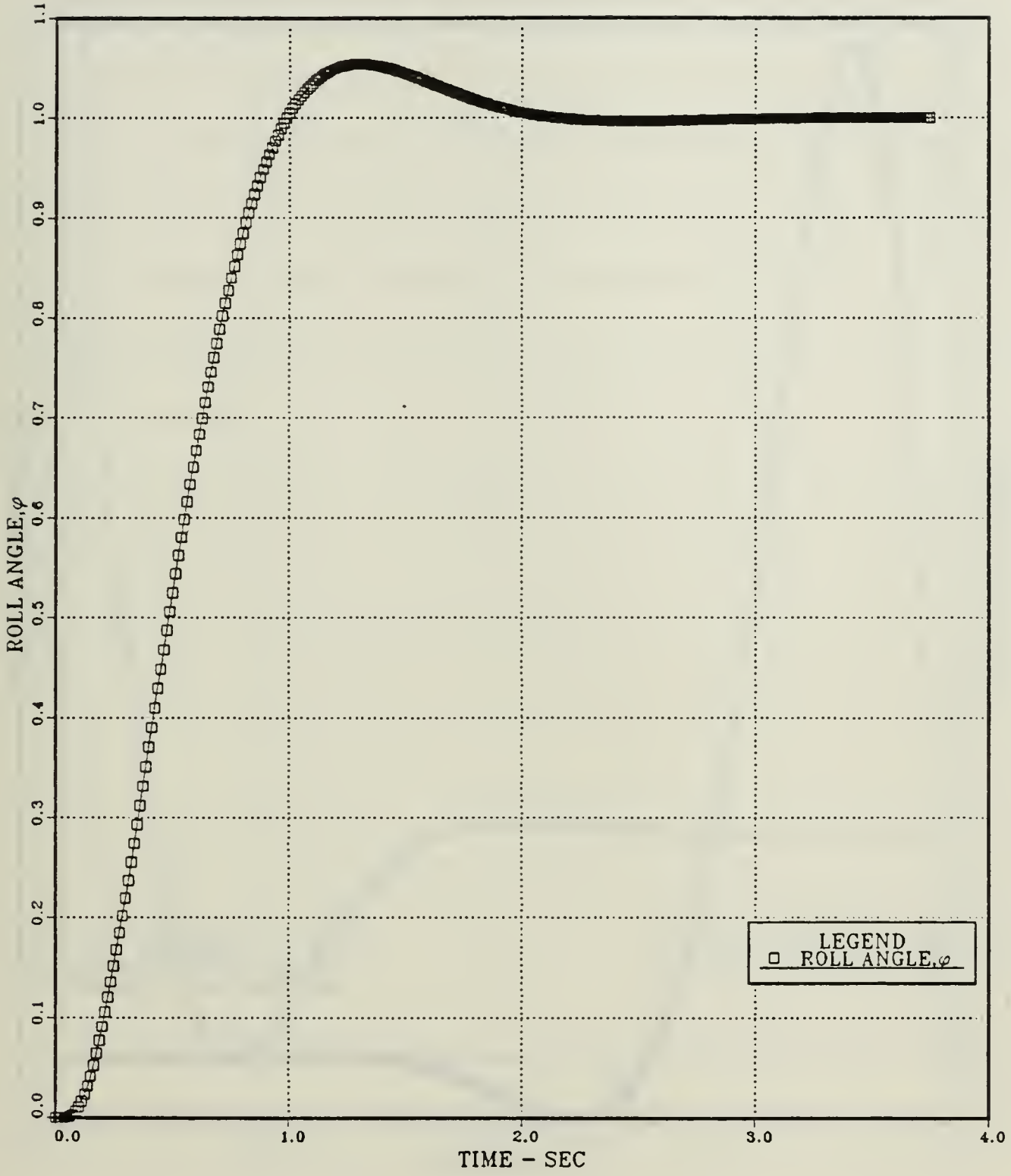

Figure 3.27 Roll Angle vs Time; Uncoupled Roll Channel Autopilot; Estimator Design; Discrete Closed Loop System; Circular Airframe

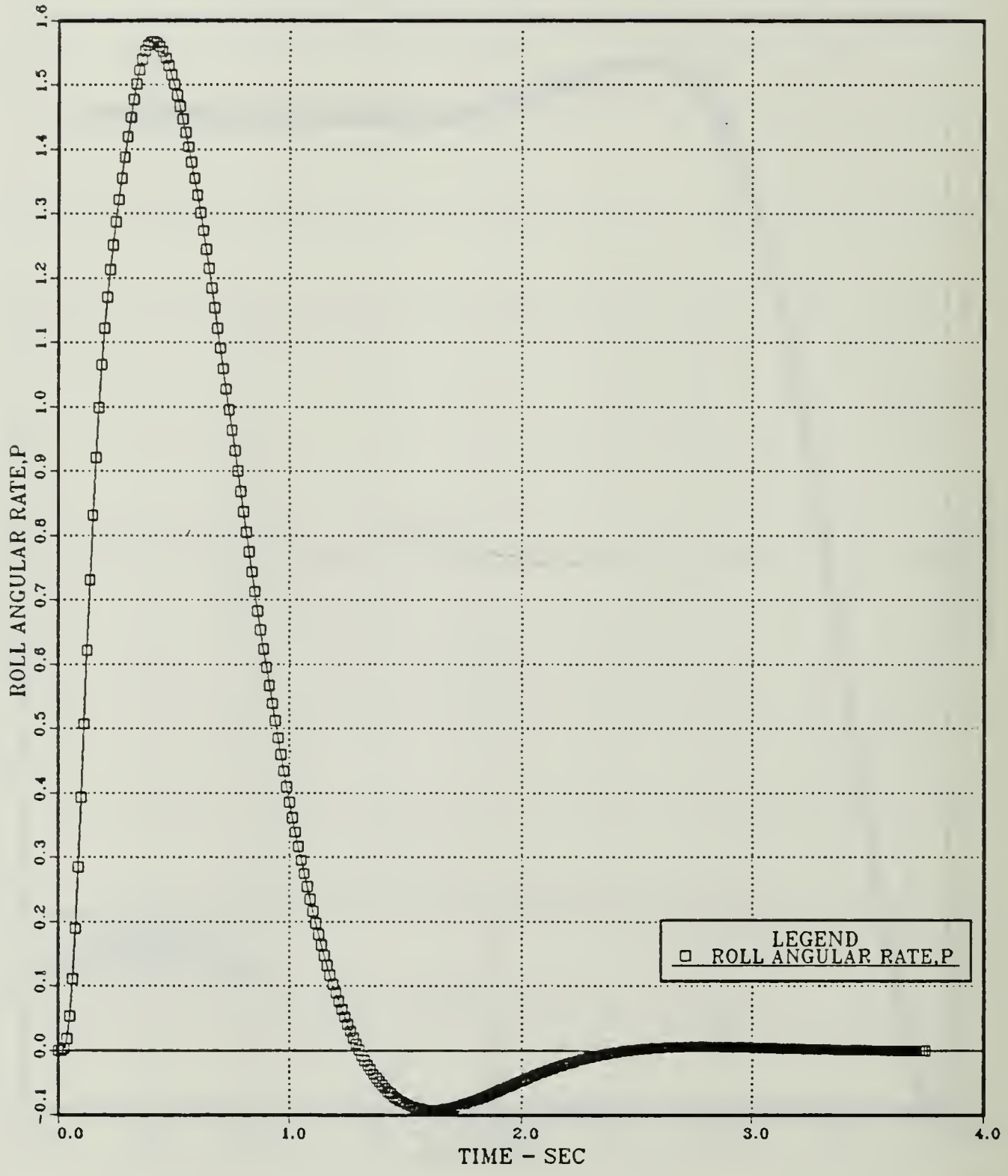

Figure 3.28 Roll Angular vs Time; Uncoupled Roll Channel Autopilot; Estimator Design; Discrete Closed Loop System; Circular Airframe

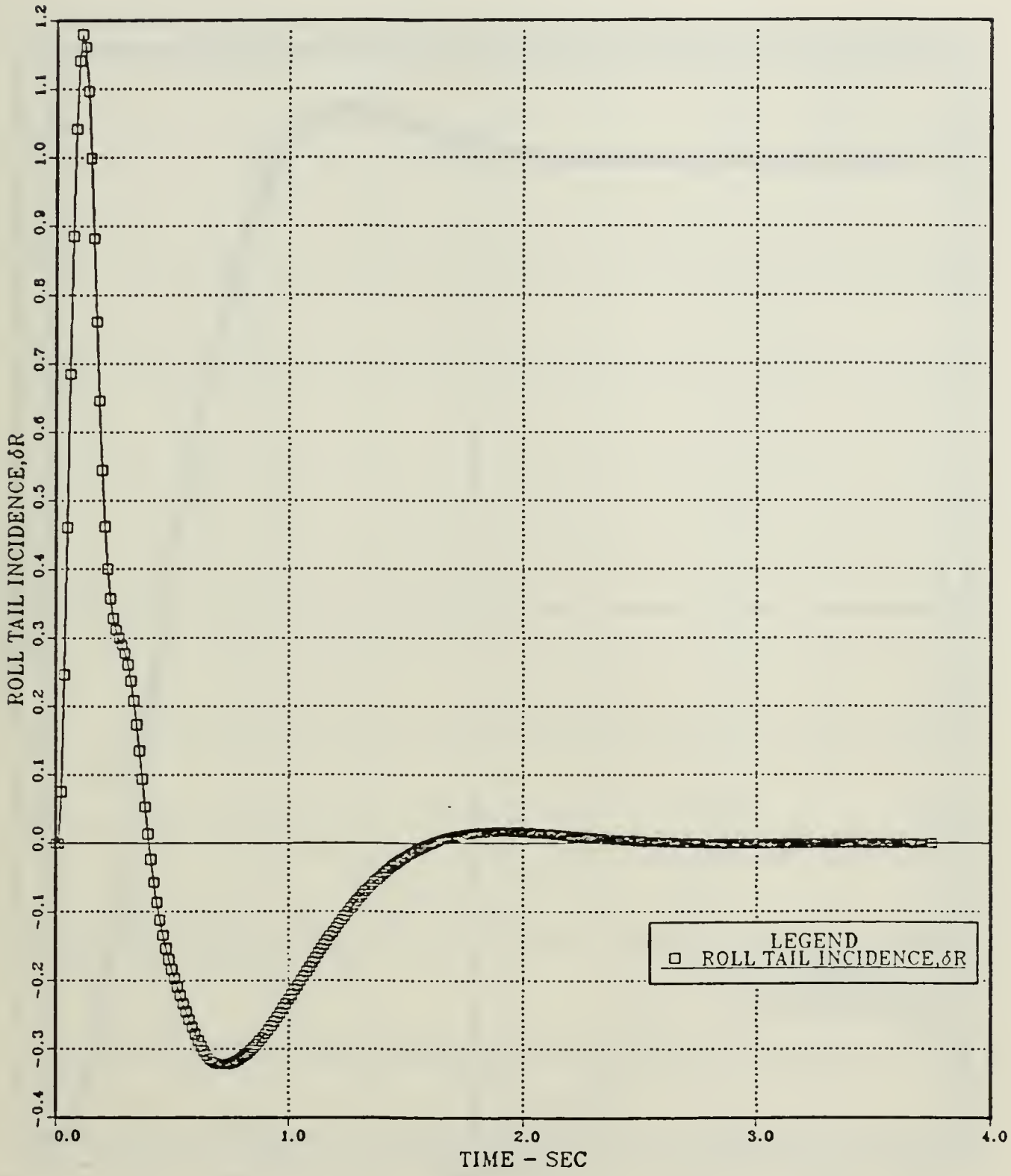

Figure 3.29 Roll Tail Incidence vs Time; Uncoupled Roll Channel Autopilot; Estimator Design; Discrete Closed Loop System; Circular Airframe

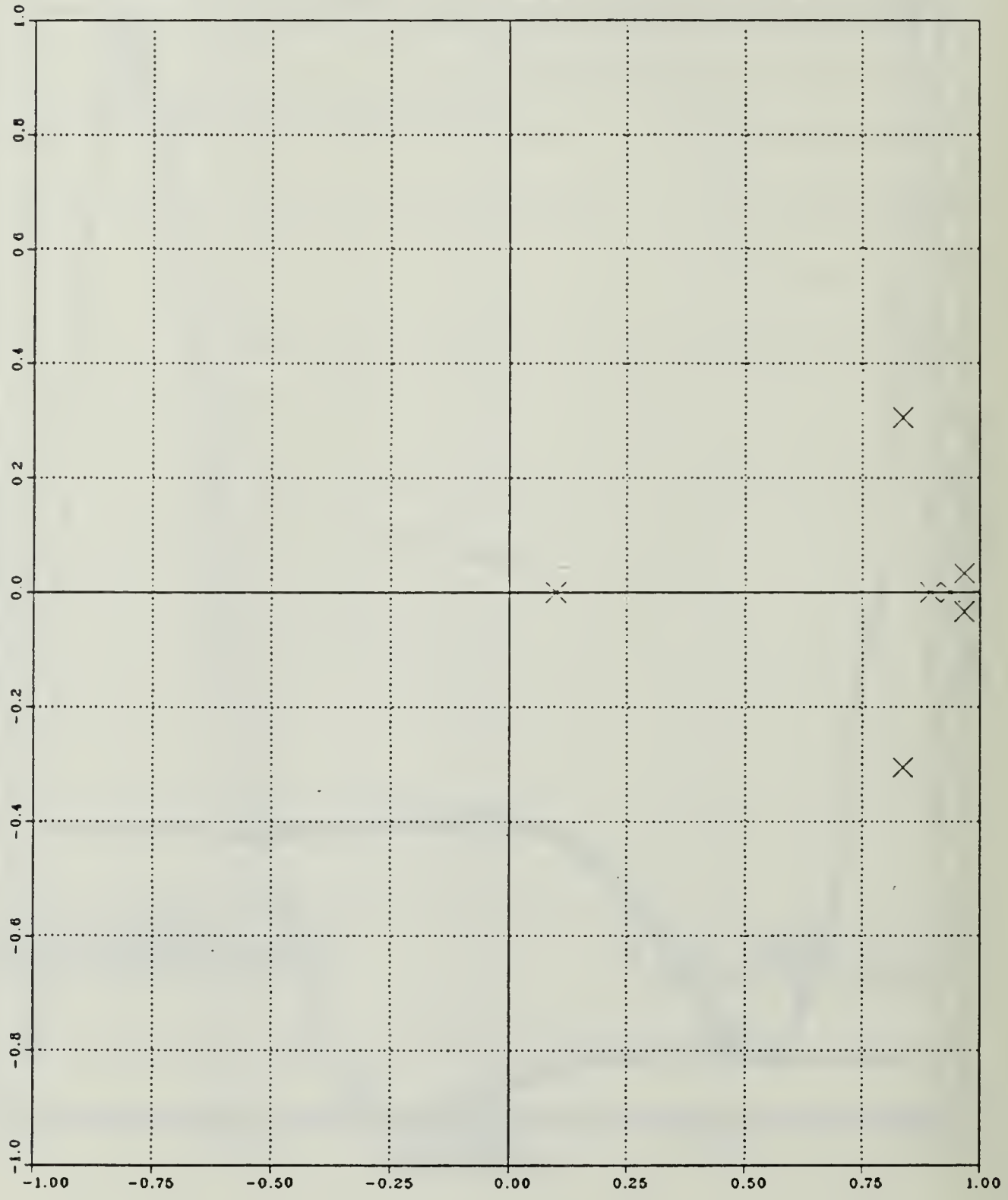

Figure 3.30 Pole-Zero Plot; Uncoupled Roll Channel Autopilot; Simplified Estimator Design; Discrete Closed Loop System; Circular Airframe

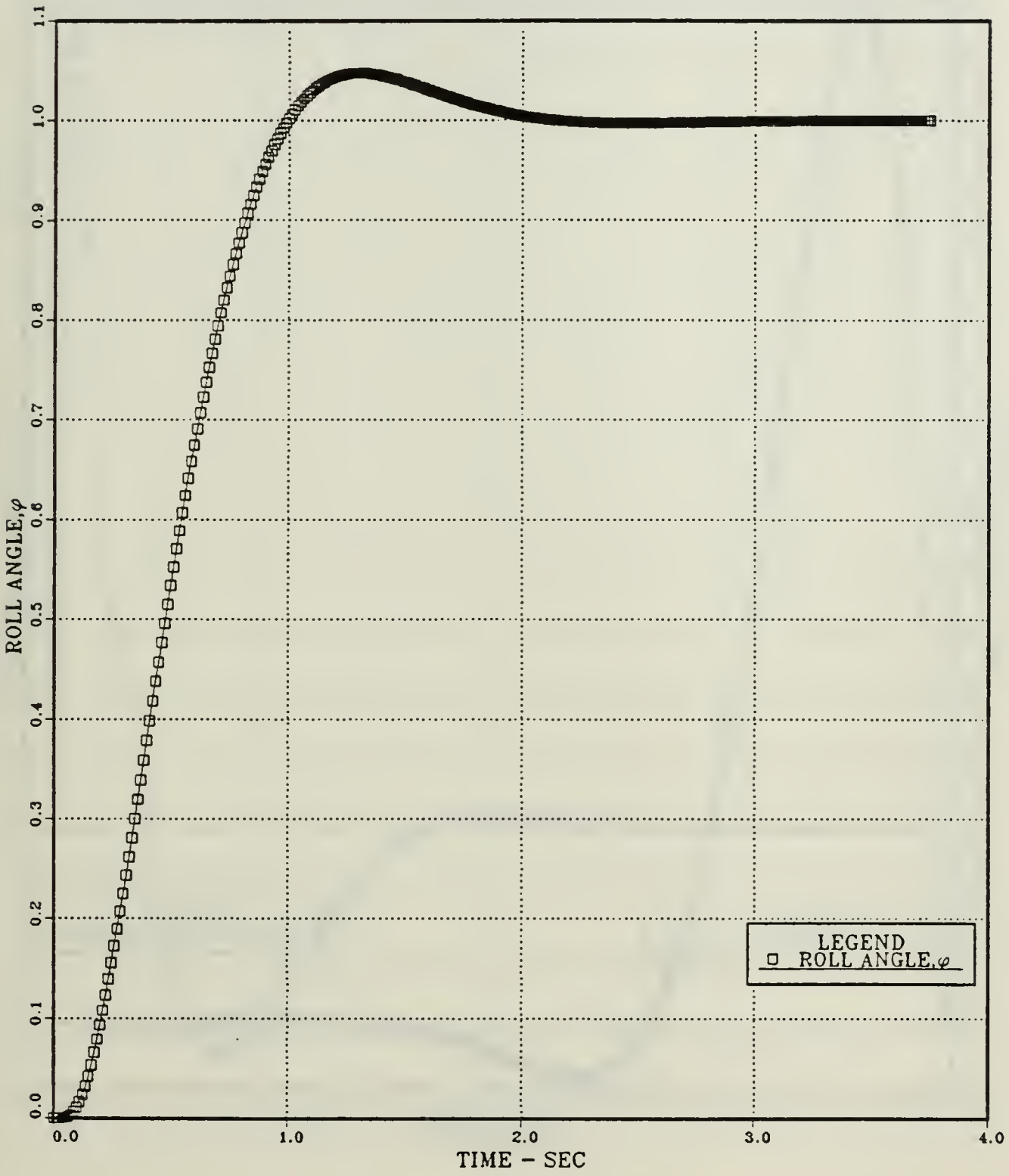

Figure 3.31 Roll Angle vs Time; Uncoupled Roll Channel Autopilot; Simplified Estimator Design; Discrete Closed Loop System; Circular Airframe

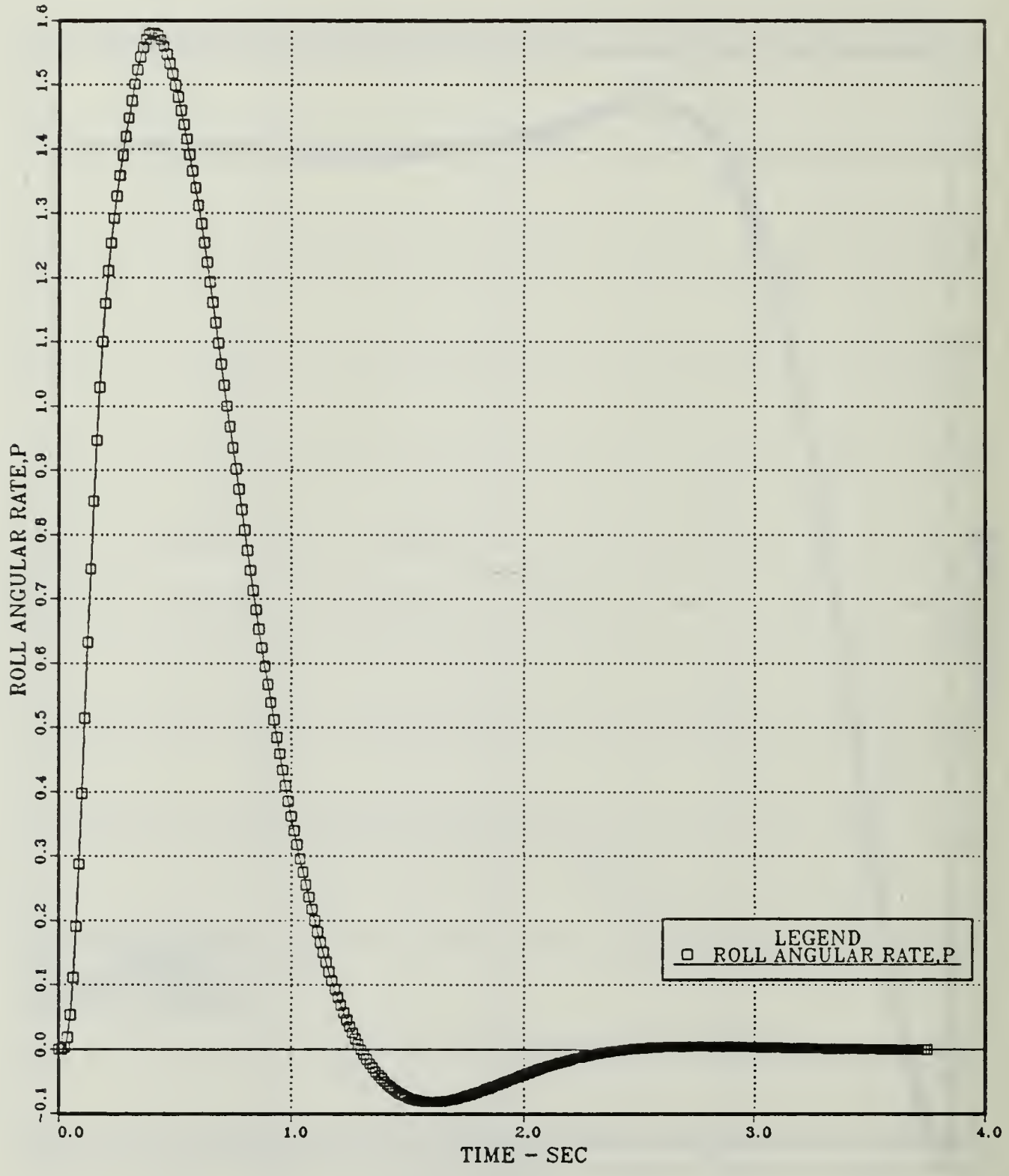

Figure 3.32 Roll Angular Rate vs Time; Uncoupled Roll Channel Autopilot; Simplified Estimator Design; Discrete Closed Loop System; Circular Airframe

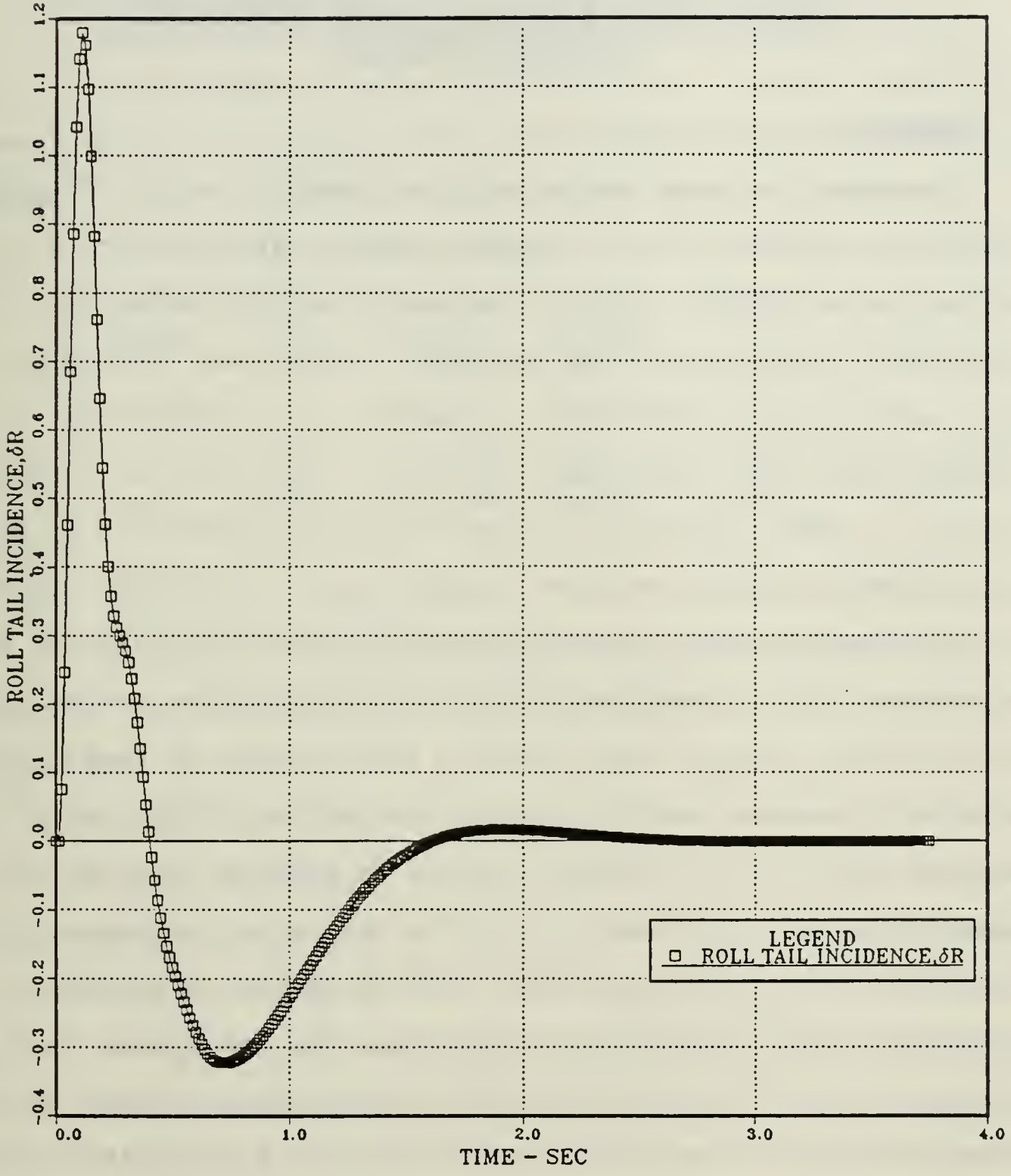

Figure 3.33 Roll Tail Incidence vs Time; Uncoupled Roll Channel Autopilot; Simplified Estimator Design; Discrete Closed Loop System; Circular Airframe

IV. MODERN CONTROL DESIGN AND ROBUSTNESS ANALYSIS OF COUPLED PITCH AND ROLL CHANNEL AUTOPILOT CIRCULAR AIRFRAME

A. GENERAL

The present chapter deals with the modern control design and robustness analysis of the discrete coupled pitch and roll channel autopilot for the circular airframe configuration. The continuous open loop coupled autopilot whose plant system and input matrices are presented in Appendix G is obtained by coupling the linear uncoupled pitch [Ref. 10] and roll (Table IV) channels. Then, utilizing analog-to-digital conversion by the aid of ORACLS program and for a sample period of 0.0125 seconds, the seventeenth-order discrete coupled system with matrices shown in Appendix H is formulated. Next, introducing the control-law and estimator designs were obtained and analyzed in terms of their transient responses and the application of the POPLAR design program [Ref. 7]. The POPLAR program is applied in order to employ singular value analysis and the use of an optimization routine to aid in pole placement control design of the above discussed linear multivariable systems. The robustness of the system is also considered by establishing singular value levels which correspond to multiloop gain and phase margins determined from the universal gain phase system diagram developed by Newsom and Mukhapadhyay at NASA Langley.

B. DISCRETE COUPLED STATE-FEEDBACK DESIGN

1. Design Approach and Analysis

The discrete coupled state-feedback designed autopilot is formulated by introducing into the original control system of Appendix H the following combined pitch [Ref. 10] and roll (III.B.1-5) control-law gain vector.

$$\begin{bmatrix} -0.0188 & -0.0279 & -0.0042 & 0.029 & 0.0041 & 0 \\ 0.0001 & 1.7732 & -2.0162 & 0.0131 & 0 & 0 \\ 0 & 0 & 0 & 0 & 0 & \\ 0 & 0 & 0 & 0 & 0 & 0 \\ 0 & 0 & 0 & 0 & 0 & 0.0004 \\ 0 & 0.0178 & -0.0179 & -1.499 & 0.0023 & \end{bmatrix} \quad \text{(IV.B.1-1)}$$

The pole-zero plot of Figure 4.1 indicates that the discrete coupled system is marginally stable, since the z-plane closed loop poles are:

$z_1 = 0.13446+j0.0320974$ (IV.B.1-2)

$z_2 = 0.13446-j0.0320974$ (IV.B.1-3)

$z_3 = 0.89699+j0.0906457$ (IV.B.1-4)

$z_4 = 0.89699-j0.0906457$ (IV.B.1-5)

$z_5 = 0.955624+j0.0299994$ (IV.B.1-6)

$z_6 = 0.953624-j0.0299994$ (IV.B.1-7)

$z_7 = 0.998202$ (IV.B.1-8)

$z_8 = 1$ (IV.B.1-9)

$z_9 = 0.995608+j0.0830713$ (IV.B.1-10)

$z_{10} = 0.995608-j0.0830713$ (IV.B.1-11)

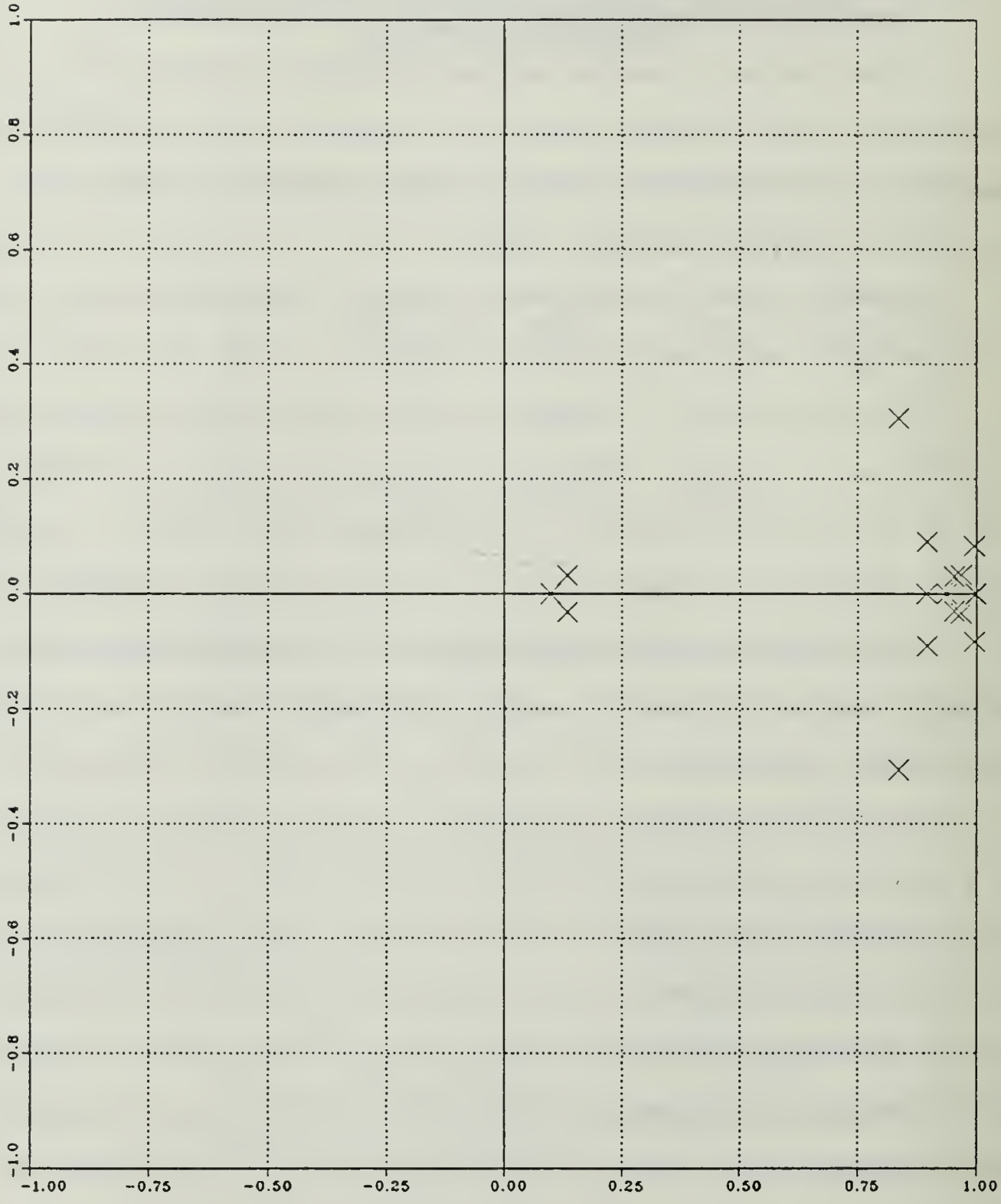

Figure 4.1 Pole-Zero Plot; Coupled Pitch and Roll Channel Autopilot; State-Feedback Design; Discrete Closed Loop System; Circular Airframe

z_{11} = 0.0993086 (IV.B.1-12)

z_{12} = 0.836555+j0.306107 (IV.B.1-13)

z_{13} = 0.836553-j0.306107 (IV.B.1-14)

z_{14} = 0.967788+j0.0334452 (IV.B.1-15)

z_{15} = 0.967788-j0.0334452 (IV.B.1-16)

z_{16} = 0.89573+j0.938133 (IV.B.1-17)

z_{17} = 0.89573-j0.938133 (IV.B.1-18)

The time response plots of the roll angle, angular rate and tail incidence are presented in Figures 4.2 through 4.4. A close observation of these plots indicate that they are identical with those of the discrete uncoupled state-feedback design of the previous chapter.

2. Robustness Analysis

Executing the POPLAR design program of [Ref. 7] with inputs the data presented in Appendix I, the minimum additive input (MIN ADD IN SV) and output (SVADMO) singular values were computed from a frequency range from 0 to 200 rad/sec.

Figures 4.5 and 4.6 which are plots of SVADMO and MIN ADD IN SV versus frequency indicate that the discrete coupled state-feedback design is robust. It is noted that for very low frequencies the values of SVADMO are above 0.8680.

Finally, in terms of optimization results, the ordered computed eigenvalues are:

z_1 = 0.07717 (IV.B.2-1)

z_2 = 0.09855 (IV.B.2-2)

z_3 = 0.25923 (IV.B.2-3)

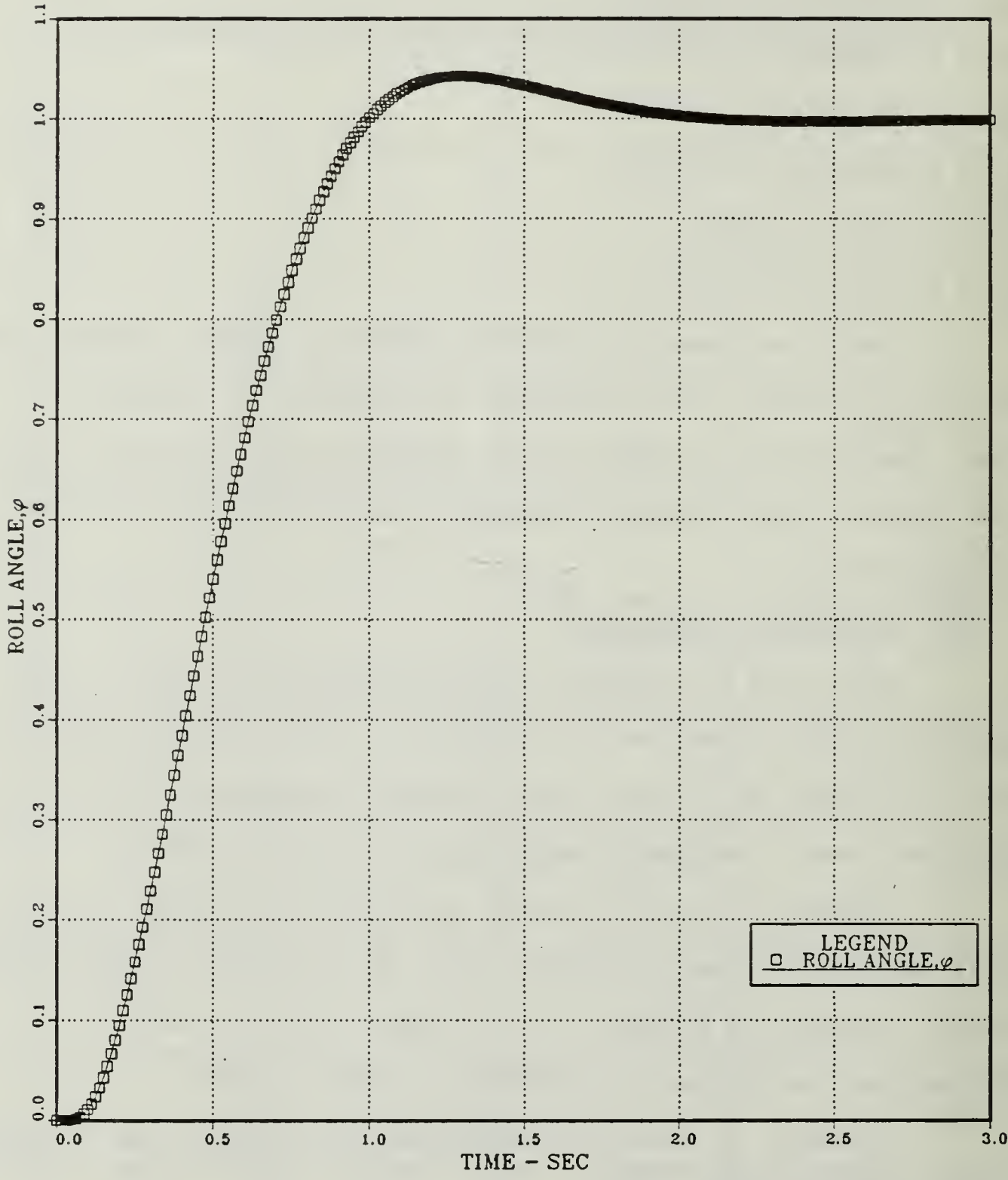

Figure 4.2 Roll Angle vs Time; Coupled Pitch and Roll Channel Autopilot; State-Feedback Design; Discrete Closed Loop System; Circular Airframe

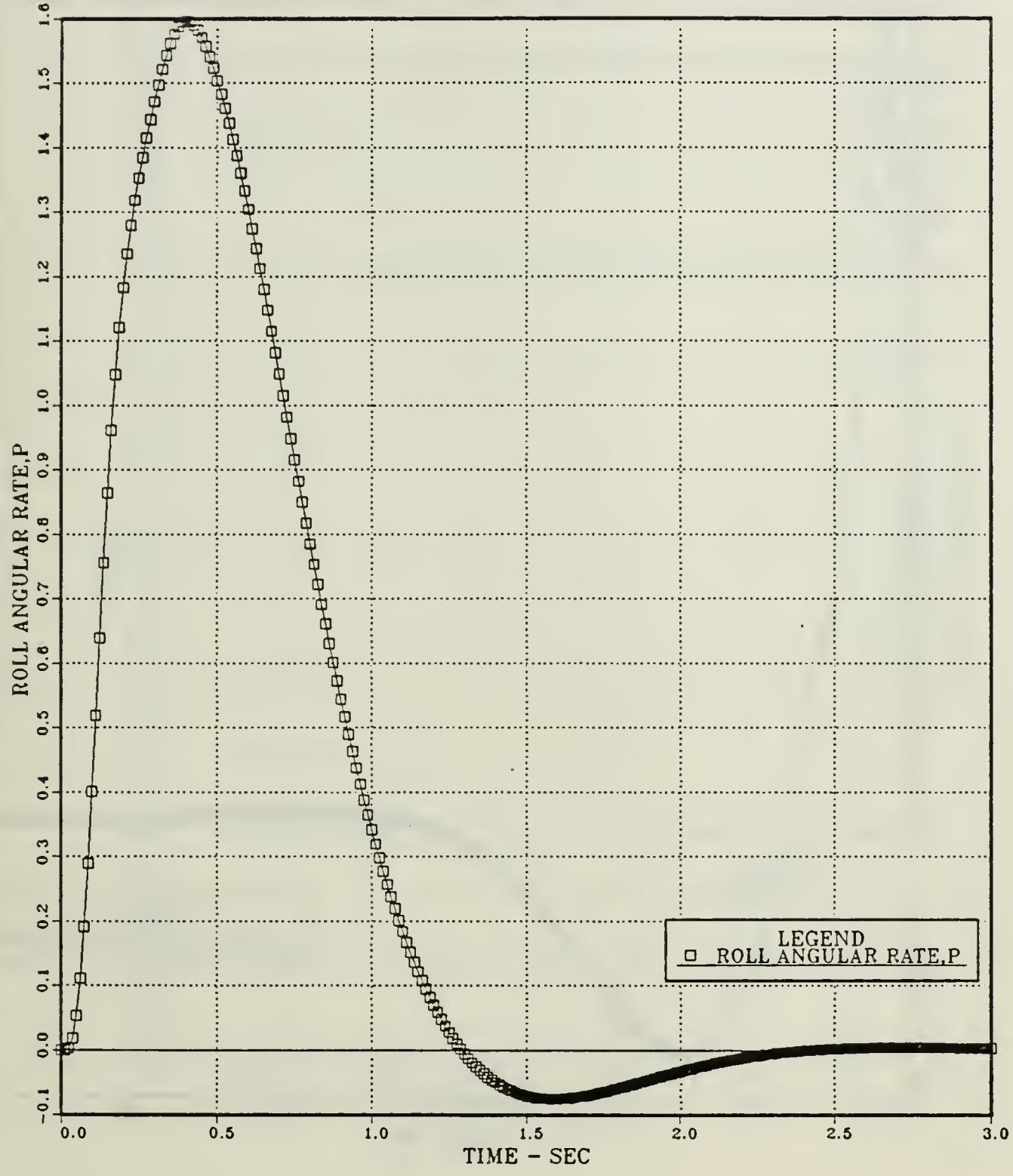

Figure 4.3 Roll Angular Rate vs Time; Coupled Pitch and Roll Channel Autopilot; State-Feedback Design; Discrete Closed Loop System; Circular Airframe

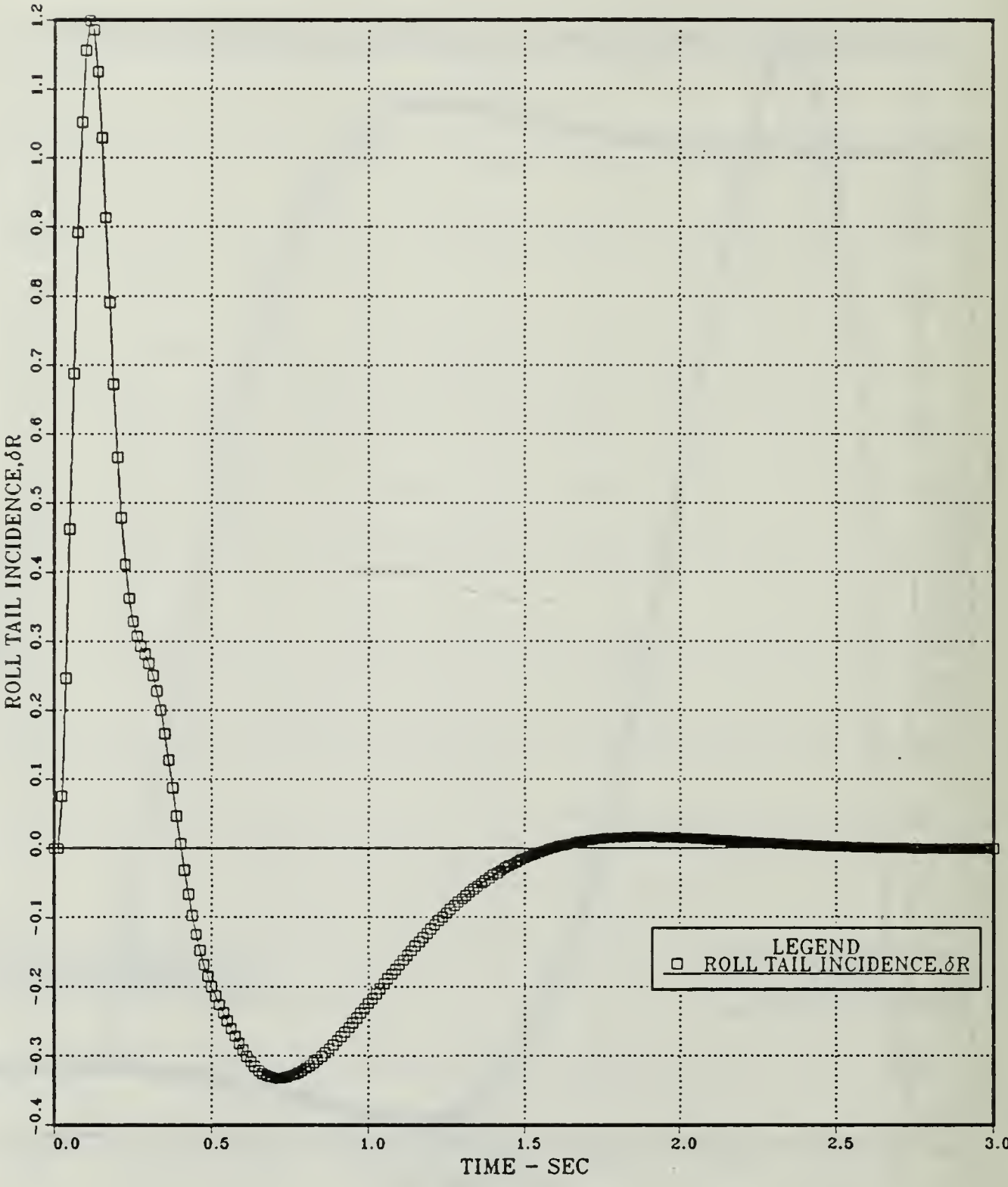

Figure 4.4 Roll Tail Incidence vs Time; Coupled Pitch and Roll Channel Autopilot; State-Feedback Design; Discrete Closed Loop System; Circular Airframe

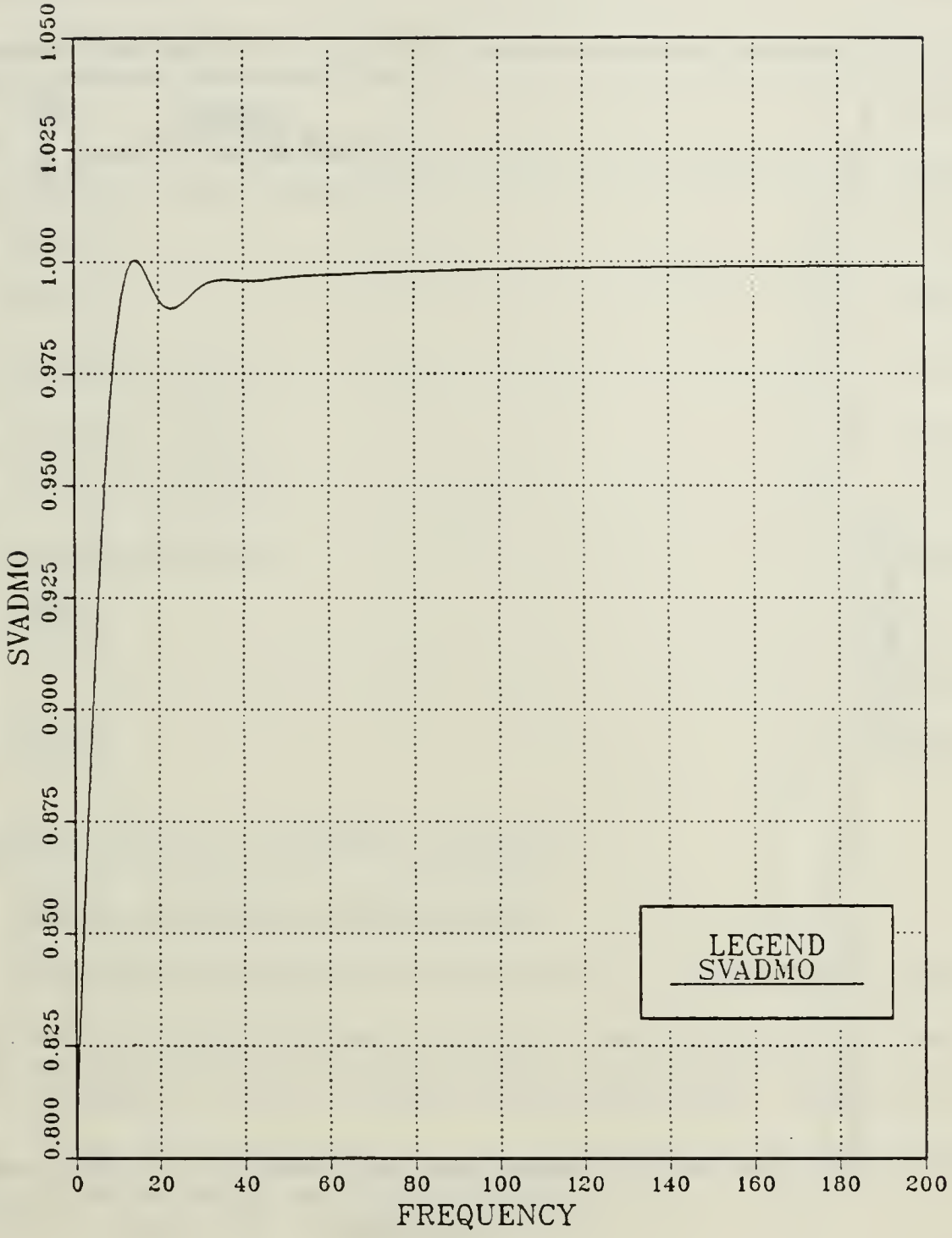

Figure 4.5 SVADMO vs Frequency; Coupled Pitch and Roll Channel Autopilot; State-Feedback Design; Discrete Closed Loop System; Circular Airframe

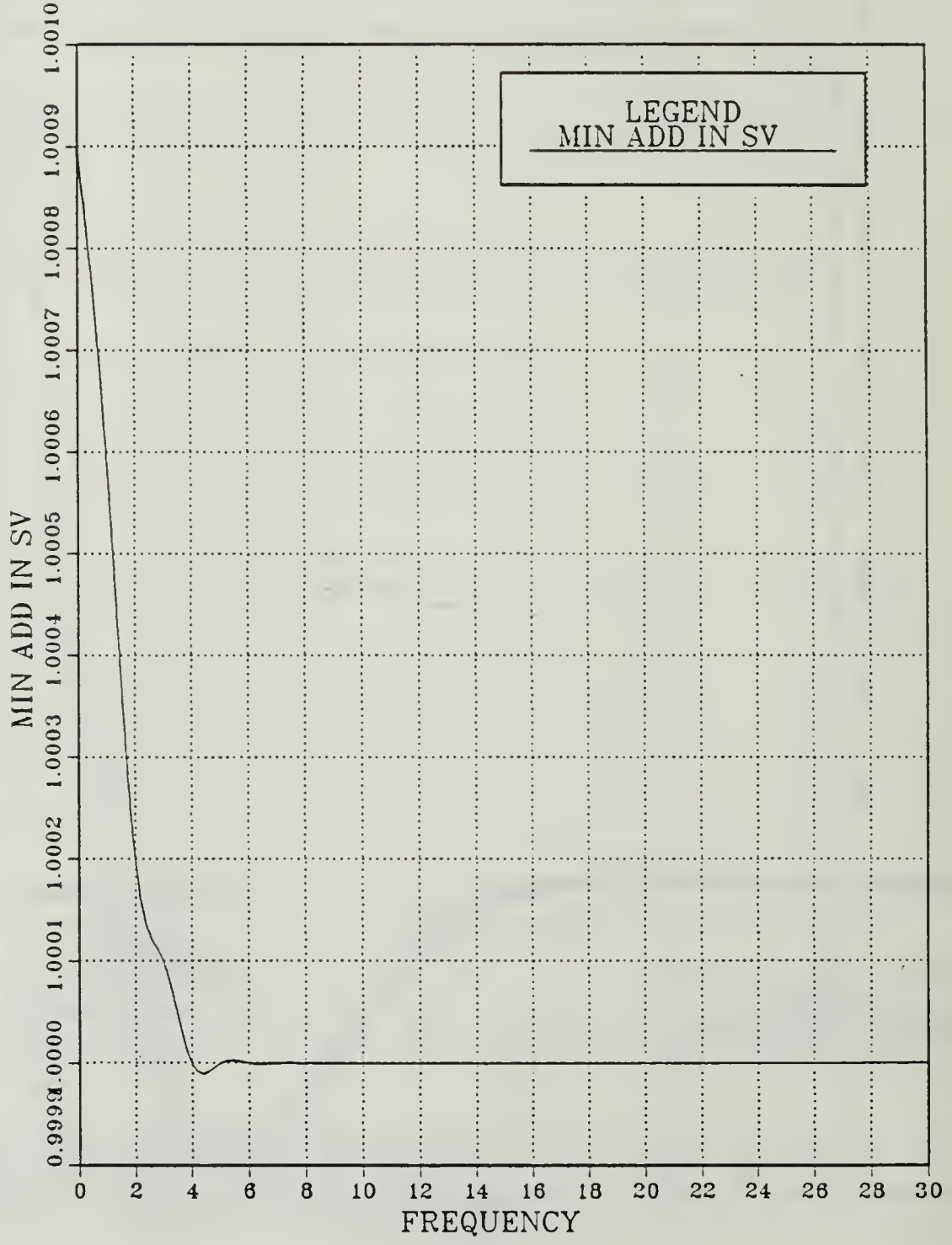

Figure 4.6 MIN ADD IN SV vs Frequency; Coupled Pitch and Roll Channel Autopilot; State-Feedback Design; Discrete Closed Loop System; Circular Airframe

$z_4 = 0.069508$ (IV.B.2-4)

$z_5 = 0.83707-j0.3014$ (IV.B.2-5)

$z_6 = 0.83707+j0.3014$ (IV.B.2-6)

$z_7 = 0.89844$ (IV.B.2-7)

$z_8 = 0.90064$ (IV.B.2-8)

$z_9 = 0.43996$ (IV.B.2-9)

$z_{10} = 0.46207$ (IV.B.2-10)

$z_{11} = 0.96562-j0.03401$ (IV.B.2-11)

$z_{12} = 0.96502+j0.03401$ (IV.B.2-12)

$z_{13} = 0.99559-j0.08307$ (IV.B.2-13)

$z_{14} = 0.99559+j0.08307$ (IV.B.2-14)

$z_{15} = 0.99820$ (IV.B.2-15)

$z_{16} = 1$ (IV.B.2-16)

$z_{17} = 1.06546$ (IV.B.2-17)

C. DISCRETE COUPLED ESTIMATOR DESIGN

1. Design Approach and Analysis

Following the same procedure as in the case of the state-feedback but for the coupled estimator gain vector the pole-zero and time response plots of the coupled estimator design are obtained. The time responses are again identical with those of the discrete uncoupled estimator design.

2. Robustness Analysis

Executing the POPLAR design program of [Ref. 7], Figures 4.7 and 4.8 are obtained which prove the robustness of the system. It is noted that for very low frequencies the values of

SVADMO are above 0.83976. Finally, in terms of optimization results the ordered computed eigenvalues are the same as in the coupled state-feedback design.

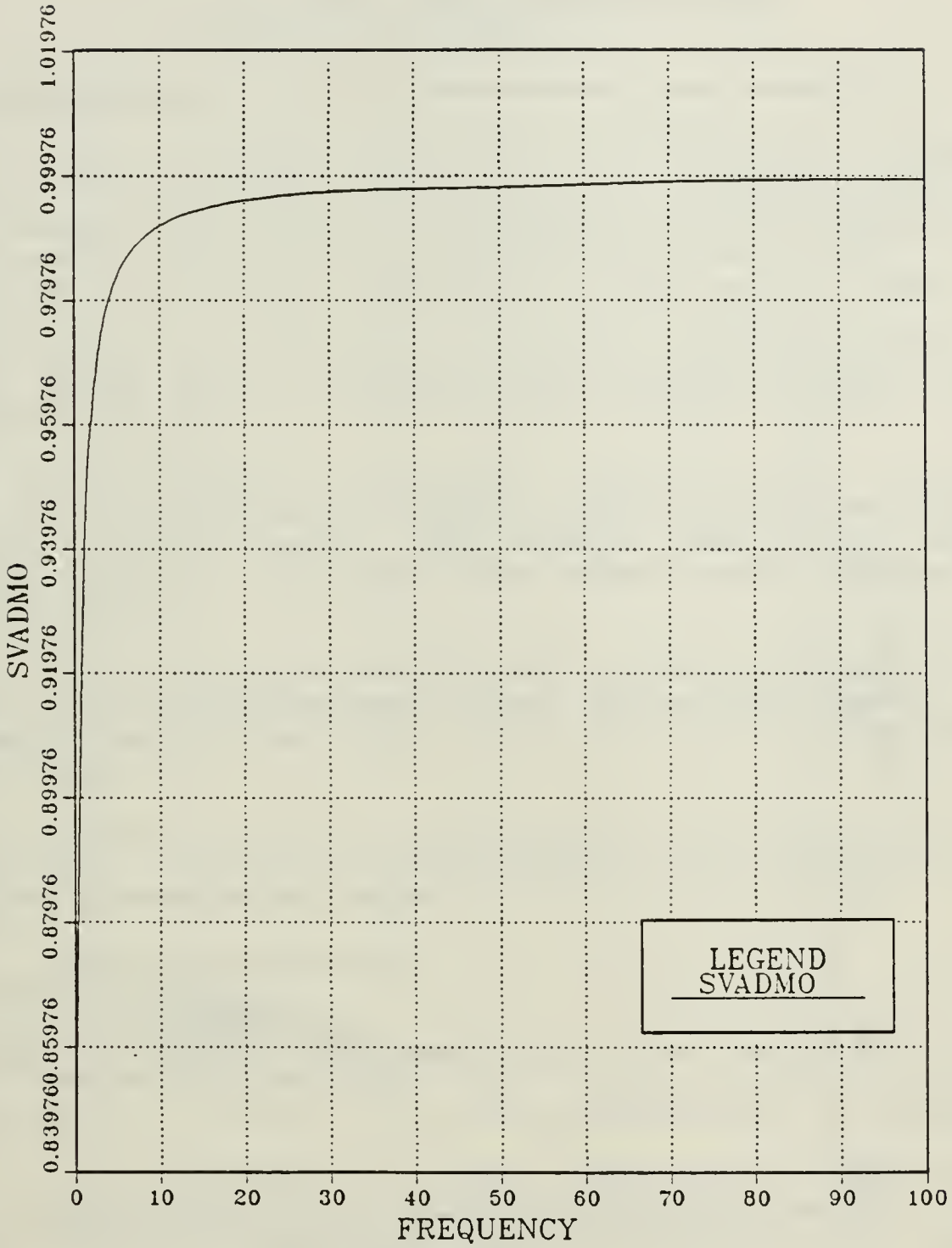

Figure 4.7 SVADMO vs Frequency; Coupled Pitch and Roll Channel Autopilot; Estimator Design; Discrete Closed Loop System; Circular Airframe

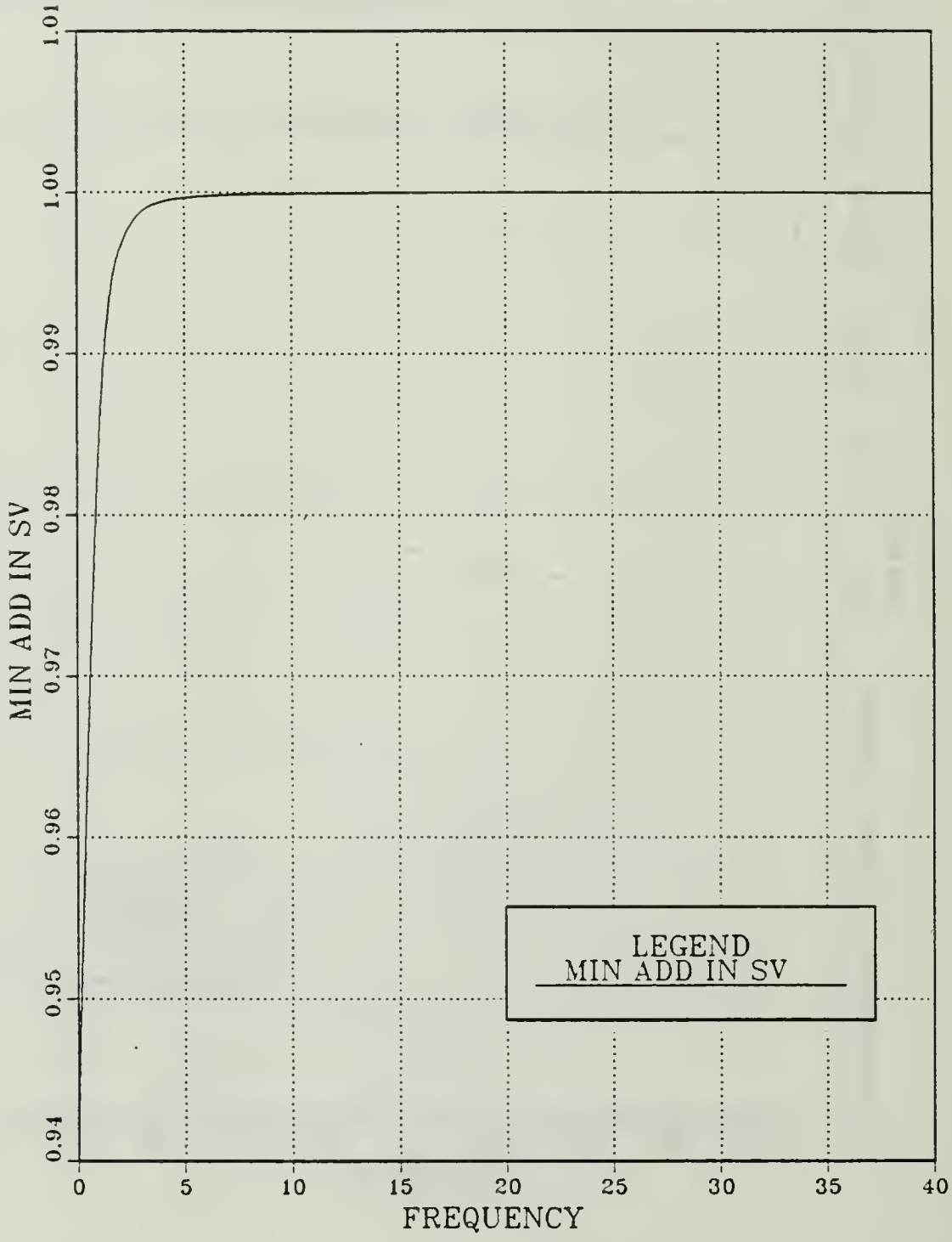

Figure 4.8 MIN ADD IN SV vs Frequency; Coupled Pitch and Roll Channel Autopilot; Estimator Design; Discrete Closed Loop System; Circular Airframe

V. CONCLUSIONS AND RECOMMENDATIONS

A. CONCLUSIONS

The goal of the present thesis was the design and analysis of discrete lateral autopilots for application to BTT missiles. The following are the principal conclusions based on this work.

1. The continuous and discrete classical designed autopilots were proved to have identical performances for the two lateral channels.

2. The state-feedback and estimator autopilots were introduced as additional dynamic designs in order to implement control to the original system. Both designs, analyzed in terms of their transient responses, were found to meet the desired requirements.

3. The simplified state-feedback and estimator designs reduced some of the returning gain loops, making the system simpler, without any significant effects on the system's performance.

4. The performance of the coupled pitch and roll channel autopilot was found to be satisfactory and the overall system proved to be robust.

B. RECOMMENDATIONS

In order to improve the simplicity of the overall system, more returning gain loops of the state-feedback and estimator design must be eliminated. A further investigation then must be conducted in order to examine if the performance of the resulting design remains unchanged.

APPENDIX A

DESIGN REQUIREMENTS FOR UNCOUPLED AUTOPILOTS

The requirements for the classical design method of the uncoupled channel autopilots [Ref. 6] are the following:

1. High Frequency Attentuation in Actuator Command Branch

a. Uncoupled Yaw Channel

It must be $\geq$ 15 db at 100 rad/sec and zero angle-of-attack and sideslip. This requirement will provide sufficient high frequency attenuation for $\geq$ 30 Hz actuator and for body bending modes when high frequency filters are added, but it limits the ability of the yaw autopilot to minimize sideslip angle.

b. Uncoupled Roll Channel

It must be $\geq$ 15 db at 100 rad/sec and zero angle-of-attack. This will provide sufficient high frequency attenuation for $\geq$ 30 Hz actuator and for elastic modes when high frequency filters are added, but this requirement limits the speed of roll angle response.

2. Relative Stability for Both Lateral Channels

Gain margins $\geq$ 6 db, phase margins $\geq 30^{\circ}$ with a goal of 12 db and 50°.

3. Acceleration Time Response

a. Uncoupled Yaw Channel

(1) 63% time constant of approximately 0.4 seconds.

(2) Overshoot $\leq$ 10%.

(3) Steady-state error need not be zero.

b. Uncoupled Roll Channel

(1) 63% time constant of 0.5 seconds.

(2) Overshoot $\leq$ 10%.

(3) Zero steady-state roll angle error.

APPENDIX B

AERODYNAMIC DATA

The overall classical design developed by Arrow [Ref. 6] was performed for the selected flight condition of Mach number 3.95 at 60000 feet altitude. The corresponding aerodynamic data presented below were taken or derived from the ICAO standard atmosphere tables.

TABLE VII

AERODYNAMIC DATA (M=3.95, H=60kft)

Temperature, T (^{o}R)	389.988
Sonic Velocity, a (ft/sec)	968.47
Pressure, p (lb/ft^2)	149.78
Density, (lb-sec^2/ft)	0.0002238
Velocity, V (ft/sec)	3825.4565
Dynamic Pressure, $\bar{q}$ (lb/ft^2)	1637.145

APPENDIX C

LINEARIZED AERODYNAMIC DERIVATIVES

The linearized aerodynamic derivatives at the selected flight condition and about a zero trim angle-of-attack are provided below for both airframe configurations [Ref. 6].

TABLE VIII

LINEARIZED AERODYNAMIC DERIVATIVES
(M=3.95, H=60kft; a=0°)

	CIRCULAR	ELLIPTICAL
C_{Y_β}	-0.065	-0.043
C_{n_β}	-0.025	0.024
	0.021	0.016
$C_{Y_{\delta_Y}}$	-0.050	-0.042
$C_{\ell_{\delta_R}}$	0.031	0.023

APPENDIX D

MISSILE SIZING AND MASS PROPERTIES

In order to provide a realistic missile based on the aerodynmamically tested configuration concepts [Ref. 5], the models were assumed to be 1/6-scale and the mass properties were developed corresponding to mass distribution which might be expected for missiles of this size. All the geometric and mass properties are presented in the following table.

TABLE IX

GEOMETRIC AND MASS PROPERTIES OF MISSILE CONFIGURATIONS

	Circular	Elliptical
Length, 1 (in)	168	168
Max. Diameter (in)	24	
Max. Major Axis (in)		41.57
Max. Minor Axis (in)		13.86
c.g. distance from L.E. (in)	100.8(0.6)	100.8(0.6)
Reference Length, d (ft)	2	2
Reference Area, S (ft)	π	π
Weight, W (lb)	2525	2475
I_{xx} (slug-ft^2)	40	40
I_{zz} (slug-ft^2)	810	853

APPENDIX E

PROGRAM LOGIC FOR APPLICATION OF ACKERMANN'S FORMULA

The program logic for computing the control-law gain vector $\underline{F}$ or the transpose of the estimator gain vector $\underline{K}^T$, taken from [Ref. 9], is given in the following table.

TABLE

PROGRAM LOGIC FOR APPLICATION OF ACKERMANN'S FORMULA

1. Read in Φ, Γ, T, and N_x, the number of states.
2. Comment: first we will read in the desired pole locations in the s-plane, convert them to z-plane polynomial coefficients, and construct $\alpha(\Phi)$.
3. **I** ← identity matrix, $N_x \times N_x$
4. **ALPHA** ← **I**
5. $k \leftarrow 1$
6. If $k > N_x$, go to step 18.
7. Read in pole location k as $a + jb$.
8. If $b = 0$, go to step 14.
9. $A_1 \leftarrow -2\exp(aT)\cos bT$
10. $A_2 \leftarrow \exp(2aT)$
11. **ALPHA** ← **ALPHA** * (Φ * Φ − $A_1\Phi$ + A_2**I**)
12. $k \leftarrow k + 2$
13. Go to step 6.
14. $A_1 \leftarrow \exp(aT)$
15. **ALPHA** ← **ALPHA** * (Φ − A_1 * **I**)
16. $k \leftarrow k + 1$
17. Go to step 6.
18. Comment: now we construct the controllability matrix.
19. **C** ← **I**
20. **E** ← Γ
21. $k \leftarrow 1$
22. If $k > N_x$, go to step 28.
23. Comment: replace column k of **C** by **E**.
24. **C**[: k] ← **E**
25. $k \leftarrow k + 1$
26. **E** ← Φ · **E**
27. Go to step 22.
28. Comment: now solve for the control law, first form e_n^T as the last row of **I**.
29. **E** ← **I**[N_x;]
30. Solve **BC** = **E** for **B**.
31. **K** = **B** * **ALPHA**
32. END

APPENDIX F

ACKERMANN FORTRAN PROGRAM

```
FILE: ACKERMAN FATFIV   A1

$JOB                                                                    ACK00010
      INTEGER      NS,K,IA,IER,I,J,NI                                   ACK00020
      REAL         PH(20,20),GA(20,20),AI(20,20),ALPHA(20,20),WK(40)    ACK00030
      REAL      A2   ,E(20,20),B(20,20),C(20),BF(20,20),DK(20,20)       ACK00040
      REAL   A,B,T,  R,ATEMP(20,20)                                     ACK00050
      REAL      A1    ,TO(20,20),TI(20,20),TS(20,20),C(20,20),TM(20,20) ACK00060
C                                                                       ACK00070
C    INPUT OF NS= NUMBER OF STATES                                      ACK00080
C              T= SAMPLE TIME                                           ACK00090
      PRINT ,  ' ENTER NUMBER OF STATES.'                               ACK00100
      READ, NS                                                          ACK00110
      PRINT,  ' ENTER SAMPLE TIME '                                     ACK00120
      READ, T                                                           ACK00130
C    INPUT OF PHI=A MATRIX                                              ACK00140
      DO 100  I=1,NS                                                    ACK00150
      DO 101  J=1,NS                                                    ACK00160
      WRITE(6,103)  I,J                                                 ACK00170
  103 FORMAT(4X,'ENTER PH(',I2,',',I2,')')                              ACK00180
      READ,PH(I,J)                                                      ACK00190
  101 CONTINUE                                                          ACK00200
  100 CONTINUE                                                          ACK00210
C    INPUT OF GA=B MATRIX                                               ACK00220
      DO 200   I=1,NS                                                   ACK00230
        J=1                                                             ACK00240
      WRITE(6,105)  I,J                                                 ACK00250
  105 FORMAT(4X,'ENTER GA(',I2,',',I2,')')                              ACK00260
      READ,GA(I,J)                                                      ACK00270
  200 CONTINUE                                                          ACK00280
C   BUILDING THE IDENTITY MATRIX                                        ACK00290
C    ALPHA=C=I                                                          ACK00300
      DO 1 I=1,NS                                                       ACK00310
      DO 5 J=1,NS                                                       ACK00320
      IF (I.EQ.J) GO TO 300                                             ACK00330
      AI(I,J)=0.                                                        ACK00340
      ALPHA(I,J)=0.                                                     ACK00350
      C(I,J)=0.                                                         ACK00360
      GO TO 5                                                           ACK00370
  300 AI(I,J)=1.                                                        ACK00380
      ALPHA(I,J)=1.                                                     ACK00390
      C(I,J)=1.                                                         ACK00400
    5 CONTINUE                                                          ACK00410
    1 CONTINUE                                                          ACK00420
      K=1                                                               ACK00430
   16 IF (K.GT.NS) GO TO 18                                             ACK00440
C                                                                       ACK00450
C     INPUT OF DESIRED POLES LOCATION                                   ACK00460
C                                                                       ACK00470
      WRITE (6,43)                                                      ACK00480
   43 FORMAT(' ENTER REAL PART OF DESIRED POLE LOCATION.')              ACK00490
      READ,A                                                            ACK00500
      WRITE(6,44)                                                       ACK00510
   44 FORMAT(' ENTER IMAGINARY PART OF DESIRED POLE LOCATION.')         ACK00520
      READ,B                                                            ACK00530
C   BUILDING ALPHA(PHI)                                                 ACK00540
      IF (B .EQ.0) GO TO 14                                             ACK00550
      A1=-2.*EXP(A*T)*COS(B*T)                                          ACK00560
      A2=EXP(2.*A*T)                                                    ACK00570
C    EVALUATE PHI*PHI                                                   ACK00580
      CALL VMULFF  (PH,PH,NS,NS,NS,20,20,TM,20,IER)                     ACK00590
C                                                                       ACK00600
      DO 2 I=1,NS                                                       ACK00610
      DO 6 J=1,NS                                                       ACK00620
        TO(I,J)=PH(I,J)*A1                                              ACK00630
        TI(I,J)=AI(I,J)*A2                                              ACK00640
        TS(I,J)=TM(I,J)+TO(I,J)+TI(I,J)                                 ACK00650
    6 CONTINUE                                                          ACK00660
    2 CONTINUE                                                          ACK00670
      CALL VMULFF (ALPHA,TS,NS,NS,NS,20,20,ATEMP,20,IER)                ACK00680
      DO 600  I=1,NS                                                    ACK00690
      DO 601  J=1,NS                                                    ACK00700
  601 ALPHA(I,J)=ATEMP(I,J)                                             ACK00710
  600 CONTINUE                                                          ACK00720
```

```
FILE: ACKERMAN WATFIV   A1

          K= K+2                                                                ACK00730
          GO TO 16                                                              ACK00740
    14    A1=EXP(A*T)                                                           ACK00750
          DO 3 I=1,NS                                                           ACK00760
          DO 7 J=1,NS                                                           ACK00770
          TO(I,J)=A(I,J)*A1                                                     ACK00780
    7     TI(I,J)=PH(I,J)-TO(I,J)                                               ACK00790
    3     CONTINUE                                                              ACK00800
          CALL VMULFF(ALPHA,TI,NS,NS,NS,20,20,ATEMP,20,IER)                     ACK00810
          DO 700 I=1,NS                                                         ACK00820
          DO 701 J=1,NS                                                         ACK00830
    701   ALPHA(I,J)=ATEMP(I,J)                                                 ACK00840
    700   CONTINUE                                                              ACK00850
          K=K+1                                                                 ACK00860
          GO TO 16                                                              ACK00870
    18    DO 9 I=1,NS                                                           ACK00880
          J=1                                                                   ACK00890
    9     E(I,J)=GA(I,J)                                                        ACK00900
          K=1                                                                   ACK00910
    22    IF (K.GT.NS) GO TO 28                                                 ACK00920
          DO 10 I=1,NS                                                          ACK00930
          C(I,K)=E(I,1)                                                         ACK00940
    10    CONTINUE                                                              ACK00950
          K=K+1                                                                 ACK00960
          CALL VMULFF (PH,E,NS,NS,1 ,20,20,E,20,IER)                            ACK00970
          GO TO 22                                                              ACK00980
    28    DO 11 J=1,NS                                                          ACK00990
    11    E( 1,J)=AI(NS,J)                                                      ACK01000
          R=0.                                                                  ACK01010
          CALL LGINF (C,20,NS,NS,R,D,20,S,WK,IER)                               ACK01020
C                                                                               ACK01030
          CALL VMULFF (E,D,1 ,NS,NS,20,20,BF,20,IER)                            ACK01040
          CALL VMULFF (BF,ALPHA,1 ,NS,NS,20,20,UK,20,IER)                       ACK01050
C                                                                               ACK01060
          PRINT, '      CONTROL GAIN  VECTOR  '                                 ACK01070
          WRITE (6,45)  (UK(1,J),J=1,NS)                                        ACK01080
    45    FORMAT(8F15.4)                                                        ACK01090
          RETURN                                                                ACK01100
          END                                                                   ACK01110
$ENTRY                                                                          ACK01120
```

APPENDIX G: PLANT SYSTEM AND INPUT MATRICES OF CONTINUOUS COUPLED PITCH AND ROLL CHANNEL AUTOPILOT

F MATRIX 17 ROWS 17 COLUMNS

-1.5000000E+02	0.0000000E+00	0.0000000E+00	0.0000000E+00	0.0000000E+00	0.0000000E+00	0.0000000E+00
0.0000000E+00	0.0000000E+00	1.5000000E+02	0.0000000E+00	0.0000000E+00	0.0000000E+00	0.0000000E+00
0.0000000E+00	0.0000000E+00	0.0000000E+00				
1.3531000E+00	0.0000000E+00	1.0000000E+00	0.0000000E+00	0.0000000E+00	0.0000000E+00	0.0000000E+00
0.0000000E+00	0.0000000E+00	0.0000000E+00	0.0000000E+00	0.0000000E+00	0.0000000E+00	0.0000000E+00
0.0000000E+00	0.0000000E+00	0.0000000E+00				
-6.5720000E+00	0.0000000E+00	-5.0000000E+00	0.0000000E+00	0.0000000E+00	0.0000000E+00	0.0000000E+00
0.0000000E+00	0.0000000E+00	0.0000000E+00	0.0000000E+00	0.0000000E+00	0.0000000E+00	0.0000000E+00
0.0000000E+00	0.0000000E+00	0.0000000E+00				
0.0000000E+00	0.0000000E+00	0.0000000E+00	0.0000000E+00	1.0000000E+00	0.0000000E+00	0.0000000E+00
-5.9263700E+01	0.0000000E+00	0.0000000E+00	0.0000000E+00	0.0000000E+00	0.0000000E+00	0.0000000E+00
0.0000000E+00	0.0000000E+00	0.0000000E+00				
0.0000000E+00	0.0000000E+00	0.0000000E+00	-4.4355700E+01	-1.4918600E-01	0.0000000E+00	0.0000000E+00
1.7887500E+00	0.0000000E+00	0.0000000E+00	0.0000000E+00	0.0000000E+00	0.0000000E+00	0.0000000E+00
0.0000000E+00	0.0000000E+00	0.0000000E+00				
0.0000000E+00	0.0000000E+00	0.0000000E+00	0.0000000E+00	0.0000000E+00	0.0000000E+00	1.0000000E+00
-7.0192000E-01	0.0000000E+00	0.0000000E+00	0.0000000E+00	0.0000000E+00	0.0000000E+00	0.0000000E+00
0.0000000E+00	0.0000000E+00	0.0000000E+00				
0.0000000E+00	0.0000000E+00	0.0000000E+00	0.0000000E+00	0.0000000E+00	-4.4355700E+01	-1.4918600E-01
-1.0433600E+03	0.0000000E+00	0.0000000E+00	0.0000000E+00	0.0000000E+00	0.0000000E+00	0.0000000E+00
0.0000000E+00	0.0000000E+00	0.0000000E+00				
0.0000000E+00	0.0000000E+00	0.0000000E+00	0.0000000E+00	0.0000000E+00	0.0000000E+00	0.0000000E+00
-1.8840000E+02	1.8840000E+02	0.0000000E+00	0.0000000E+00	0.0000000E+00	0.0000000E+00	0.0000000E+00
0.0000000E+00	0.0000000E+00	0.0000000E+00				
-4.6083900E-01	-2.2308300E+00	-3.4058000E-01	2.2308300E+00	3.4058000E-01	0.0000000E+00	0.0000000E+00
-2.0134600E+01	-1.4300000E-01	0.0000000E+00	0.0000000E+00	0.0000000E+00	0.0000000E+00	0.0000000E+00
0.0000000E+00	0.0000000E+00	0.0000000E+00				
0.0000000E+00	0.0000000E+00	0.0000000E+00	0.0000000E+00	0.0000000E+00	0.0000000E+00	-1.0000000E+00
8.8712400E+02	-8.8842200E+02	0.0000000E+00	0.0000000E+00	0.0000000E+00	0.0000000E+00	0.0000000E+00
0.0000000E+00	0.0000000E+00	0.0000000E+00				
0.0000000E+00	0.0000000E+00	0.0000000E+00	0.0000000E+00	0.0000000E+00	0.0000000E+00	0.0000000E+00
0.0000000E+00	0.0000000E+00	0.0000000E+00	0.0000000E+00	0.0000000E+00	0.0000000E+00	0.0000000E+00
0.0000000E+00	0.0000000E+00	8.3534620E+00				
0.0000000E+00	0.0000000E+00	0.0000000E+00	0.0000000E+00	0.0000000E+00	0.0000000E+00	0.0000000E+00
0.0000000E+00	0.0000000E+00	0.0000000E+00	0.0000000E+00	1.0000000E+00	0.0000000E+00	0.0000000E+00
0.0000000E+00	0.0000000E+00	0.0000000E+00				
0.0000000E+00	0.0000000E+00	0.0000000E+00	0.0000000E+00	0.0000000E+00	0.0000000E+00	0.0000000E+00
0.0000000E+00	0.0000000E+00	0.0000000E+00	0.0000000E+00	0.0000000E+00	-1.7600000E+01	-8.0000000E+00
0.0000000E+00	0.0000000E+00	0.0000000E+00				
0.0000000E+00	0.0000000E+00	0.0000000E+00	0.0000000E+00	0.0000000E+00	0.0000000E+00	0.0000000E+00
0.0000000E+00	0.0000000E+00	0.0000000E+00	-7.5325000E-01	-8.8352000E-01	3.5165000E-01	-5.0000000E+00
0.0000000E+00	0.0000000E+00	-4.0334000E-01				
0.0000000E+00	0.0000000E+00	0.0000000E+00	0.0000000E+00	0.0000000E+00	0.0000000E+00	0.0000000E+00
0.0000000E+00	0.0000000E+00	0.0000000E+00	0.0000000E+00	0.0000000E+00	0.0000000E+00	0.0000000E+00
-6.0000000E+00	0.0000000E+00	6.2329100E-01				
0.0000000E+00	0.0000000E+00	0.0000000E+00	0.0000000E+00	0.0000000E+00	0.0000000E+00	0.0000000E+00
0.0000000E+00	0.0000000E+00	0.0000000E+00	-1.0271000E-01	-1.2048000E-01	4.7950000E-02	1.4318200E+01
-1.4181840E+01	-1.5000000E+01	-1.4067000E-01				
0.0000000E+00	0.0000000E+00	0.0000000E+00	0.0000000E+00	0.0000000E+00	0.0000000E+00	0.0000000E+00
0.0000000E+00	0.0000000E+00	0.0000000E+00	0.0000000E+00	0.0000000E+00	0.0000000E+00	0.0000000E+00
0.0000000E+00	1.0795320E+04	-1.8840000E+02				

G MATRIX 17 ROWS 2 COLUMNS

0.0000000E+00	0.0000000E+00
-1.3531000E+00	0.0000000E+00
6.5720000E+00	0.0000000E+00
0.0000000E+00	0.0000000E+00
0.0000000E+00	0.0000000E+00
0.0000000E+00	0.0000000E+00
0.0000000E+00	0.0000000E+00
0.0000000E+00	0.0000000E+00
4.6083900E-01	0.0000000E+00
0.0000000E+00	0.0000000E+00
0.0000000E+00	0.0000000E+00
0.0000000E+00	0.0000000E+00
0.0000000E+00	1.7600000E+01
0.0000000E+00	8.8352000E-01
0.0000000E+00	0.0000000E+00
0.0000000E+00	1.2048000E-01
0.0000000E+00	0.0000000E+00

APPENDIX H: PLANT SYSTEM AND INPUT MATRICES OF DISCRETE COUPLED PITCH AND ROLL CHANNEL AUTOPILOT

A MATRIX 17 ROWS 17 COLUMNS

1.5795753E-01	3.5369325E-02	5.5845972E-03	-3.5415286E-02	-5.0350633E-03	1.4378905E-03	-6.9550195E-03	
3.1215038E+00	-2.7434696E+00	8.4950341E-01	0.0000000E+00	0.0000000E+00	0.0000000E+00	0.0000000E+00	
0.0000000E+00	0.0000000E+00	0.0000000E+00					
7.3702121E-03	1.0001647E+00	1.2143713E-02	-1.8110329E-04	-2.8707303E-05	6.4803277E-06	-4.3143367E-05	
2.3554415E-02	-2.1657925E-02	9.0789743E-03	0.0000000E+00	0.0000000E+00	0.0000000E+00	0.0000000E+00	
0.0000000E+00	0.0000000E+00	0.0000000E+00					
-3.5755072E-02	-8.9683355E-04	9.3927554E-01	8.7928241E-04	1.3937755E-04	-3.1463045E-05	2.0946996E-04	
-1.1434246E-01	1.0515494E-01	-4.4066551E-02	0.0000000E+00	0.0000000E+00	0.0000000E+00	0.0000000E+00	
0.0000000E+00	0.0000000E+00	0.0000000E+00					
6.3641914E-04	4.8072547E-03	7.3780452E-04	9.9134592E-01	1.1724094E-02	1.0389178E-07	-1.0276906E-06	
-2.5772733E-01	-4.3736676E-01	3.6239694E-04	0.0000000E+00	0.0000000E+00	0.0000000E+00	0.0000000E+00	
0.0000000E+00	0.0000000E+00	0.0000000E+00					
-1.2632605E-04	-8.8102183E-04	-1.3508452E-04	-9.5242591E-01	9.9481481E-01	-1.1955039E-08	1.3487756E-07	
1.1052479E-01	1.0875558E-01	-5.6530062E-05	0.0000000E+00	0.0000000E+00	0.0000000E+00	0.0000000E+00	
0.0000000E+00	0.0000000E+00	0.0000000E+00					
5.0058503E-05	3.4706702E-04	5.3521335E-05	-3.4235257E-04	-5.4232194E-05	9.9653837E-01	1.2473878E-02	
-4.3837950E-02	-4.3103149E-02	2.2370223E-05	0.0000000E+00	0.0000000E+00	0.0000000E+00	0.0000000E+00	
0.0000000E+00	0.0000000E+00	0.0000000E+00					
1.1198372E-02	8.4559715E-02	1.2932664E-02	-8.2578336E-02	-1.3194430E-02	-5.5328815E-01	9.9465984E-01	
-4.5313172E+00	-7.6933073E+00	6.3774425E-03	0.0000000E+00	0.0000000E+00	0.0000000E+00	0.0000000E+00	
0.0000000E+00	0.0000000E+00	0.0000000E+00					
-1.8197865E-03	-1.6475935E-02	-2.5342871E-03	1.5914437E-02	2.5927483E-03	-7.6937268E-07	6.1129260E-06	
1.9658256E-02	8.2551826E-01	-1.8117691E-03	0.0000000E+00	0.0000000E+00	0.0000000E+00	0.0000000E+00	
0.0000000E+00	0.0000000E+00	0.0000000E+00					
-2.4201118E-03	-2.6250703E-02	-4.0468111E-03	2.5078784E-02	4.1674975E-03	-2.2085612E-06	1.4659039E-05	
-1.0104558E-01	8.5213330E-01	-3.0636457E-03	0.0000000E+00	0.0000000E+00	0.0000000E+00	0.0000000E+00	
0.0000000E+00	0.0000000E+00	0.0000000E+00					
8.5120362E-03	7.7170206E-02	1.1870299E-02	-7.4535066E-02	-1.2144650E-02	3.4647518E-03	-1.2502640E-02	
4.6563462E+00	-3.8405597E+00	1.0075610E+00	0.0000000E+00	0.0000000E+00	0.0000000E+00	0.0000000E+00	
0.0000000E+00	0.0000000E+00	0.0000000E+00					
0.0000000E+00	0.0000000E+00	0.0000000E+00	0.0000000E+00	0.0000000E+00	0.0000000E+00	0.0000000E+00	
0.0000000E+00	0.0000000E+00	0.0000000E+00	9.9773873E-01	-2.7013690E-03	1.0245896E-03	2.2685736E-01	
-2.2392478E-01	3.2285155E+00	3.6730433E-02					
0.0000000E+00	0.0000000E+00	0.0000000E+00	0.0000000E+00	0.0000000E+00	0.0000000E+00	0.0000000E+00	
0.0000000E+00	0.0000000E+00	0.0000000E+00	1.2492612E-02	9.9999121E-01	3.3686339E-06	7.9213881E-04	
-7.8251019E-04	1.6120665E-02	3.2146565E-04					
0.0000000E+00	0.0000000E+00	0.0000000E+00	0.0000000E+00	0.0000000E+00	0.0000000E+00	0.0000000E+00	
0.0000000E+00	0.0000000E+00	0.0000000E+00	-1.3299604E-03	-2.0935729E-01	9.0483727E-01	-3.6881965E-05	
3.6451129E-05	-9.6597313E-04	-2.6908370E-05					
0.0000000E+00	0.0000000E+00	0.0000000E+00	0.0000000E+00	0.0000000E+00	0.0000000E+00	0.0000000E+00	
0.0000000E+00	0.0000000E+00	0.0000000E+00	-9.0797723E-03	-1.1024037E-02	3.9997202E-03	9.2763032E-01	
1.1630732E-02	-1.7007972E-01	-2.6023512E-03					
0.0000000E+00	0.0000000E+00	0.0000000E+00	0.0000000E+00	0.0000000E+00	0.0000000E+00	0.0000000E+00	
0.0000000E+00	0.0000000E+00	0.0000000E+00	-1.7343942E-04	-2.3717899E-04	7.8554533E-05	1.7374049E-02	
9.1059431E-01	2.4502210E-01	2.7257510E-03					
0.0000000E+00	0.0000000E+00	0.0000000E+00	0.0000000E+00	0.0000000E+00	0.0000000E+00	0.0000000E+00	
0.0000000E+00	0.0000000E+00	0.0000000E+00	-1.9081030E-03	-2.3081830E-03	8.4609805E-04	1.5280715E-01	
-1.5037418E-01	7.4697747E-01	-1.1429485E-03					
0.0000000E+00	0.0000000E+00	0.0000000E+00	0.0000000E+00	0.0000000E+00	0.0000000E+00	0.0000000E+00	
0.0000000E+00	0.0000000E+00	0.0000000E+00	-6.2875715E-02	-7.5602497E-02	2.8176191E-02	5.6122435E+00	
-5.5314055E+00	4.3323648E+01	5.1340685E-02					

B MATRIX 17 ROWS 2 COLUMNS

-7.5609829E-03	0.0000000E+00
-1.6449186E-02	0.0000000E+00
7.9821623E-02	0.0000000E+00
-9.9881803E-04	0.0000000E+00
1.3285612E-04	0.0000000E+00
-7.2448726E-05	0.0000000E+00
-1.7575515E-02	0.0000000E+00
3.4315550E-03	0.0000000E+00
5.4807555E-03	0.0000000E+00
-1.6073019E-02	0.0000000E+00
0.0000000E+00	2.7013690E-03
0.0000000E+00	8.7926971E-06
0.0000000E+00	2.0935729E-01
0.0000000E+00	1.1024087E-02
0.0000000E+00	2.6717899E-04
0.0000000E+00	2.3081830E-03
0.0000000E+00	7.5602497E-02

APPENDIX I

COUPLED STATE-FEEDBACK DESIGN INPUT DATA FOR POPLAR PROGRAM

```
FILE: FEEDBACK DATA      A1

 1000     0
      200.0          0.0          1.0
          1            0            0
        0.4          0.4          0.0      0
    0     0     0      5     3      3 1000     0
17171702171702171717
    1.5795758E-01    3.6369326E-02    5.5848592E-03   -3.5415286E-2   -5.6350634E-3
    1.4376905E-03   -6.8550195E-3     3.1215038OE+0   -2.7434696E+0    8.4960341E-01
                0                0                0               0               0
                0                0
    7.3702121E-03    1.0001847E-00    1.2145713E-02   -1.8110829E-4   -2.8707903E-5
    6.4803277E-06   -4.3148367E-5     2.3554415E-02   -2.1657925E-2    9.0789743E-03
                0                0                0               0               0
                0                0
   -3.5755072E-2    -8.9683556E-4    9.3927554E-01    8.7928240E-04   1.3937755E-04
   -3.1463045E-5     2.0946996E-04   -1.1434246E-1    1.0513494E-01   -4.4066551E-2
                0                0                0               0               0
                0                0
    6.3641914E-04    4.8072347E-03    7.3780452E-04    9.9184592E-01   1.1724094E-02
    1.0389178OE-7    -1.0276906E-6   -2.5772733E-1    -4.3730676E-1   3.6239694E-04
                0                0                0               0               0
                0                0
   -1.2632605E-4    -8.8102133E-4    -1.3508452E-4    -5.5242591E-1   9.9431481E-01
   -1.1935039E-8     1.3487757E-07    1.1052479E-01    1.0373553E-01   -5.6530062E-5
                0                0                0               0               0
                0                0
    5.0058503E-05    3.4906702E-04    5.3521335E-05   -3.4235257E-4   -5.4232194E-5
    9.9653887E-01    1.2473878E-02   -4.3837960E-2    -4.3103149E-2    2.2390223OE-5
                0                0                0               0               0
                0                0
    1.1198072E-02    8.4589715E-02    1.2982664E-02   -8.2578336E-2   -1.3194430E-2
   -5.5328815E-1     9.9465984E-01   -4.5313172E-0    -7.6933073E-0    6.3774424E-03
                0                0                0               0               0
                0                0
   -1.8197865E-3    -1.6475936E-2    -2.5342871E-3    1.5914437E-02   2.5927489E-03
   -7.6937268E-7     6.1129260E-06    1.9658256E-02    8.2551326E-01   -1.6117691E-3
                0                0                0               0               0
                0                0
   -2.4201118E-3    -2.6250703E-2    -4.0468111E-3    2.5078784E-02   4.1674975E-03
   -2.2085612E-6     1.4659039E-05   -1.0104558E-1    8.5213330E-01   -3.0606437E-3
                0                0                0               0               0
                0                0
    8.5120361E-03    7.7170206E-02    1.1870299E-02   -7.4535066E-2   -1.2144650E-2
    3.4647518E-03   -1.2502640E-2     4.6503462E-00   -3.8409597E-0    1.0075610E-00
                0                0                0               0               0
                0                0                0               0               0
                0                0                0               0               0
    9.9773878E-01   -2.7013690E-3     1.0245896E-03    2.2685736E-01   -2.2392478E-1
    3.2285155E-00    3.6730433E-02
                0                0                0               0               0
                0                0                0               0               0
    1.2492612E-02    9.9999121E-01    3.3686339E-06    7.9213881E-04   -7.3251019E-4
    1.6120605E-02    3.2146565E-04
                0                0                0               0               0
                0                0                0               0               0
   -1.3299604E-3    -2.0935729E-1     9.0483727E-01   -3.6881965E-5    3.6451128E-05
   -9.6597318E-4    -2.6908370E-5
                0                0                0               0               0
                0                0                0               0               0
   -9.0797723E-3    -1.1024087E-2     3.9997292E-03    9.2763032E-01   1.1630732E-02
   -1.7007972E-1    -2.0028512E-3
                0                0                0               0               0
                0                0                0               0               0
   -1.7340942E-4    -2.0717899E-4     7.8564538E-05    1.7374049E-02   9.1059431E-01
    2.4505510E-01    2.7257510E-03
                0                0                0               0               0
                0                0                0               0               0
   -1.9081030E-3    -2.3061830E-3     8.4609805E-04    1.5230715E-01   -1.5037418E-1
    7.4692747E-01   -1.1429485E-3
                0                0                0               0               0
                0                0                0               0               0
```

FILE: FEEDBACK DATA A1

-6.2875718E-2	-7.3602497E-2	2.8176191E-02	5.6122435E-00	-5.5314055E-0
4.3323648E+01	5.1043685E-02			
-7.5609829E-3	0			
-1.6449186E-2	0			
7.9821623E-02	0			
-9.9881608E-4	0			
1.8285612E-04	0			
-7.2448726E-5	0			
-1.7575515E-2	0			
3.4315556E-03	0			
5.4807555E-03	0			
-1.6073019E-2	0			
0	2.7013690E-03			
0	8.7926971E-06			
0	2.0935729E-01			
0	1.1024087E-02			
0	2.0717899E-04			
0	2.3081830E-03			
0	7.5602497E-02			
1.0000000E-00	0	0	0	0
0	0	0	0	0
0	0	0	0	0
0				
0	1.0000000E-00	0	0	0
0	0	0	0	0
0	0	0	0	0
0				
0	0	1.0000000E-00	0	0
0	0	0	0	0
0	0	0	0	0
0				
0	0	0	1.0000000E-00	0
0	0	0	0	0
0	0	0	0	0
0				
0	0	0	0	1.0000000E-00
0	0	0	0	0
0	0	0	0	0
0				
1.0000000E-00	0	0	0	0
0	0	0	0	0
0	0	0	0	0
0				
0	1.0000000E-00	0	0	0
0	0	0	0	0
0	0	0	0	0
0				
0	0	0	0	0
0	0	1.0000000E-00	0	0
0	0	0	0	0
0				
0	0	0	0	0
0	0	0	1.0000000E-00	0
0	0	0	0	0
0				
0	0	0	0	0
0	0	0	0	1.0000000E-00
0	0	0	0	0
0				
0	0	0	0	0
0	0	0	0	0
1.0000000E-00	0	0	0	0
0				
0	0	0	0	0
0	0	0	0	0
0	1.0000000E-00	0	0	0
0				
0	0	0	0	0
0	0	0	0	0
0	0	1.0000000E-00	0	0
0				
0	0	0	0	0

FILE: FEEDBACK DATA A1

```
                    0                    0                    0                    0                    0
                    0                    0                    0   1.0000000E-00                    0
                    0                    0
                    0                    0                    0                    0                    0
                    0                    0                    0                    0   1.0000000E-00
                    0                    0
                    0                    0                    0                    0                    0
                    0                    0                    0                    0                    0
                    0                    0                    0                    0                    0
  1.0000000E-00     0                    0
                    0                    0                    0                    0                    0
                    0                    0                    0                    0                    0
                    0                    0                    0                    0                    0
                    0   1.0000000E-00
 -0.0188000E-00    -0.0279000E-00   -0.0042000E-00    0.0290000E+00    0.0041000E+00
  0.0000000E+00     0.0001000E+00    1.7732000E+00   -2.0162000E+00    0.0131000E+00
  0.0000000E+00     0.0000000E+00    0.0000000E+00    0.0000000E+00    0.0000000E+00
  0.0000000E+00       0.0000000E+0
  0.0000000E+00     0.0000000E+00    0.0000000E+00     0.0000000E+0     0.0000000E+00
  0.0000000E-00     0.0000000E+00     0.0000000E+0     0.0000000E+0      0.0000000E+0
  0.0000000E+00     0.0000000E-00    0.0000000E+00     0.0178000E-0    -0.0179000E-0
 -1.4990000E-00     0.0023000E-00
0 0 0 0 0 0 0 0 0 0 0 0 0 0 0 0 0 0 0 0 0
0 0 0 0 0 0 0 0 0 0 0 0 0 0 0 0 0 0 0 0 0
   -10000      10000
 0.13199300   0.0319377 0
 0.13199300  -0.0319377 0
 0.89698700   0.0906708 0
 0.89698700  -0.0906708 0
 0.95362500   0.0299850 0
 0.95362500  -0.0299850 0
 0.99820200   0.0000000 0
 1.00000000   0.0000000 0
 0.99560800   0.0830713 0
 0.99560800  -0.0830713 0
 0.09928050   0.0000000 0
 0.83521600   0.3097360 0
 0.83521600  -0.3097360 0
 0.96908700   0.0328588 0
 0.96908700  -0.0328588 0
 0.89379700   0.0000000 0
 0.93707500   0.0000000 0
```

APPENDIX J

COUPLED ESTIMATOR DESIGN INPUT DATA FOR POPLAR PROGRAM

```
FILE: ESTIMATO DATA     A1

 1000     0
     100.0         0.0         1.0
         1           0           0
       0.4         0.4         0.0     0
    0    0    0    5    3    3 1000    0
1717170217170217 17
   1.5795758E-01   3.6369326E-02   5.5348592E-03  -3.5415236E-2  -5.6850634E-3
   1.4376905E-03  -6.3550195E-3   3.1215038OE+0  -2.7434696E+0   8.4960341E-01
                0               0              0              0              0
                0               0
   7.3702121E-03   1.0001847E-00   1.2145713E-02  -1.8110829E-4  -2.8707903E-5
   6.4803277E-06  -4.3148367E-5   2.3554415E-02  -2.1657925E-2   9.0789743E-03
                0               0              0              0              0
                0               0
  -3.5755072E-2   -8.9683556E-4   9.3927554E-01   8.7328240E-04   1.3937755E-04
  -3.1463045E-5    2.0946996E-04  -1.1434246E-1   1.0513494E-01  -4.4066551E-2
                0               0              0              0              0
                0               0
   6.3641914E-04   4.8072347E-03   7.3780452E-04   9.9184592E-01   1.1724094E-02
   1.0389178OE-7  -1.0276906E-6  -2.5772733E-1  -4.3730676E-1   3.6239694E-04
                0               0              0              0              0
                0               0
  -1.2632605E-4   -8.8102183E-4  -1.3508452E-4  -5.5242591E-1   9.9481481E-01
  -1.1935039E-8    1.3487757E-07   1.1052479E-01   1.0873558E-01  -5.6530062E-5
                0               0              0              0              0
                0               0
   5.0058503E-05   3.4906702E-04   5.3521335E-05  -3.4235257E-4  -5.4232194E-5
   9.9653887E-01   1.2473878E-02  -4.3837960E-2  -4.3103149E-2   2.2390223OE-5
                0               0              0              0              0
                0               0
   1.1198072E-02   8.4589715E-02   1.2932664E-02  -8.2578336E-2  -1.3194430E-2
  -5.5328815E-1    9.9465984E-01  -4.5313172E-0  -7.6933073E-0   6.3774424E-03
                0               0              0              0              0
                0               0
  -1.8197865E-3   -1.6475936E-2  -2.5342871E-3   1.5914437E-02   2.5927489E-03
  -7.6937268E-7    6.1129260E-06   1.9653256E-02   8.2551826E-01  -1.6117691E-3
                0               0              0              0              0
                0               0
  -2.4201118E-3   -2.6250703E-2  -4.0468111E-3   2.5073784E-02   4.1674975E-03
  -2.2085612E-6    1.4659039E-05  -1.0104558E-1   8.5213330E-01  -3.0606437E-3
                0               0              0              0              0
                0               0
   8.5120361E-03   7.7170206E-02   1.1870299E-02  -7.4535066E-2  -1.2144650E-2
   3.4647516E-03  -1.2502640E-2   4.6563462E-00  -3.6409597E-0   1.0075610E-00
                0               0              0              0              0
                0               0
                0               0              0              0              0
                0               0              0              0              0
   9.9773878E-01  -2.7013690E-3   1.0245896E-03   2.2685736E-01  -2.2392478E-1
   3.2285155E-00   3.6730433E-02
                0               0              0              0              0
                0               0              0              0              0
   1.2492612E-02   9.9999121E-01   3.3686339E-06   7.9213881E-04  -7.8251019E-4
   1.6120605E-02   3.2146565E-04
                0               0              0              0              0
                0               0              0              0              0
  -1.3299604E-3   -2.0935729E-1   9.0483727E-01  -3.6881965E-5   3.6451128E-05
  -9.6597318E-4   -2.6908370E-5
                0               0              0              0              0
                0               0              0              0              0
  -9.0797723E-3   -1.1024087E-2   3.9997292E-03   9.2763032E-01   1.1630732E-02
  -1.7007972E-1   -2.0028512E-3
                0               0              0              0              0
                0               0              0              0              0
  -1.7340942E-4   -2.0717899E-4   7.8564538E-05   1.7374049E-02   9.1059431E-01
   2.4505510E-01   2.7257510E-03
                0               0              0              0              0
                0               0              0              0              0
  -1.9081030E-3   -2.3081830E-3   8.4609805E-04   1.5280715E-01  -1.5037418E-1
   7.4692747E-01  -1.1429485E-3
                0               0              0              0              0
                0               0              0              0              0
```

FILE: ESTIMATD DATA A1

-6.2875718E-2	-7.5602497E-2	2.8176191E-02	5.6122435E-00	-5.5314055E-0
4.3323648E+01	5.1040665E-02			
-7.5609829E-3	0			
-1.6449186E-2	0			
7.9821623E-02	0			
-9.9881608E-4	0			
1.8285612E-04	0			
-7.2448720E-5	0			
-1.7575515E-2	0			
3.4315526E-03	0			
5.4807555E-03	0			
-1.6073019E-2	0			
0	2.7013690E-03			
0	8.7926971E-06			
0	2.0935729E-01			
0	1.1024087E-02			
0	2.0717899E-04			
0	2.3081830E-03			
0	7.5602497E-02			
1.0000000E-00	0	0	0	0
0	0	0	0	0
0	0	0	0	0
0	0			
0	1.0000000E-00	0	0	0
0	0	0	0	0
0	0	0	0	0
0	0			
0	0	1.0000000E-00	0	0
0	0	0	0	0
0	0	0	0	0
0	0			
0	0	0	1.0000000E-00	0
0	0	0	0	0
0	0	0	0	0
0	0			
0	0	0	0	1.0000000E-00
0	0	0	0	0
0	0	0	0	0
0	0			
1.0000000E-00	0	0	0	0
0	0	0	0	0
0	0	0	0	0
0	0			
0	1.0000000E-00	0	0	0
0	0	0	0	0
0	0	0	0	0
0	0			
0	0	0	0	0
0	0	1.0000000E-00	0	0
0	0	0	0	0
0	0			
0	0	0	1.0000000E-00	0
0	0	0	0	0
0	0	0	0	0
0	0			
0	0	0	0	1.0000000E-00
0	0	0	0	0
0	0	0	0	0
0	0			
1.0000000E-00	0	0	0	0
0	0	0	0	0
0	0	0	0	0
0	0			
0	1.0000000E-00	0	0	0
0	0	0	0	0
0	0	0	0	0
0	0			
0	0	1.0000000E-00	0	0
0	0	0	0	0
0	0	0	0	0

FILE: ESTIMATO DATA A1

```
                0                   0                   0                   0                   0
                0                   0                   0   1.0000000E-00                   0
                0                   0
                0                   0                   0                   0                   0
                0                   0                   0                   0   1.0000000E-00
                0                   0
                0                   0                   0                   0                   0
                0                   0                   0                   0                   0
                0                   0                   0                   0                   0
  1.0000000E-00                     0
                0                   0                   0                   0                   0
                0                   0                   0                   0                   0
                0                   0                   0                   0                   0
                0   1.0000000E-00
 -1.8784000E-00   0.0200000E-00  -0.0972000E-00   0.0219000E+00   0.0041000E+00
 -0.0016000E+00   0.3860000E+00   0.0720000E+00   0.0007000E+00  -0.3370000E+00
  0.0000000E+00   0.0000000E+00   0.0000000E+00   0.0000000E+00   0.0000000E+00
  0.0000000E+00    0.0000000E+0
  0.0000000E+00   0.0000000E+00    0.0000000E+00    0.0000000E+0   0.0000000E+00
  0.0000000E-00   0.0000000E+00     0.0000000E+0    0.0000000E+0    0.0000000E+0
  0.0040000E+00   0.0000000E+00    0.0000000E+00   -0.0002000E-0   0.0003000E-0
  0.0000000E+00  -0.0492000E-00
0 0 0 0 0 0 0 0 0 0 0 0 0 0 0 0 0
0 0 0 0 0 0 0 0 0 0 0 0 0 0 0 0 0
   -10000      10000
 0.13199300  0.03193770
 0.13199300 -0.03193770
 0.89698700  0.09067080
 0.89698700 -0.09067080
 0.95362500  0.02998500
 0.95362500 -0.02998500
 0.99820200  0.00000000
 1.00000000  0.00000000
 0.99560800  0.08307130
 0.99560800 -0.08307130
 0.09928050  0.00000000
 0.83521600  0.30973600
 0.83521600 -0.30973600
 0.96908700  0.03285880
 0.96908700 -0.03285880
 0.89379700  0.00000000
 0.93707500  0.00000000
```

LIST OF REFERENCES

1. Best, D., "An Analysis of Polar Missile Control," Journal of the Royal Acoustic Society, August 1960.

2. Thomas, A.N., Jr., "New Generation Ramjets-A Promising Future," Astronautics and Aeronautics, June 1980.

3. NASA CR-3325, Bank-to-Turn Control Technology Survey for Homing Missiles, Riedel, F. W., September 1980.

4. NASA CR-3420, Homing Performance Comparison of Selected Airframe Configurations Using Skid-to-Turn and Bank-to-Turn Steering Policies, Reichert, R. T., May 1981.

5. NASA TM-74079, Aerodynamic Characteristics of a Monoplanar Missile Concept with Bodies of Circular and Elliptical Cross Sections, Graves, E. B., December 1977.

6. NASA CR-3644, An Analysis of Aerodynamic Requirements for Coordinated Bank-to-Turn Autopilots, Arrow, A., November 1982.

7. Gordon, V. C., Pole Placement and Robustness Design Program, Ph.D. Thesis, Naval Postgraduate School, Monterey, California, December 1984.

8. Ogata, K., Modern Control Engineering, Prentice-Hall Inc., 1970.

9. Franklin, G. F., and Powell, D., Jr., Digital Control of Dynamic Systems, Addison-Wesley Publishing Co., June 1981.

10. Karaiskos, I., The Effects of Digital Control on Longitudinal Autopilots for Bank-to-Turn and Skid-to-Turn Missiles, Master Thesis, Naval Postgraduate School, Monterey, California, December 1985.

BIBLIOGRAPHY

Kuo, C. B., Automatic Control Systems, 1982.

Garnell, P., Guided Weapon Control Systems, 1980.

INITIAL DISTRIBUTION LIST

		No. Copies
1.	Defense Technical Information Center Cameron Station Alexandria, Virginia 22304-6145	2
2.	Library, Code 0142 Naval Postgraduate School Monterey, California 93943-5000	2
3.	Department Chairman, Code 67 Department of Aeronautics Naval Postgraduate School Monterey, California 93943-5000	1
4.	Professor D. J. Collins, Code 67Co Department of Aeronautics Naval Postgraduate School Monterey, California 93943-5000	3
5.	Professor H. A. Titus, Code 62Ts Department of Electrical and Computer Engineering Naval Postgraduate School Monterey, California 93943-5000	2
6.	Hellenic General Naval Staff 2nd Branch, Education Department Stratopedo Papagou Athens, Greece	4
7.	Christos I. Karadimas Kolokotroni 156, Piraeus Athens, Greece	5
8.	Ioannis C. Karaiskos Pelopos 1, Koridallos, Piraeus Athens, Greece.	1

216673

Thesis
K142573
c.1

Karadimas
Design and analysis of discrete lateral autopilots for coordination bank-to-turn missiles.